UNIVERSITA' DEGLI STUDI DI VERONA

Department of Neurosciences, Biomedicine and Movement

Graduate School of Life and Health Sciences

Doctoral program in Biomolecular Medicine

29th cycle, 2014-2016

Oligomerization of RNase A and onconase: structural determinants and influence on the functional features of the two enzymes

S.S.D. BIO/10 Biochemistry

Coordinator: Prof. De Franceschi Lucia

Tutor: Prof. Gotte Giovanni

Doctoral Student: Dott. Fagagnini Andrea

Contents

Abstract

1) Extensive deamidation of RNase A limits its oligomerization through 3D domain swapping (3D-DS)

Bovine pancreatic ribonuclease A (RNase A, 13.7 KDa) is the prototype of the 'pancreatic-type' ribonuclease superfamily. When subjected to lyophilization from 40% acetic acid solutions or to alternative unfolding procedures at high protein concentration, natively monomeric RNase A forms oligomers through a mechanism named 3D domain swapping (3D-DS). The oligomers form through the swapping of the N- and/or C-terminal domain of RNase A monomer. RNase A can undergo deamidation, especially of residue N67, to form Asp or isoAsp residues that modify both protein net charge and enzymatic activity. Furthermore, it is known that deamidation affects, although slightly, also the self-association of RNase B, that is one of the glycosylated forms of RNase A.

In the work described in chapter 3, we report and analyze the strong influence of RNase A deamidation on the enzyme tendency to oligomerize through the three-dimensional domain swapping mechanism. In fact, N67 deamidation decreases the yield of RNase A oligomers obtained after lyophilization from 40% acetic acid, and the Asp containing RNase A affects less the oligomerization compared to the isoAsp-containing protein. On the contrary, deamidation occurring at additional Asn or Gln residues nullifies the propensity of RNase A to oligomerize, as well as its enzymatic activity. Using 2D and 3D NMR, we identified some residues more prone to undergo deamidation, and we studied the difference existing among the tertiary structures of native and deamidated RNase A monomer, in combination with CD spectroscopy. Finally, the effect induced by deamidated residues on RNase

A dimers structures was studied with an *in silico* approach.

2) Different properties of RNase A dimers depend on the oligomerization process of the protein

Bovine pancreatic ribonuclease A (RNase A, 13.7 KDa), the 'pancreatic-type' ribonuclease superfamily prototype, is able to oligomerize through a mechanism called 3D domain swapping. RNase A oligomerization takes place when the monomeric protein is lyophilized from 40% acetic acid solutions or when it is submitted to thermal incubation in various solvents, especially EtOH, at high protein concentration.

Considering that the toxicity of oligomeric species of proteins involved in proteopathies often depends on the pathway through which oligomers form, we planned to analyze if also RNase A oligomers are affected by the production method. Thus, as reported in chapter 4, we analyzed how two different methods useful to obtain RNase A oligomers can possibly alter the structure and the function of its monomeric and dimeric forms. RNase A monomer and dimers were treated/obtained through 40% acetic acid lyophilization or thermal treatments at 60 °C in 20 or 40% EtOH and they were purified through cation exchange chromatography. Their structural differences were studied through cathodic native PAGE, far- and near-UV CD, ANS fluorescence and limited proteolysis with subtilisin. Tertiary structure differences, related to hydrophobic residues exposure and N-terminal region modifications, were confirmed only for the monomer using ANS fluorescence. In fact, no significative conformational differences were detectable using other analytical approaches. Contrarily, EtOH treatments demonstrated to form dimers with higher catalytic activity against ds-RNA poly(A):poly(U), with respect to the same species obtained after acid lyophilization.

3) Onconase oligomerizes producing a cytotoxic 3D domain-swapped dimer

Onconase (ONC, 11.8 KDa) is a protein produced in *Rana pipiens* oocytes and early embryos, belonging to the pancreatic-type RNase superfamily. This protein is currently used in Phase II and IIIb clinical trials against human non-small cell lung cancer and mesothelioma. In fact, despite its monomeric state, ONC structure allows it to avoid the interaction with the cytosolic RNase inhibitor and to exert its strong cytotoxicity by cleaving various types of RNA (mRNA, rRNA, tRNA, interfering RNA).

In the work reported in chapter 5, we found for the first time that ONC spontaneously forms dimeric trace amounts that increase about four times after acid lyophilization of the protein. This dimer was purified from the monomer, together with low amounts of ONC larger oligomers, through size exclusion chromatography (SEC). We found that dimeric ONC forms through the 3D domain swapping of its N-terminal domain, because the C-terminus is blocked by the presence of a disulfide involving the last cysteine residue. This was demonstrated by cross-linking the dimer with divinyl sulfone (DVS), and by the production of the H10A mutant, that resulted unable to oligomerize. Thus, the dimeric ONC has been modeled starting from the known structure of the N-swapped RNase A dimer and the structures of ONC dimer and monomer were compared using far- and near-UV CD and fluorescence. Although no significant differences involving secondary and tertiary structures were found, ONC monomer resulted to expose hydrophobic residues at a higher extent than the dimer.

Finally, we noticed that, at low concentrations, ONC dimer is more cytotoxic and pro-apoptotic than the monomer against PaCa44 pancreatic cancer cell line, and the cytotoxic effect is increased when the ONC species are combined with the antitumor drug gemcitabine.

Chapter 1

Introduction

1.1 Ribonucleases

The metabolism of ribonucleic acid (RNA), which represents the intermediate step in the genetic information transfer from DNA to proteins, is under the control of two classes of enzymes: RNA polymerases and RNA depolymerases or Ribonucleases (RNases)[1]. RNA polymerases take part in the synthesis of RNA molecules, while their degradation is catalyzed by RNases.

In living cells, RNA turnover is regulated by more than 20 exo- and endoribonucleases (RNases), whose function is to process RNA into mature forms[2]. In this way, RNases participate in RNA metabolism, but are also involved in other pathways, such as cell maturation, apoptosis, angiogenesis and defense against exogenous RNA viruses[3,4]. Moreover, some different RNases are also cytotoxic, including the wild-type binase from *Bacillus intermedius*[5], RNase Sa from *Streptomyces aureofaciens*[6], α-sarcin from *Aspergillus giganteus*[7], ranpirnase (also called Onconase) from *Rana pipiens*[8] and bovine seminal RNase (BS-RNase) from *Bos taurus*[3,9,10], and also mutants[11–15] or chemically modified[16,17] or engineered forms[18,19] of human and bovine pancreatic RNases.

Hence, it is evident that numerous RNase variants are known, forming a large family of enzymes. In non-herbivorous species, an important classification addresses the different secretory RNases into two superfamilies: the pancreatic and the non-pancreatic-type. The pancreatic-type RNases are present at very low levels (with respect to those of bovine pancreas) in secretory organs and body fluids such as pancreas, prostate, seminal fluid, milk and saliva[20–28]. They are characterized by sequence, structure and catalytic properties similar to those of bovine or human pancreatic RNases and their positive amino acid residues are localized in the vicinity of their active site[29,30]. Instead, the non-pancreatic-type RNases, present in spleen, liver, kidney, urine and serum[22,23,26,31–35], display sequence and catalytic properties similar to those of bovine kidney RNase K2 or human EDN/liver RNase, and their basic amino acid residues are distant from the active site[29,30].

1.2 RNase A

1.2.1 RNase A structure

Bovine pancreatic ribonuclease (RNase A, 13686 Da)[36] from *Bos taurus* is secreted in large quantities by the bovine pancreas, possibly due to the large amount or RNA produced by the bacteria present in the rumen[37]. The "A" refers to the most abundant isoform of the protein. In fact, other glycosylated isoforms accompany RNase A, such as RNase B[38–40], which is a mixture of glycoforms in which $Man_{5-9}GlcNAc_2$ are bound to the side-chain nitrogen of Asn34, and the less abundant RNase C and D[41,42], even more heterogeneous in their glycosylation profiles. RNase A was the first enzyme and the third protein whose amino acid sequence was determined[43,44], and the third enzyme and fourth protein whose structure was solved through X ray diffraction[45] (Fig. 1.1). It is a single-domain protein, composed by 124 amino acids (including all natural amino acids, except tryptophan), which originates a three-dimensional structure composed of three α-helices and seven β-strands: helix I (residues 3–13), helix II (24–34) and helix III (50–60), and an antiparallel β-sheet comprising β-strand I (43–49), β-strand II (61–63), β-strand III (72–74), β-strand IV (79–87), β-strand V (96–111), and β- strand VI (116–124). The structure is stabilized by four disulfide bonds at positions 26-84, 40-95, 58-110 and 65-72. These disulfide bonds are crucial for the stability of the protein, since the mutation of any cysteine in alanine[46] or serine[47,48] residues decreases its melting temperature. The prevalence of basic residues (four Arg, four His and ten Lys) over acidic residues (five Asp and five Glu) confers to the protein a positive net charge, with a resulting pI of 9.3[49]. The N-terminal domain (residues 1-15), includes the first α-helix, and is connected to the protein core through a flexible loop (residues 16-23). On the contrary, the C-terminal β-hairpin is composed by two β-strands (residues 105-124), in which a higher number of hydrophobic residues are present with respect to the N-terminus of the protein[50].

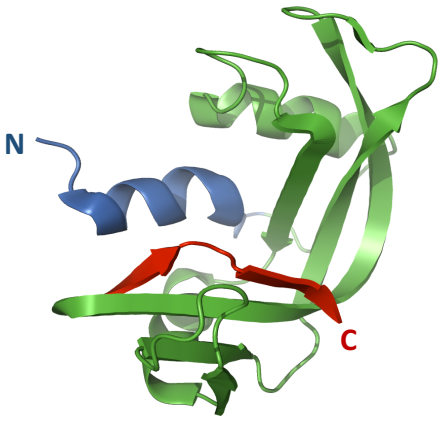

Figure 1.1 – Crystal structure of wild-type bovine pancreatic ribonuclease A (PDB: 5RSA[51]). The N- and C-termini are highlighted in blue and red, respectively.

In vivo, RNase A activity is strongly reduced or lost due to the presence of cytosolic inhibitors (Fig. 1.2) that inglobate the protein in their structure[12,52–54]. The most potent inhibitor of RNase A is the "ribonuclease inhibitor" (RI), a ~ 50 kDa protein present in mammalian cells. The role of RI is very presumably to protect the cytosolic RNA from the invasion of external pancreatic ribonucleases, and its function has been very well studied ($K_d \approx 10^{-14}$ M, $K_i \approx 10^{-13}$ M)[55,56]. The cytotoxic properties of other pancreatic-type ribonucleases, such as onconase or BS-RNase, seems to be principally due to their ability to evade RI[57–59].

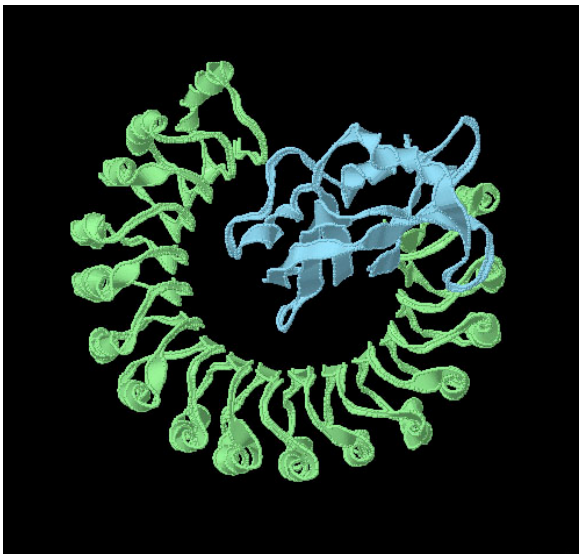

Figure 1.2 – Interaction between RNase A inhibitor (green) and RNase A (light blue)[60].

1.2.2 Catalytic activity of RNase A

RNase A is active on single-stranded RNA (ss-RNA). Moreover, some experiments demonstrated that it is also able to bind one of the two strands of the double-stranded DNA (ds-DNA) molecule, leading to its destabilization[61]. The binding involves more amino acid residues that take part to different interactions with more nucleic acids[62,63] (Fig. 1.3). RNase A displays several subsites, three of which (B1, B2 and B3) interact with the bases of a bound substrate. The B1 subsite (Thr45, Asp83) interacts only with pyrimidine residues[64,65], with higher preference for cytosine with respect to uracil. In contrast, B2 (Asn71, Glu111) and B3 subsites (unknown) are less specific, B2 having a preference for adenine[66], while B3 prefers purine bases[67,68]. Subsites P0 (Lys66), P1 (Gln11, His12, Lys41, His119 and Asp121) and P2 (Lys7, Arg10) interact with the phosphoryl group of the bound substrate[63].

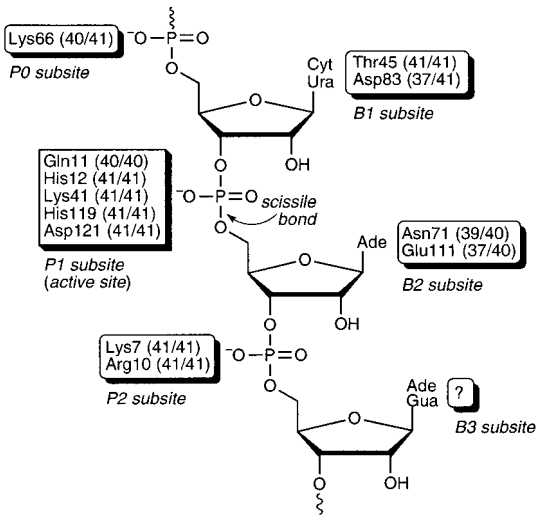

Figure 1.3 – RNase A residues involved in the interactions with the bound RNA molecule, and constituting B1 (Thr45, Asp83), B2 (Asn71, Glu111), B3 (unknown), P0 (Lys66), P1 (Gln11, His12, Lys41, His119, Asp121) and P2 (Lys7, Arg10) subsites. Numbers in parentheses refer to the conservation of the indicated residues in pancreatic ribonucleases. (Modified from Raines, 1998[69]).

The P1 subsite is the active site that catalyzes the cleavage of the bound P-O$^{5'}$ bond[70–75]. It is composed by Gln11 and His12, located in the N-terminal domain, by His119 and Asp121, in the C-terminus, and by Lys41, located in the protein core. In the first part of the first reaction, the transphosphorylation, His12 acts as a general base, removing a proton from the 2'oxygen of the substrate[51,76] (Fig. 1.4A). Instead, His119 acts as an electrophile, to allow the protonation of the 5' oxygen, and to favor the cleavage of the P-O bond between two RNA bases. This event leads to the formation of a nucleoside 2',3'-cyclic phosphodiester. In the second reaction (Fig. 1.4B), the hydrolysis of the nucleoside 2',3'-cyclic phosphodiester is induced by a nucleophilic attack of a water molecule to the 3'phosphate, facilitated by the action of His119 as a general base, with the protonation of the 2' oxygen and the deprotonation of His12 (Fig. 1.4B).

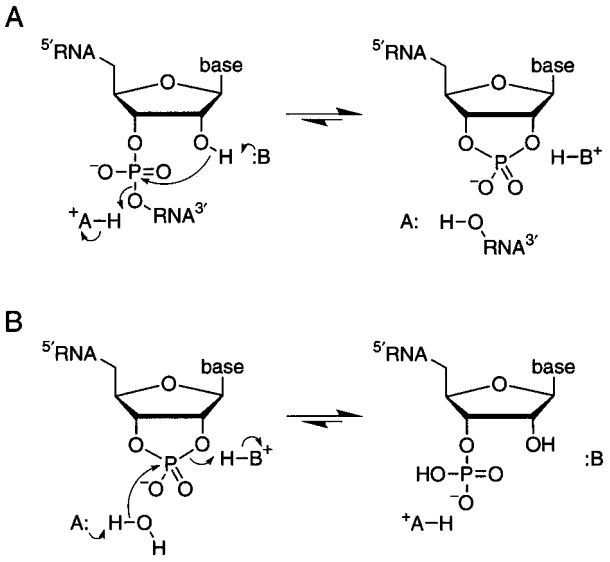

Figure 1.4 – Mechanisms of transphosphorylation (A) and hydrolysis (B) reactions catalyzed by RNase A. "B:" = His12, "A:" = His119. (Modified from Raines, 1998[69]).

RNase A cleaves CpX substrates and hydrolizes C>p (2',3'-cyclic cytidilate) 2-fold faster than the corresponding uridylyl substrates[69]. Poly(C) is cleaved about 20-fold faster than poly(U), while poly(A) is hydrolyzed at a rate that is 10^3- to 10^4-fold lower with respect to poly(U)[29,77].

1.2.3 RNase A oligomerizes through 3D Domain Swapping (3D-DS)

In the last two decades, RNase A has become a model to study protein aggregation. In fact, under specific conditions such as lyophilization from 40% acetic acid or incubation at high protein concentration in various solvents at high temperatures[50,78,79], monomeric RNase A forms aggregates, some of which have been characterized[80–82]. These species include metastable oligomers ranging from dimers, trimers, tetramers and larger oligomers, up to tetradecamers[83,84]. RNase A oligomerizes through 3D domain swapping mechanism[85]. The term 3D-DS was used for the first time by Eisenberg and co-workers[86] to describe the structure of a diphtheria toxin dimer (DT), but the mechanism was previously proposed in 1962[78]

by Crestfield et al., for RNase A. Then, to the end of the past decade, the structures of more than sixty domain-swapped protein dimers or oligomers had been solved[87]. 3D-DS occurs when one or more domains of a monomeric protein are reciprocally exchanged to form a dimer or a larger oligomer (Fig. 1.5). In a monomer, the domain(s) involved in the swapping leading to the oligomers formation contacts a part of its body, in the so-called closed interface (C-interface)[88](Fig. 1.5A). Mildly denaturing conditions, such as temperature or pH variation, as well as a high protein concentration, allow a monomer to reach the necessary $\Delta G^{\ddagger}$ to switch a domain and form an "open" monomer (Fig. 1.5A). Two identical domains are then reciprocally exchanged by different monomers, forming a dimer or an oligomer in which the interfaces present in the native monomer are re-estabilished. Then, also a new, additional, interface not present in the monomer, and referred to as the Open interface (O-interface)[88] (Fig. 1.5B), forms between the two swapped subunits.

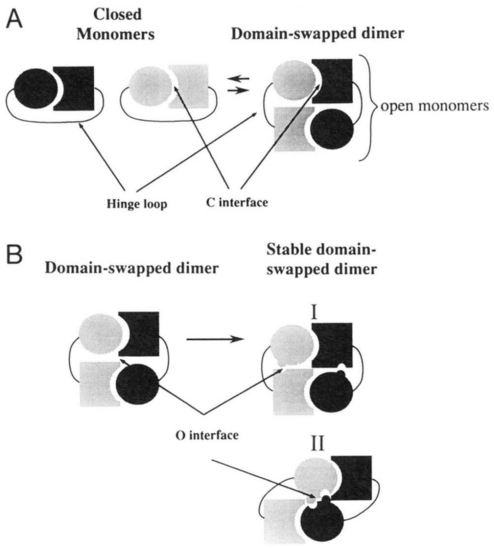

Figure 1.5 – Formation of a 3D domain-swapped metastable (A) and stable (B) dimer. Closed monomers are composed by the protein body (square) and the swappable domain (circle), linked through a polypeptide linker (hinge loop). The interface between the protein body and the swappable domain present in both monomer and dimer is the closed interface (C-interface). The open monomer can dimerize through 3D domain swapping, leading to the formation of a new open interface (O-interface), not present in the monomeric species. The O-interface can involve domains of the same subunit (BI) and/or different subunits (BII). Mutations may stabilize the O-interface, and consequently the dimeric forms. (Modified from Bennett at al., 1995[88]).

When the $\Delta G°_{oligomerization}$ is positive, metastable oligomers (such as RNase A oligomers, DT dimer) are generated, whereas stable oligomers form when $\Delta G°_{oligomerization}$ is negative (such as BS-RNase, IL-5 or βB2-crystallin dimers)[88] (Fig. 1.6). Three factors contribute to the Gibbs free energy difference among monomers and 3D-swapped oligomers: the oligomerization entropy makes the monomer more thermodynamically favored, while the new contacts generated in the swapped oligomers by the hinge loops and/or the new O-interface interactions make the domain-swapped oligomer more favorable[80,89–91].

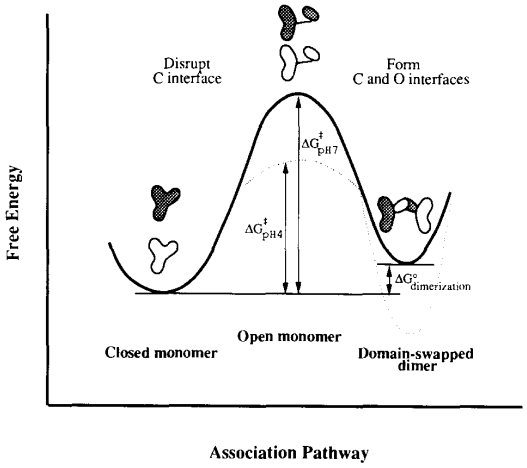

Figure 1.6 – Free energy in the formation of a domain-swapped dimer form two DT monomers. The difference in Gibbs free energy is positive, according to the metastable nature of the dimer formed. The dashed line refers to the formation of a stable domain-swapped dimer, favored by a negative difference in Gibbs free energy. (Modified from Bennett at al., 1995[88]).

The swapping domain may have different secondary structures: one α-helix, one β-strand, several α-helices, several β-strands, or a mixture of α-helices and β-strands. This demonstrates that 3D-DS does not need a particular type of primary or secondary structure[85]. Also the very flexible loop connecting the swapping domain to the protein body, the so-called hinge loop, can adopt a variety of secondary structures. Some hinge loops are coils, some α-helices and other form β-strands[81]. The stabilization of the swapped oligomers depends on various conditions, such as

buffer type, buffer concentration and pH, temperature, time and/or mutation of key residues[84,92–97].

3D-DS may also occur as a consequence of multiple mutations, causing monomer destabilization, such as the hinge loop shortening (for example in Staphylococcal nuclease)[98–101], or mutation(s) causing electrostatic repulsions between the swapping domain and the protein body (βB2-crystallin)[102]. On the other hand, amino acid substitution could form new contacts between the subunits of the same or different monomers constituting the oligomer and stabilize the O-interface[88].

3D-DS is also implicated in protein evolution. In fact, some proteins may acquire different activity with respect to the monomeric forms upon oligomerization, and if it confers an advantage to the organism, the oligomers will be selected in the process of natural evolution[88].

1.2.4 RNase A 3D domain-swapped N- and C-dimers

The most abundant species obtained through the induced oligomerization of RNase A are two different dimers. The crystallographic structures of both dimers were solved[80,81]. The first dimer forms through the swapping of the N-terminal domain (residues 1-15) of two RNase A monomers, and for this reason has been called N-dimer (N_D, PDB entry 1A2W), while the swapping of the C-terminus (residues 116-124) leads to the formation of the so-called C-dimer (C_D, PDB entry 1F0V), as shown in figure 1.7. The active site is reconstituted in both dimers, and the enzymatic activity is hence maintained[78,103].

RNase A constitutively forms traces of N-dimer[79,104]. In the N_D (Fig. 1.7A), the swapped N-terminus of each monomer contacts the major domain (residues 23-124) of the other. The two subunits interact through their three-stranded β-sheets, forming a six-stranded β-sheet through an O-interface stabilized by six H-bonds[81]. These specific stabilizing contacts are warranted by the two subunits disposed at approximately 160 degrees[81,105], because the two hinge loops acquire a different conformation: one forms a coil, whereas the other forms a helix.

In the C_D (Fig. 1.7B), the C-terminus of each monomer accommodates to the core of the other, forming a dimer that is larger in size with respect to the N_D, due to its different conformation, with a surface area of 13411 $Å^2$, instead of the 12236 $Å^2$ of the N_D[80]. In the C-terminal domain of the two subunits two β-strands form a β-hairpin richer in hydrophobic residues with respect to the N-terminus, and molecular dynamics simulations suggest that C_D is more flexible than N_D[105,106]. Moreover, the C_D conformation allows this isoform to expose a higher positive charge than N_D. The different sizes and charge exposition of N- and C-dimers allow to separate these two isoforms through size exclusion or cation exchange chromatographies[103,107].

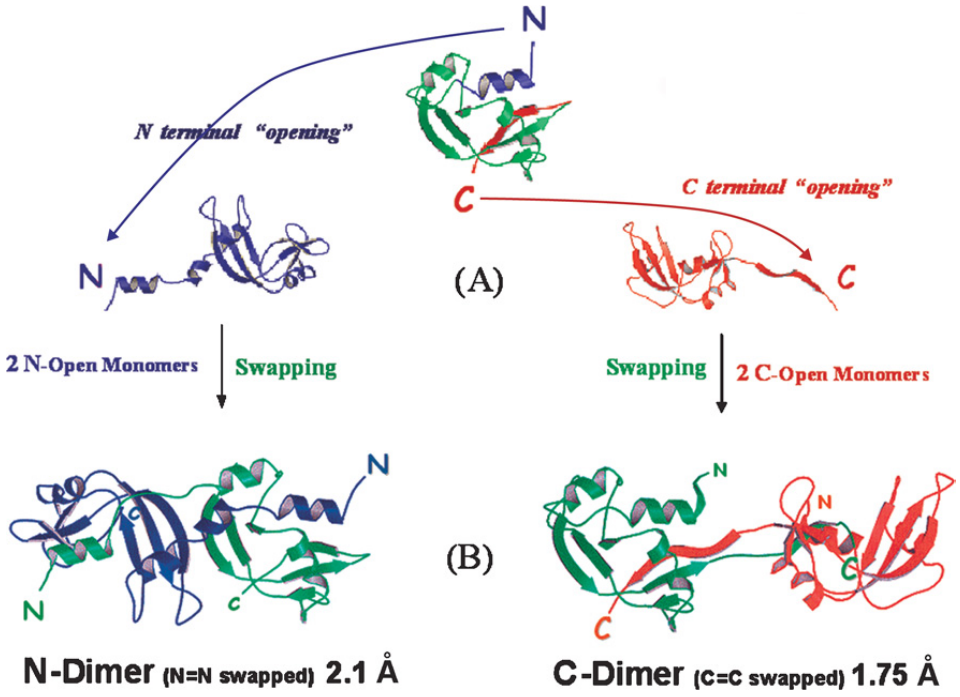

Figure 1.7 – A) N-terminal (blue) and C-terminal (red) opening of RNase A monomer, with B) the formation of the N-dimer (left PDB: 1A2W[81]) and the C-dimer (right, PDB: 1F0V[80]), respectively. (Modified from Libonati and Gotte, 2004[50]).

1.2.5 RNase A 3D domain-swapped trimers, tetramers and larger oligomers

RNase A forms also oligomers larger than dimers; in fact, there are two types of trimers: the NC-trimer (Fig. 1.8B), whose structure has been modeled as a linear trimer[82,94], and the C-trimer (Fig. 1.8A), whose structure has been solved[82] (PDB entry, 1JS0).

According to the proposed model, whose validity has been experimentally confirmed, the NC-trimer forms when a central monomer simultaneously swaps both its N-and C termini with two other monomers. It can be envisaged as a N-dimer, one subunit of which swaps the C-terminus with another monomer or, alternatively, as a C-dimer swapping the N-terminus of one subunit with a third monomer.

Instead, the structure of the C-trimer shows that the molecule generates through the swapping of the C-terminal domain of three monomers. Each monomer swaps its C-terminus into the core of the next monomer, forming a structure similar to a propeller whose surface is richer in basic charges with respect to NC-trimer.

The possibility to simultaneously swap both termini enlarges the oligomerization potential of RNase A: in fact, fewer amounts of different tetrameric isoform generate[80,82,83,85,94,107,108]. Four of them have been partially characterized and modeled (Fig. 1.8). Finally, also traces of pentamers, hexamers and larger oligomers have been detected and partially characterized[84,107,109,110].

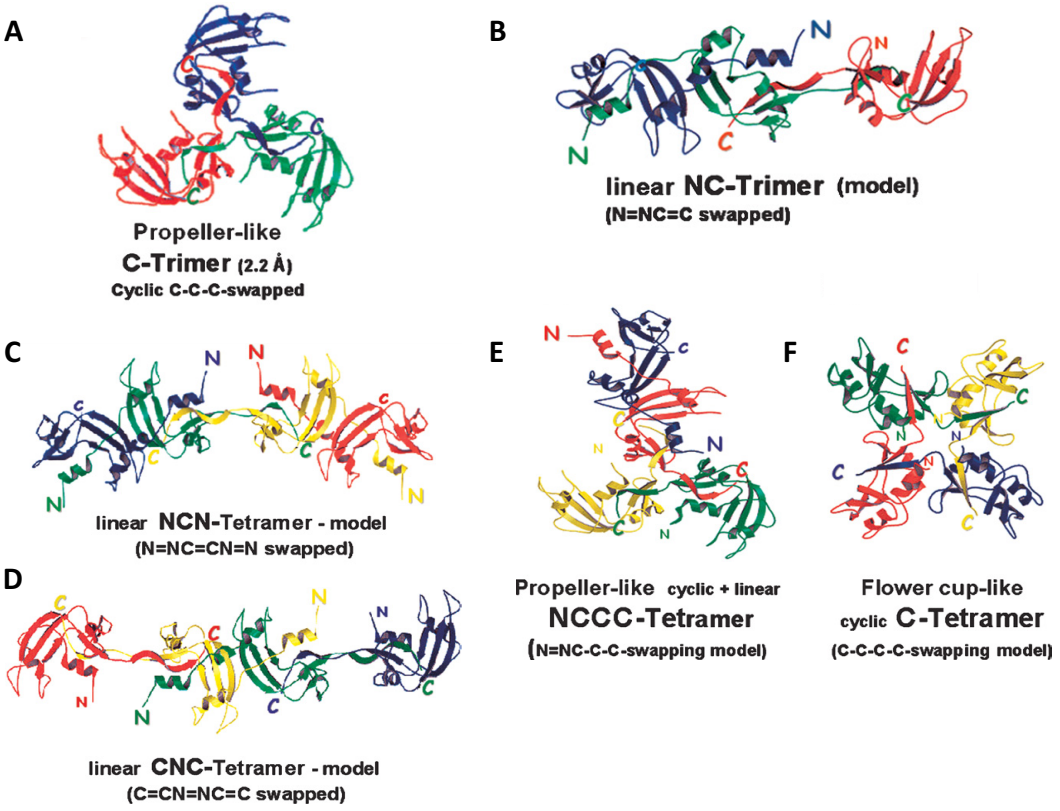

Figure 1.8 – Structure of A) C-trimer, and models of B) NC-trimer, C) NCN-tetramer, D) CNC-tetramer, E) NCCC-tetramer, F) C-tetramer. (Modified from Libonati and Gotte, 2004[50]).

1.2.6 Enzymatic activity of RNase A oligomers

Due to the reconstitution of a composite active site, RNase A oligomers are enzymatically active[78,80,81,88,103]. There is no difference among monomer and oligomers activity against 2',3'-cyclic cytidylate[78,103,111], while using single stranded (ss) yeast RNA as substrate, oligomers display a ribonucleolytic activity between 40 and 80% of monomeric RNase A[79,83,107,112]. In this case, the larger the oligomer, the lower the catalytic activity. With polyuridylate (polyU) and polycytidylate (polyC) as substrates, the activity of the oligomers falls between 70 and 90% of that of RNase A monomer[83,107]. The activities of the oligomers have to be considered per mole of oligomeric molecule, as the activity expressed per mole of species is about 60% of the activity of the monomer. In fact, when more subunits

are bound together, they are unable to simultaneously bind the substrate, but only a fraction of them can attack the substrate, reducing in this way the catalytic activity per mg of oligomer[50]. The higher catalytic activity that oligomers display against poly(U) and poly(C) with respect to yeast RNA could be due to the greater length and homogeneity of these substrates, that allow a better binding to the RNase A subsites[69,113,114]. Moreover, because of its heterogeneous sequence, the folding of yeast RNA leads to a complicated structure, which RNase A can attack less efficiently.

On the contrary, double stranded-RNA (ds-RNA) is degraded less efficiently by RNase A, due to the difficult enzyme-substrate interactions[115]. However, RNase A oligomerization leads to the gain of depolymerization activity against double-stranded RNA, such as the synthetic polyribonucleotide poly(A):poly(U). This activity increases with the size of oligomers, augmenting from dimers to trimers to tetramers, and so on[82,83,107,112]. Moreover, the activity varies among the oligomers with the same size, with the one exposing more positive charge being more active[107]. Thus, the C-swapped oligomers are generally more active than the N-swapped ones. This is due to the different basicity localized by the active sites of the oligomers, with a consequent different interaction with the negative charges of RNA phosphate groups.

RNase A is not highly active against poly(A), likely because purine bases can only bind the B2 and B3 subsites, but not the B1[69]. On the contrary, its oligomers become more active, and this activity increases with the size of the oligomers, probably due to the stronger electrostatic interaction[83,107,116].

1.2.7 Cytotoxic activity of RNase A oligomers

The catalytic activity of RNase A is responsible of its cytotoxicity against some types of cancer cells[117]. RNase A, in fact, demonstrated to display weak antitumor activity at high doses against Ehrlich carcinoma in mice (above 10 mg/Kg)[118,119]. On the contrary, RNase A oligomers are characterized by an *in vitro* and *in vivo* cytotoxic activity against some types of cancer cells such as ML-2 (human myeloid

leukemia) and HL-60 (human promyelocytic leukemia cells), as well by an aspermatogenic action, that generally increases with the increasing size, catalytic activity and, consequently, basic charge of RNase A oligomers[108]. Experimental evidence of these points is supported by the acidic, non-cytotoxic RNase Sa from *Streptomyces aurefaciens*, that becomes cytotoxic against NIH3T3 and v-*ras* transformed NIH3T3 cells after the replacement of five acidic residues with lysines[120] and by the decreased cytotoxicity of the ribotoxin α-sarcin against human rhabdomyosarcoma cells after the removal of a highly positively charged β-hairpin belonging to its N-terminus[121]. It was supposed that the cytotoxicity of RNase A oligomers is principally ascribed to their ability to evade the cytosolic RNase A inhibitor (cRI)[12,122]. Their structure, in fact, does not allow the cRI to retain them, contrarily to RNase A monomer, for which it shows high affinity[123,124]. Supporting this hypothesis, it was demonstrated that RNase A monomer acquires significant antitumor activity when conjugated with PEG[125] and is cytotoxic against k-562 cells when submitted to site directed mutagenesis in order to decrease the interaction with cRI[126]. However, the mechanism of RNase A oligomers endocytosis has not been clarified yet, but it has been hypothesized that the high positive charges exposed allow them to interact with the negative surfaces of the target cells, that successively incorporate them through endocytosis[108]. Once inside the cell, oligomers are allowed to attack various type of RNA, such as mRNA, tRNA, rRNA, siRNA, and DNA:RNA hybrid molecules. Putative targets of RNase A are also RNAs circulating in the blood plasma, including pre-miRNAs and miRNAs implicated in the control of oncogenesis and invasion[127].

The cytotoxic activity of RNase A oligomers depends on their stability, that is difficult to be analyzed during *in vitro* or *in vivo* experiments. In general, the higher the oligomer size, the lower its stability[94]. However, when tested in very complex environments composed by a huge number of different molecules, such as cell cultures or *in vivo* tissues, it is impossible to predict the stability of these species.

1.2.8 RNase A as a model to study the mechanism through which amyloid fibers form

The mechanism of 3D domain swapping has been found to be involved in the formation of amyloid fibers. Amyloid deposits are formed by proteins that are otherwise soluble in their physiological role. All amyloids fibers share three specific characteristics: i) they can be stained by organic dyes, such as the bis-diazo Congo Red[128], ii) they appear composed by uniform, straight and rigid fibers, of about 100 Å diameter[129,130], and iii) they are formed by the so-called repetitive cross-β structure[131], in which β-strands are perpendicular to the fiber axis. Some human diseases are caused by the accumulation of localized amyloid deposits. Amyloid β-protein, α-synuclein, and prion protein, for example, are able to form amyloid fibrils, causing the known pathologies of Alzheimer, Parkinson and prion diseases (such as spongiform encephalopathies and scrapie), respectively[132]. Then, human cystatin C (HCC, a cysteine protease inhibitor), that can generate amyloid fibrils that accumulate in the brain arteries of elderly patients suffering from cerebral amyloid angiopathy, and β_2-microglobulin (the invariant light chain of the class I major histocompatibility antigens), that forms dialysis related amyloid fibers, are examples of proteins able to form oligomers through 3D-DS[133–135]. In these contexts, 3D-DS, the mechanism shared by RNase A, has been proposed as a possible mechanism responsible for amyloid fibers formation. Anyway, the only pancreatic-type RNase that is able to form amyloid fibrils is the eosinophil cationic protein (ECP)[136]. RNase A does not form amyloid fibrils in its wild-type (wt) form, but produces amyloid type fibrils when modified through the addition of 10 Gln residues in the proximity of the C-terminal domain, or by the addition of some Gly residues before its N-terminus[137,138]. Moreover, it has been demonstrated that fibrils are not the direct cause of toxicity that is rather related to the presence of smaller oligomers that are the fibril precursors[139]. It was recently demonstrated that these oligomers may be toxic or not depending on the way they form[139].

In this context, RNase A can be taken as a model to study and understand the mechanism of self-association of amyloid precursors, although the wt protein does not form fibrils (Chapter 4).

1.2.9 RNase A deamidation

3D-DS self-association is quantitatively affected by several factors, such as molecular crowding[96], glycosylation[140], mutations affecting the polarity of N- and C-swapping termini[93], or mutations of key-residues[92,95]. These parameters affect the relative proportions of RNase A N-swapped or C-swapped oligomers[92,93,140,141]. Another factor that limits RNase A oligomerization may be deamidation, although this link has been only investigated for RNase B[107,140].

Protein deamidation principally involves Asn but also Gln residues. Asn deamidation starts with a nucleophilic attack on its amide carbonyl performed by the nitrogen of the peptide group linking the Asn to the following residue, generally a Gly. The result of this reaction is the formation of a cyclic succinimidyl intermediate that can undergo hydrolysis at both the sides of the imide nitrogen, forming either a normal aspartic derivative (D) or an isoaspartic one (<u>*D*</u>)[142,143] (Fig. 1.9). On the other hand, Gln deamidation leads to the formation of a Glu residue and a slower forming γ-Glu product[144,145].

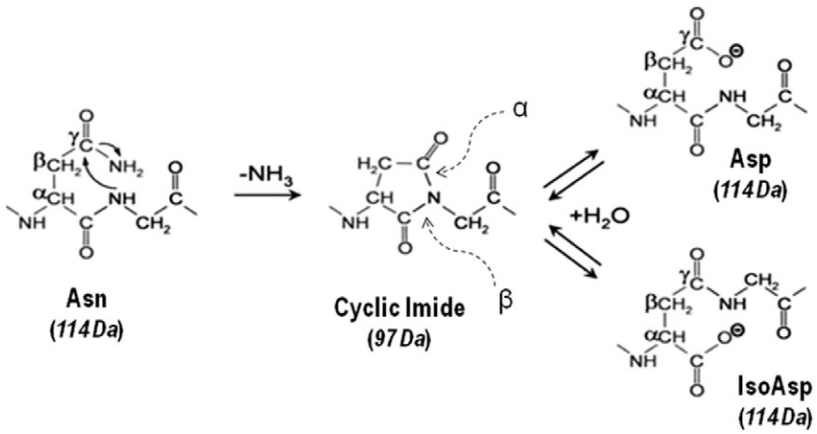

Figure 1.9 – Asn deamidation proceeds through a cyclic succinimidyl intermediate that can be hydrolyzed at both sides of the imide nitrogen, producing either an aspartate (α-derivative) or an isoaspartate (β-derivative) residue.

Protein deamidation occurs during purification or long-time storage of a protein, thus it has been proposed to occur during protein aging[144,146,147]. Deamidation, in

fact, spontaneously affects several proteins[144,145,148,149].

The deamidation of specific residues of some proteins can alter their propensity to aggregate, with opposite effects. For example, the natural structural variant D76N of β_2-microglobulin increases its fibrillogenic capacity with respect to the wt protein[150], while deamidation is able to induce the aggregation of other proteins such as γD-crystallin, amylin and SOD1[151–153]. In addition, it has to be underlined that Asn263 deamidation in the fibronectin type I repeat (FN-I5) is able to increase endothelial cell adhesion and proliferation[154].

In the case of BS-RNase, the deamidation of Asn67 of both subunits occurs as a post-translational modification[146,155]. In its native structure RNase A is very resistant to deamidation, probably due to the rigidity of the backbone of the loop between Cys65 and Cys72, that is stabilized by a disulfide bond between these two residues and by the β-turn at residues 66-68, which could hinder the formation of the cyclic imide[156]. It is possible to selectively deamidate the Asn67 of RNase A, and this modification results in both a reduction of its catalytic activity against yeast ss-RNA for both the isoAsp and Asp derivatives, and a reduction in the folding rate of the isoAsp derivative[157].

The influence of deamidation on the oligomerization of RNase A is deeply analyzed in chapter 3.

1.3 Onconase

1.3.1 Onconase structure

Onconase (ONC) (Fig. 1.10A), also known as P30 protein[158] or Ranpirnase, is a small basic protein (11.8 kDa). It is the smallest member of the pancreatic-type RNase super-family[159], despite a sequence identity of only 30% with RNase A, and it is isolated from oocytes and early embryos of *Rana pipiens*, the northern leopard

frog[158,160,161]. ONC extracted from oocytes is polymorphic at positions 11, 20, 25, 85 and 103, and *R. pipiens* genome seems to contain four or more genes coding for ONC variants[160–163]. ONC shares common structural elements with RNase A, particularly the position of the three α-helices, the two 3-stranded anti-parallel β-sheets, the active sites residues, the hydrophobic clusters, and three out of four disulfide bonds (Cys19-Cys68, Cys30-Cys75, Cys48-Cys90)[164] (Fig.1.10B). Nevertheless, ONC differs from RNase A for the presence of a N-terminal pyroglutamate residue[161,164], formed by the spontaneous cyclization of the amino-terminal glutamine residue or as a product of glutaminyl cyclase, which tethers the N-terminus to the protein body, and of a disulfide bond involving the C-terminal cysteine (Cys87-Cys104). Both features contribute to the high thermal stability of ONC, whose melting temperature is of about 90 °C, that is 25-30 °C higher than that of RNase A[165,166]. In fact, hindering the formation of the N-terminal pyroglutamyl bond by retaining the N-terminal Met results in a decrease of ONC Tm of about 5 °C, and in a ~40-fold reduction of its catalytic activity against yeast RNA, measured in the presence of 0.05 M NaCl. This demonstrates that the pyroglutamate takes part also in the catalytic mechanism[166]. On the other hand, the loss of the C-terminal disulfide bond results to a decreasing of the melting temperature of about 19 °C, but it does not affect the catalytic activity[166].

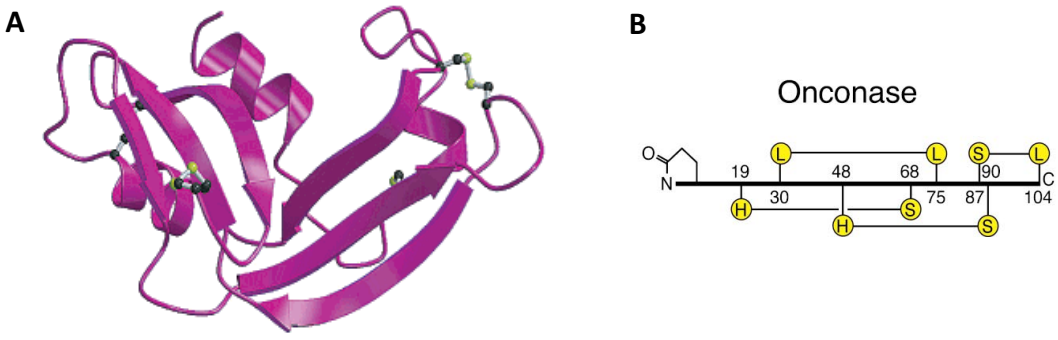

Figure 1.10 – A) Crystal structure of wild type onconase (ONC, PDB entry, 1ONC[164]) and B) schematic representation of the disulfide bonds present in ONC tertiary structure. The secondary structural context of each half-cystine is indicated by H (helix), S (sheet), or L (loop). (Modified from Lee and Raines, 2003[167] and from Leland and Raines, 2001[168]).

1.3.2 ONC enzymatic activity

The catalytic residues of RNase A (His12, Lys41, His119) are conserved in ONC, and are His10, Lys31, His97[161] (Fig. 1.11). The B1 subsite of ONC is composed by Thr35, Asp67 and Phe98, while the B2 subsite is supposed to be formed by Thr89 and Glu91[169].

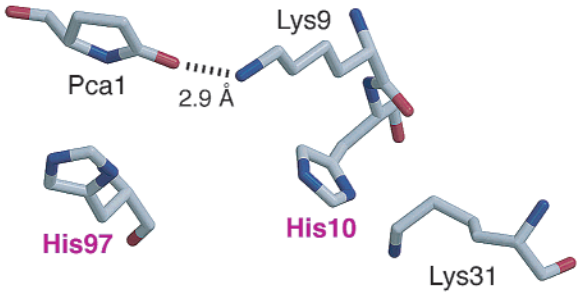

Figure 1.11 – Active-site residues of ONC. His10, Lys31, and His97 are conserved in the RNase A superfamily. (Modified from Lee and Raines, 2003[167]).

The catalytic activity of ONC toward the synthetic substrate 6-FAM-dArUdGdA-6-TAMRA is three-five orders of magnitude lower than that of RNase A[167]. While RNase A homologs bind a pyrimidine residue on the 5' side of the phosphodiester bond[51,67,77,170], ONC prefers to bind a guanine on the 3' side[167]. This preference is typical of frog ribonucleases, but not of mammalian homologs. The ONC target is the intracellular RNA, and some experiments demonstrated that it is able to cleave tRNA[171]. In this case, the cleavage sequence for ONC is the guanosine-guanosine phosphodiester bond in the variable loop of the D-arm of t-RNA[172]. ONC is 100-fold more active against polyuridylic than polycytidilyc acids and 10-fold more active against uridylyl 3',5' guanosine than cytidilyl 3',5' guanosine[173]. Hence, somewhat surprisingly, ONC displays a different base specificity when interacting with synthetic substrates or tRNA molecules[172,174].

1.3.3 ONC cytotoxicity

Onconase is both cytotoxic and cytostatic towards several tumor cell lines. Its action is explicated by arresting the cell cycle in the G1 phase[8,58]. Its LC_{50} in vitro is about 10^{-7} M, but it depends on the type of cancer cell. It is used in Phase II and Phase IIIb clinical trials against non-small cell lung cancer and unresectable malignant mesothelioma, respectively[175]. Recently, ONC showed to be remarkably active against other several human cancer cell types, such as glioma cells and lymphoma B cells[176,177] or, finally, against human pancreatic adenocarcinoma cell lines through an autophagy-mediated and ROS-dependent pathway[178]. Some studies demonstrated that it is an effective chemotherapeutic agent in mice[179]. Moreover, ONC is able to inhibit human immunodeficiency virus type 1 replication[174,180]. Renal toxicity is dose-limiting, but it can be overcome by discontinuing treatments.

Like the other cytotoxic RNases, except for the RNases from *Rana catesbeiana* (RC-RNase) and *Rana japonica* (RJ-RNase), which lead to cell death through their binding to the cell membrane[181], ONC explicates its cytotoxicity after its cellular internalization, that occurs through endocytosis[9]. The cell membrane receptors involved in ONC internalization are still elusive. After the releasing from the endosome to the cytoplasm, ONC and RNases in general are free to meet the target RNA, but they must resist to the attack of proteases.

The degradation of rRNA was proposed to be the reason for ONC cytostatic and cytotoxic activity, due to the inhibition of protein synthesis[58]. Subsequently, the cleavage of tRNA induced by this protein was supposed to lead to the activation of the caspase cascade in mammalian cells, resulting in apoptosis[182]. Another proposed mechanism for ONC action is the generation of intracellular interfering RNA (RNAi), whose final result is also the induction of apoptosis[183].

ONC cytotoxicity, like that of BS-RNase and RNase A oligomers (Section 1.2.7), is principally ascribed to its ability to evade the cytosolic RNase inhibitor, a ~ 50 kDa protein. Although being monomeric, the low sensitivity of ONC to the inhibitor ($K_i \geq 10^{-6}$ M) seems to be related to the lack of many of the residues present in RNase A sequence that are known to mediate the interaction with the inhibitor[19,57].

1.3.4 ONC oligomerization

At the time of this study, no data reporting the capacity of ONC to self-associate were available. Since RNase A oligomerization greatly enhances its activity and cytotoxicity, we wished to assess whether ONC oligomerization could lead to similar improvements in the therapeutic potential, and simultaneously reduce the side effects associated with the treatment.

It is well known that RNase A, when lyophilized from 40% acetic acid solution and redissolved in sodium-phosphate buffer (section 1.2.3), produces oligomers with an increasing cytotoxic activity as a function of the molecular weight. So far, no oligomers of ONC have been reported or characterized in their cytotoxic activity. In the work reported in chapter 5, we obtained a ONC dimer and traces of larger oligomers through lyophilization from 40% acetic acid. We studied the structural and functional properties of the dimer and we tested its cytotoxic effects induced on a pancreatic cancer cell line, PaCa44.

Chapter 2

Aim of the thesis

The main intent of this PhD thesis was to deepen the investigation of the structural determinants that affect the self-association tendency of pancreatic-type RNases[50,79,95,184].

In particular, I started to study the effect played by deamidation on the aggregation propensity of RNase A, an aspect that was only marginally mentioned in the past[107].

Then, I analysed the differences detectable between RNase A oligomers obtained after acid lyophilization[78] or, alternatively, through the thermal treatment of concentrated solutions of the protein dissolved in various solvents[79].

Finally, I focused my attention on the oligomerization process of onconase, the amphibian pancreatic-type RNase variant already known to be cytotoxic in its native form.

1) Extensive deamidation of RNAse A limits its oligomerization through 3D domain swapping

Protein deamidation is ascribable to processes taking part during the protein purification steps, but also to protein storage. Moreover, some studies demonstraded that it also occurs as a consequence of protein aging[144,146,147]. When a protein undergoes deamidation, some of its structural and/or functional properties can be altered in different ways. For example, when the Asp present in position 76 of β_2-microglobulin is replaced by Asn, the protein increases its fibrillogenic propensity[150], while the deamidation of proteins such as γD-crystalline, amylin and SOD1 promotes their aggregation[151–153].

The cation exchange chromatography pattern of a commercial type of RNase A (RNase A-type IA, Sigma-Aldrich) is consistent with the presence of deamidated species, as judged from the comparison with RNase B, previously studied[107]. Moreover, with respect to the purer RNase A (Type XIIA, Sigma-Aldrich), RNase A-IA produced less oligomers after lyophilization from 40% acetic acid solution. Our hypothesis was that RNase A deamidation could influence its propensity to oligomerize. RNase A deamidation was hence induced to study the oligomerization

ability of the resulting deamidated species, following the protocol of Di Donato et al.[157]. N67D-RNase A, a deamidated derivative previously deeply characterized, as well as its two subspecies, Asp and isoAsp derivatives, and other poly-deamidated species that were chromatographically isolated, were induced to oligomerize. In order to study how extensive deamidation of RNase A inhibits its oligomerization ability and alters its enzymatic activity, CD spectroscopy, 2D and 3D NMR, immunoblotting, *in silico* structural analyses and Kunitz enzymatic assays were used (Chapter 3).

2) Different properties of RNase A dimers depend on the oligomerization process of the protein

Natively monomeric RNase A (13.7 KDa) can oligomerize under determined conditions, such as lyophilization from 30-50% acetic acid[78] or thermal treatments in various solvents[79], producing dimers, trimers, tetramers and larger oligomers[50,84,110], through a mechanism named three-dimensional domain swapping (3D-DS)[88]. This mechanism had also been unveiled to lead to the formation of cross-β spine aggregates and fibrils involved in deposition diseases[185]. It is known that, in the context of amyloid deposition diseases, the toxicity is not due to fibrils, but rather to early oligomeric aggregates. Again, more recently, some studies demonstrated that these oligomers can be toxic or not toxic, as a function of possibly different aggregation pathways[139].

Considering that RNase A forms the same type of oligomers following two different protocols, in the work reported in chapter 4 we aimed to evaluate if the process of production of RNase A oligomers could somehow affect their functional properties. To do so, we focused our attention on RNase A N-dimer(s)[81] and C-dimer(s)[80] obtained through the two different methods mentioned above: 1) lyophilization from 40% acetic acid[78] and 2) thermal treatment of highly concentrated solution of the protein in 20% and 40% EtOH[79]. We measured and analyzed the differences in the enzymatic activities of monomer and dimers treated/obtained with the

mentioned conditions and, using CD spectroscopy, ANS fluorescence, and limited proteolysis with subtilisin, we analyzed their structural and stability differences.

3) Onconase oligomerizes producing a cytotoxic 3D domain-swapped dimer

Onconase (ONC), a small member of the pancreatic-type RNases superfamily, is a cytotoxic and cytostatic protein expressed in oocytes and early embryos of *Rana pipiens*[158,160,161]. This protein is used in Phase II and Phase IIIb clinical trials against non-small cell lung cancer and unresectable malignant mesothelioma[175], respectively, and it is also active against other several human cancer cell types[176–178], as well as against human immunodeficiency virus type 1[174,180].

Because of the structural similarity existing among ONC and RNase A despite the low sequence identity (about 30%), we attempted to induce ONC oligomerization by lyophilizing it from 40% acetic acid, in order to investigate if ONC could be able to produce 3D domain-swapped oligomers, similarly to the prototype RNase A[50,78,79], even if the C-terminus of ONC is blocked by a disulfide bond involving the last C-terminal cysteine (Cys104). For this reason, we hypothesized that the C-terminal domain could not be available to take part in the swapping process. In fact, after acid lyophilization, only one peak eluting before the ONC monomer was detected in size exclusion chromatography. The species eluted in this peak was deeply characterized using CD spectroscopy, fluorescence, Kunitz assays and *in silico* analysis. To confirm that the ONC dimer formed through N-terminal domain swapping, a cross-linking reaction with divinyl sulfone was performed and a H10A mutant was produced and analyzed. Finally, since RNases generally increase their biological activities upon oligomerization[50,186], the cytotoxic activity and the apoptosis induction of ONC dimer was tested against a pancreatic cancer cell line, and compared to the already known cytotoxicity of ONC monomer[178]. The whole work performed is described and discussed in chapter 5.

Chapter 3

Extensive deamidation of RNase A hinders its oligomerization through 3D domain swapping

3.1 Materials

RNase A from bovine pancreas (Type IA-S and XII-A) and poly(A):poly(U) were purchased from Sigma-Aldrich. Yeast RNA (ss-RNA) was from Boehringer. All other chemicals were used at the highest purity available. ONC cDNA was kindly provided by prof. Delia Picone and dr. Eugenio Notomista (University of Naples, Federico II).

3.2 Methods

3.2.1 Quantification of the various RNase A species

The concentration of the RNase A monomeric and oligomeric species was determined measuring the sample absorbance at 280 nm, $\varepsilon^{1\%}_{280} = 7.3\ M^{-1}cm^{-1}$, with a Jasco V-650 spectrophotometer. Oligomerization does not affect the molar extinction coefficient value (unpublished data).

3.2.2 Induction of RNase A deamidation

Deamidation of RNase type XII-A was carried out incubating the protein at a concentration of 2 mg/ml in 1% NH_4HCO_3, at 37 °C, following the procedure of Di Donato & coll.[157]. 500 μg aliquots of the protein were withdrawn at different times (0-48-134-256 h) and the reaction was stopped by adding 0.2 M NaH_2PO_4/Na_2HPO_4 (NaPi) buffer, pH 6.7. Then, the NaPi concentration of the aliquots was lowered to 50 mM with Amicon Plus and Amicon Mini ultrafilters (3 kDa or 10 kDa cut-off, Merck-Millipore) for subsequent cation exchange chromatography analyses.

3.2.3 Purification of RNase type IA-S, deamidated RNase type XII-A and RNase A oligomers

Each species deriving from RNase type IA-S or from the deamidation reaction of RNase type XII-A was purified through cation exchange chromatography, with a Source 15S HR 10/10 column attached to an ÄKTA-FPLC system (GE-Healthcare), and equilibrated with 60 mM NaPi buffer, pH 6.7, at a flow rate of 1 ml/min.

RNase A oligomers were purified at a flow rate of 2 ml/min, with a 70 mM NaPi concentration to elute the monomer, 90 mM to elute the N-dimer, and a 1h gradient from 90 to 200 mM to elute the C-dimer and the larger oligomers[107].

To better resolve the polydeamidated species, the same column was equilibrated with 0.1 M sodium acetate-acetic acid buffer, pH 5.0, and 0.05 M NaCl, and a 120 min NaCl gradient was applied from 0.05 M to 0.35 M to elute samples. The flow rate was of 1 ml/min.

Chromatographic patterns and areas of the resulting peaks were analyzed with the Unicorn 5.01 Software (GE Healthcare).

3.2.4 Purification of Aspartic and IsoAspartic derivatives through hydrophobic interaction chromatography (HIC)

One peak resulting from the deamidation reaction corresponds to the monodeamidated species at Asn67[157]. To better resolve the Asp (N67D) and IsoAsp (N67*D*) derivatives, the peak corresponding to N67D/N67*D* was collected after cation exchange chromatography, dyalized against ddH_2O and lyophilized. The resulting powder was redissolved in 2.0 M $(NH_4)_2SO_4$/0.1 M NaPi, pH 6.0, and injected onto a Phenyl Sepharose column equilibrated with the same buffer. The samples were eluted with a gradient from 2.0 M to 0.5 M $(NH_4)_2SO_4$, in 90 min, an elution strategy that resembles the one described by Di Donato et al.[157].

3.2.5 Enzymatic activity on single strand (ss-) RNA

Kunitz assays[187] were performed on 0.6 mg/ml yeast RNA ($A_{300} \approx 0.6$) solubilized in 0.1 M sodium acetate buffer, pH 5.0, using a Jasco V-650 spectrophotometer. Enzymes' concentration was 0.75 ng/µl. The decrease of A_{300} was recorded for 300 seconds, in the linearity range. The blank measure was performed acquiring the absorbance of 0.1 M sodium acetate buffer, pH 5.0. Negative controls were performed by measuring the absorbance of the yeast-RNA solution without the addition of the enzyme, in order to exclude the presence of contaminant RNases. The enzymatic activities of the protein samples were calculated as $\Delta A/(\Delta min \cdot \mu g)$.

3.2.6 RNase A oligomers production and purification

Each species purified by cation exchange chromatography and/or by HIC was dialyzed against 2x distilled water (ddH_2O), and then lyophilized from 40% aqueous acetic acid solutions at the concentration of 50 mg/ml, following the procedure of Crestfield & coll[78]. The resulting powder was then suspended at different concentrations, ranging from 1 to 10 mg/ml, in 0.4 M NaPi buffer, pH 6.7, and analyzed by size exclusion chromatography (SEC), with a Superdex 75 HR 10/300 column attached to an ÄKTA-FPLC system (GE-Healthcare). The column was equilibrated with the same NaPi buffer and the mixtures were eluted at a flow rate of 0.10-0.15 ml/min. Chromatographic patterns and areas of the resulting peaks were analyzed with the Unicorn 5.01 Software (GE Healthcare).

3.2.7 SDS-PAGE and immunoblotting analysis

SDS-PAGE was performed using a 12.5% acrylamide gel and Tris/glycine buffer, pH 8.3. Five µg of each sample were run at 200 V, for 60 min.

The transfer of each protein sample on a PVDF (Immobilon-P) membrane, was carried out in ice bath, using a constant amperage of 300 mA, for 1 h. The

membrane was then transferred in a 5% BSA in TBST solution (50 mM Tris-HCl, pH 7.5, 0.9% NaCl, 0.1% Tween20), for 1 h. IgG anti-HP-RNase (IgTech, Salerno, Italy), kindly provided by Dr. E. Pizzo (University of Naples, Federico II), was added in a 1:1000 (antibody stock:TBST solution) ratio, and the membrane was transferred at 4 °C, overnigth. After TBST washing, the membrane was developed with anti-rabbit IgG peroxidase-conjugate antibody (1:2000, Cell Signaling Tech, Danvers, MA, USA) and detected with a chemiluminescent detection system (Immun-Star WesternC Kit, Bio-Rad, Hercules, CA). Blotted proteins were then detected with ChemiDoc XRS Imaging System (Bio-Rad).

3.2.8 Nondenaturing cathodic PAGE

Nondenaturing cathodic PAGE[188] was performed using a 12.5-15% acrylamide gel, in β-alanine (0.35%)/acetic acid buffer, pH 4.0. Samples were electrophoresed with a constant voltage of 200 V, for 90 min, in ice. Gels were subsequently transferred in 12.5% 2,2,2-trichloroacetic acid for 90 min, stained with 0.1% Coomassie Brilliant Blue, and destained in 10% CH_3COOH, 20% EtOH solution.

3.2.9 Circular dichroism and thermal unfolding analyses

A Jasco J-810 spectropolarimeter was used to measure far-UV CD spectra. Spectra of native and deamidated monomeric RNase A (Sigma, type XII-A) were recorded at 25 °C using the following parameters: bandwidth = 1.2 nm, scan speed = 20 nm/min, number of scans = 6, substracting the spectrum of the 5 mM K_2HPO_4/KH_2PO_4 buffer recorded using the same parameters.

The thermal denaturation of RNase A species was carried out with a protein concentration ranging from 0.25 to 0.5 mg/ml, diluted in 10 mM NaPi buffer, pH 6.7, and submitting the protein to a thermal gradient of 1.5 °C/min, from 25 to 90 °C. The reaction was monitored in the far-UV, at 218 nm, with a Jasco J-810 spectropolarimeter equipped with a programmable Peltier device for the

temperature control. The signal was recorded every 0.5 °C, with a bandwidth of 2 nm. The T_m of each monomer was hence derived from the 50% far-UV CD signal.

3.2.10 NMR experiments

NMR spectra were recorded in collaboration with prof. D. V. Laurents (CSIC, Madrid) at 25 °C in buffer containing 10% D_2O, 10 mM NaPi (pH 6.65) and 0.5 mM 4,4-dimethyl-4-silapentane-1-sulfonic acid (DSS) as the internal chemical shift reference. NMR spectra were acquired on a Bruker Advance Spectrometer, operating at 800 MHz (1H) and equipped with a triple resonance cryoprobe and z-gradients. The mixing time of the ^{1}H NOESY was 150 ms, 2024 × 320 pt. matrix (132 scans per increment) and a 12.0 × 12.0 ppm sweep width. Spectra were processed and analyzed with the TOPSPIN 2.1 program and peaks were assigned with the aid of the Sparky program. In order to identify which Asn and Gln residues actually suffer deamidation in ^{1}H homonuclear NMR spectra, 3 mg of ^{13}C, ^{15}N-labeled RNase A were dissolved in 20 mM NaH_2PO_4 buffer (pH 4.6) with 15% D_2O and a series of 1D ^{1}H, 2D ^{1}H-^{15}N HSQC and 3D HN(CO)CA and HNCACB NMR spectra were recorded at 35 °C. On the basis of the correlations observed in the 2D and 3D spectra, and of the comparison with previous assignments under similar conditions[48,189] the chemical shifts of the ^{1}HN, ^{15}N, ^{13}Cα and ^{13}Cβ of the Asn and Gln residues and their sequential neighbors were corroborated. Next, to afford deamidation, 1% NH_4HCO_3 was added, the sample's pH was increased to 8.2 and the sample incubated for seven days at 37 °C. Afterwards, the sample was transferred by a short gel filtration step back into 20 mM NaH_2PO_4 buffer (pH 4.6) with 15% D_2O, concentrated by ultrafiltration and a second series of 1D ^{1}H, 2D ^{1}H-^{15}N HSQC and 3D HN(CO)CA and HNCACB NMR spectra were recorded. The identification of deamidated peaks was performed by the quantitative integration of their signals in 2D HSQC spectra or by visual inspection for weak or missing peaks in 3D spectra, or both. Whereas side chain Asn/Gln H_2N-resonances will be sensitive probes of deamidation, we used backbone HN-signals to identify residues undergoing deamidation, since they are more disperse, have been previously

assigned and give rise to peaks with superior signal/noise ratios in standard ^{13}C, ^{15}N 3D NMR spectra.

3.2.11 Molecular Modeling

The coordinate files of the RNase A N-dimer (PDB ID: 1A2W[81]) and C-dimer (PDB ID: 1F0V[80]) were used as templates for *in silico* mutational analysis, performed in collaboration with doctor R. Montioli. Mutations Asn→Asp and Glu→Gln were constructed via *in silico* amino acid substitution using the Molecular Operating Environment (MOE) software provided by Chemical Computing Group Inc. (Montreal, Quebec, Canada) mutagenesis tool. The Asn→isoAsp substitution was carried out by the modeling tool of MOE software using the available structure of N67*D* mutant (PDB ID: 1DY5[190]) as the source for the isoAsp residue structure. The protonation state was calculated by setting the parameters that reflect physiological conditions (37°C, ionic strength given by NaCl 0.15 M, pH 7.4), using the Protonate 3D application of MOE. All mutated structures were refined by potential energy minimization applying the CHARM27 force field in implicit solvent. The structure alignment and non-covalent interactions prediction were carried out using the MOE software. Local changes of the secondary structure, and/or side chains orientation, and contact(s) detection were analyzed by visual inspection.

3.3 Results

3.3.1 The yield of oligomerization of less pure RNase A is lower than that of the purer one

RNase type IA and XIIA powders were separately lyophilized from 40% acetic acid solution and then redissolved in 50 mM NaPi buffer, pH 6.7. RNase A oligomers were purified through cation exchange chromatography, by increasing the concentration of NaPi buffer, pH 6.7. The result is that the lower the purity of RNase A, the lower the oligomerization yield, as it is visible in figure 3.1, where the pattern of oligomerization of RNase A type IA (black dashed curve) is compared with the one of the purest type XIIA (continuous curve).

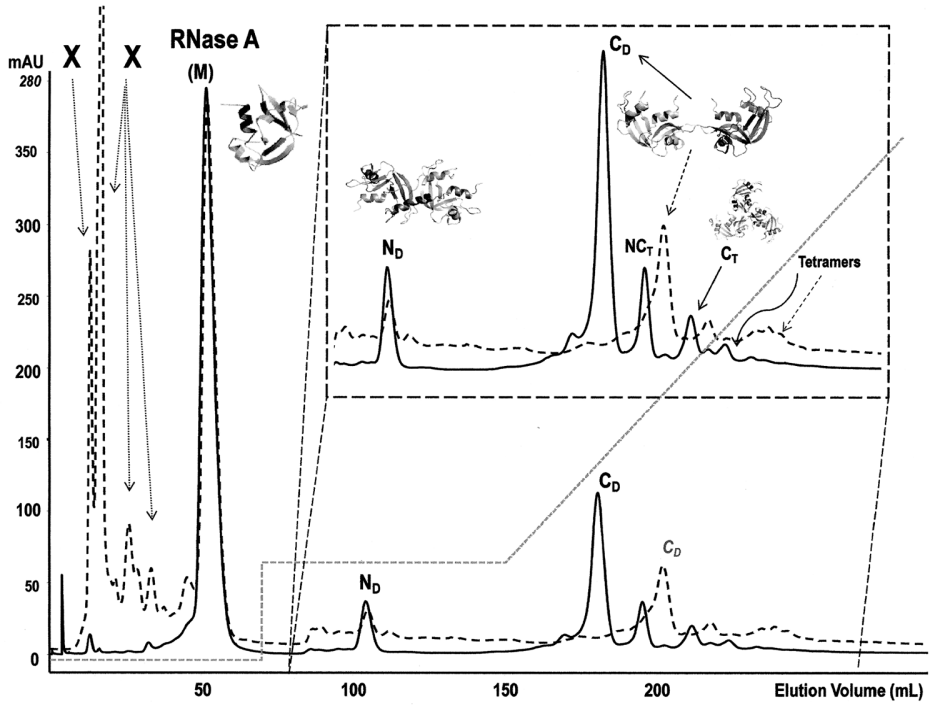

Figure 3.1 – Cation exchange of RNase type IA (dashed curve) and type XII A (continuous curve) performed with a Source 15S HR 10/10 after lyophilization from 40% acetic acid solution and resuspension in 50 mM NaPi buffer. X = unknown, probably polydeamidated species, M = monomer, N_D = N-terminal domain swapped dimer, C_D = C-terminal domain swapped dimer, NC_T = N- and C-terminal domain swapped trimer, C_T = C-terminal domain swapped trimer. The structures of each known species are reported next to their corresponding elution peak. Patterns were normalized on the monomer area with the Unicorn 5.01 Software (GE Healthcare).

Both the reduced oligomerization yield and the position of the impurities (identified with "X" in figure 3.1) recall previous results displayed by RNase A when oligomerization was affected by impurities attributed to deamidated variants of the protein[107].

3.3.2 Induction of deamidation of RNase A and purification and preliminar characterization of the obtained species

To assess if the X species were deamidated RNase A products, deamidation was induced on the purer RNase A XIIA, by incubating the monomer at a concentration of 2 mg/ml in a 1% ammonium bicarbonate buffer, following the procedure described by Di Donato & coll.[157]. 1 mg aliquots of the protein were withdrawn at 0, 48, 134 and 256 h and analyzed through cation exchange chromatography, using a constant NaPi buffer concentration of 60 mM, pH 6.7.

The described reaction promotes the formation of new peaks whose area increases with time, until 256 h, in line with the decreasing quantity of native RNase A monomer. The two main peaks, called *dd* and N67D, elute at about 10 and 17 ml, respectively (Fig. 3.2). The position of the former is the same of the peaks corresponding to the unknown impurities found in RNase type IA (dotted black line), while the latter resembles the characteristics of RNase A deamidated at position 67 (N67D), previously studied by Di Donato & coll.[157].

A nondenaturing cathodic PAGE[188] (Fig. 3.2, upper inset) displays that X and *dd* are a qualitatively similar mix of more species, less basic than native RNase A and N67D. For this reason, they are probably deamidated at different and/or various residues[157]. N67D shows a lower mobility than monomeric RNase A, according to the presence of Asp67 carboxyl group in spite of the Asn67 amide.

To confirm that all RNase type IA impurities and all the species formed by the deamidation reaction of RNase type XIIA were RNase A derivatives, a Western blot analysis was performed on X, *dd* (1 and 2), N67D and monomeric RNase A. Each species can be recognized by the IgG anti-HP-RNase, definitely confirming that the species analyzed are RNase A derivatives (Fig 3.2, lower inset).

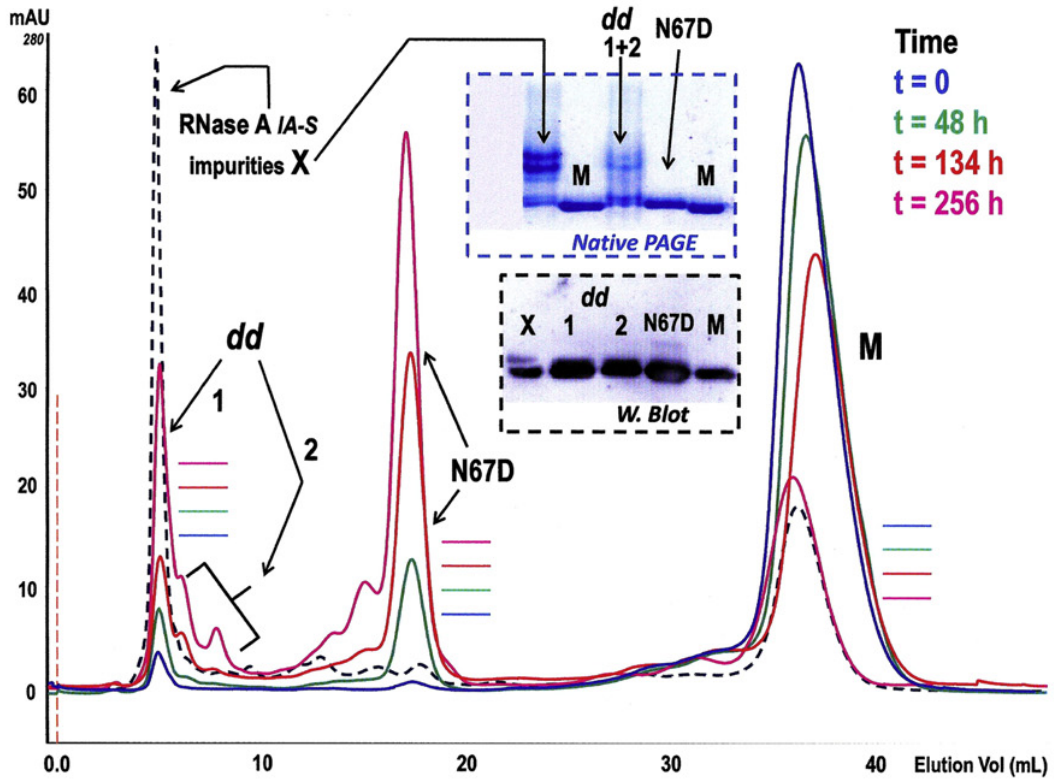

Figure 3.2 – Pattern of RNase XIIA deamidated species purified through cation exchange chromatography performed on a Source 15S HR 10/10 equilibrated with 60 mM NaPi buffer, pH 6.7. Four aliquots of 1 mg each have been withdrawn at different times from the deamidation reaction and chromatographed (blue curve-0h, green curve-48h, red curve-134h, violet curve-256h). *dd* = polydeamidated RNase A species, N67D = deamidated RNase A at residue 67. The pattern of RNase A-IA is superimposed as a black dashed curve. The results of RNase A derivatives submitted to a 15% native cathodic PAGE and to Western blot analysis performed on a 12.5% SDS-PAGE are shown in the central insets.

Moreover, each peak eluting from the cation exchange chromatography was separately collected and analyzed through SEC, onto a Superdex 75 HR 10/300 column and in a 12.5% SDS-PAGE (Fig. 3.3). Figure 3.3 shows that samples elute at the same volume (about 14 ml) and migrate with the same mobility of native RNase A.

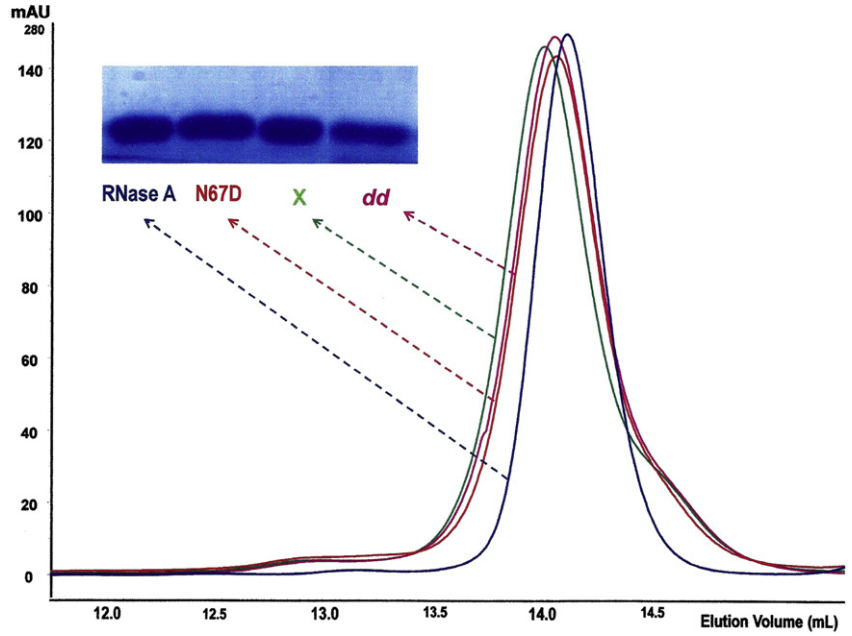

Figure 3.3 – SEC separation in a Superdex 75 HR 10/300 column of native, monomeric RNase A (blue curve), N67D (red curve), impurities of RNase type IA (X, green curve) and polydeamidated species obtained from the deamidation reaction of RNase type XIIA (*dd*, violet curve), performed with 0.4 M NaPi buffer, pH 6.7. A 12.5% SDS-PAGE of each species is reported as an inset.

3.3.3 Comparison of the enzymatic activities of the obtained species against yeast ss-RNA

The enzymatic activity against yeast ss-RNA of each RNase A purified species was measured by Kunitz assays[187]. Activities were calculated as the decrease of absorbance with respect to time, per mg of protein. The obtained data demonstrate that N67D retains about 74% of RNase A activity, while X and *dd* species maintain about 4 and 6% of it, respectively (Tab. 3.1). The values, despite the very low X and *dd* activities, further confirm that they all are RNase A derivatives. The decreased activity could be due to Asn71 and Gln11 deamidation, which affect RNase A B2 and P1 binding subsites, respectively[70,191]. Moreover, the deamidation of other Asn/Gln residues could increase the net negative charge, that would interfere with the binding of the substrate.

RNase A species	% residual Kunitz activity	% residual monomer
RNase A	100.0	62.4 ± 0.6
N67D	73.9	71.8 ± 1.7
X	4.0	97.0 ± 1.1
dd	5.7	98.1 ± 0.6
1:1 *dd*:native RNase A mix	-	89.6 ± 1.0

Table 3.1 – Kunitz activity and mean percentages of the residual monomer after lyophilization from 40% acetic acid of RNase A monomer, N67D, X, *dd* species and 1:1 RNase A:*dd* mix. The activities of all the species are reported as percentages of the RNase A monomer activity (100%). All percentages were calculated from three or more different experiments.

3.3.4 Oligomerization of the variously deamidated RNase A derivatives

Each peak eluted from the cation exchange was desalted, lyophilized, and submitted to another lyophilization step from 40% acetic acid (40 mg/ml), in order to obtain RNase A oligomers. Each lyophilized sample was then resuspended in 0.4 M NaPi buffer, pH 6.7, at a concentration of 10 mg/ml, and immediately injected onto a SEC Superdex 75 HR 10/300 column. The obtained patterns are superimposed in figure 3.4.

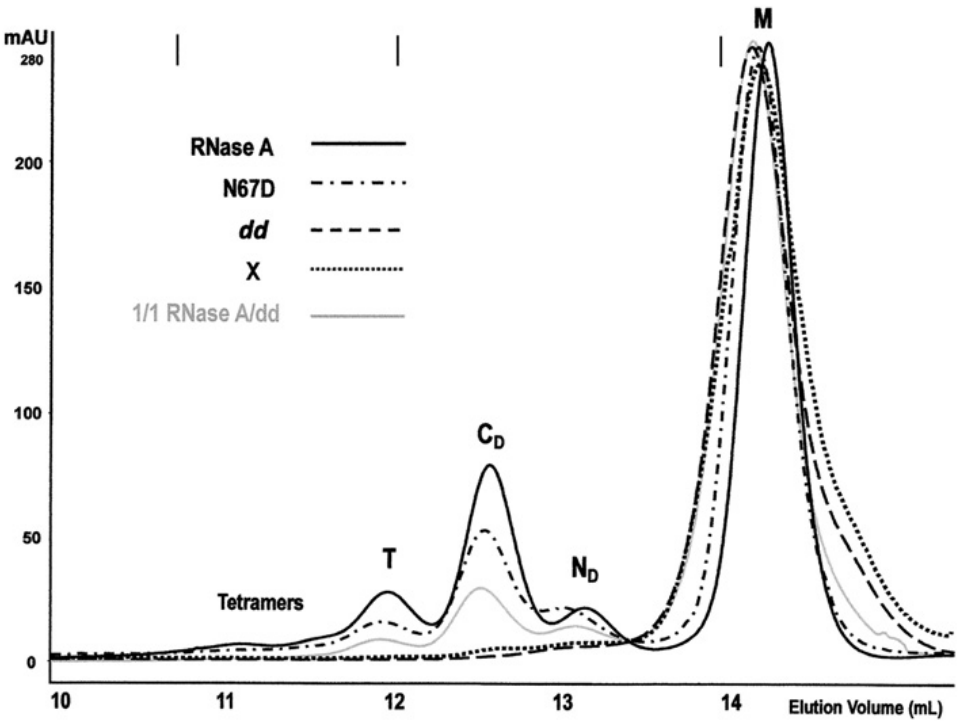

Figure 3.4 – SEC chromatography of the obtained oligomers of RNase A (continuous line), N67D (dashed-dotted line), *dd* (dashed line), X (dotted line) and 1:1 RNase A:*dd* mix (grey line). The chromatographic purification was performed with a Superdex 75 HR 10/300 equilibrated with 0.4 M NaPi buffer, pH 6.7. M = monomer, N_D = N-terminal domain swapped dimer, C_D = C-terminal domain swapped dimer, T = trimer. Vertical bars represent the elution positions of M.W. standards: Ovalbumin (44 kDa), Carbonic Anhydrase (29 kDa) Cytochrome C (12.3 kDa). Patterns were normalized on the monomer area with the Unicorn 5.01 Software (GE Healthcare).

Contrarily to RNase A, that forms about 38% oligomers (residual monomer 62.4%, Table 3.1), *dd* and X do not oligomerize at all. In fact, since the percentage of oligomers obtained from *dd* and X is about 2% and 3%, respectively, and considering that RNase A constitutively forms 1-2% of N_D, the aggregation propensity of *dd* and X derivatives is actually reduced to zero by extensive protein deamidation. The aggregation is instead only partially compromised by deamidation of Asn67, since only 28% oligomers are obtained from N67D (Table 3.1). Moreover, the aggregation propensity of native RNase A is lowered by the presence of equal amounts of impurities (1:1 mix of RNase type XIIA:X, 10% obtained oligomers), in line with the lowered aggregation yield obtained with

RNase A type IA (Fig. 3.1). It is interesting to note that the yield of oligomers (especially C_D and trimers) obtained from this mix is lower with respect to the expected average calculated as the average of the oligomers obtained from the pure native RNase A monomer and X or *dd*.

3.3.5 Purification and induced oligomerization of N67D and N67*D* RNase A derivatives

When an asparagine residue undergoes deamidation, it passes through a cyclic succinimidyl intermediate that can successively generate either an aspartic or a β-aspartic residue, depending on the position (α or β) in which hydrolysis takes place (Introduction, Fig. 1.9). Also glutamine residues are susceptible to deamidation reaction, that leads to the formation of either glutammic or γ-glutammic acid. Also racemization, producing D-Asp and D-isoAsp or D-Glu and D-γ-Glu, may occur, but it has never been so far detected in RNase A.

It had been demonstrated that N67D is a mix of two isoforms; one characterized by the presence of an aspartic acid in position 67 (N67D), and another with an isoaspartic acid occupying the same position (N67*D*)[157]. In order to study the differences in the oligomerization propensity among these two species, we separated the two isoforms through HIC. Fig. 3.5 shows the result of the purification of N67D from N67*D*. The former elutes at about 48 ml, while the latter elutes 4 ml before, at a volume of about 44 ml. The ratio N67*D*:N67D, calculated as the area of the eluting peaks, was about 55:45, confirming previous results and indicating that the slightly predominant isoform is the isoAsp derivative[157]. To avoid the reciprocal contamination of the two species, only the ascending fraction of N67*D* peak and the descending fraction of N67D were collected.

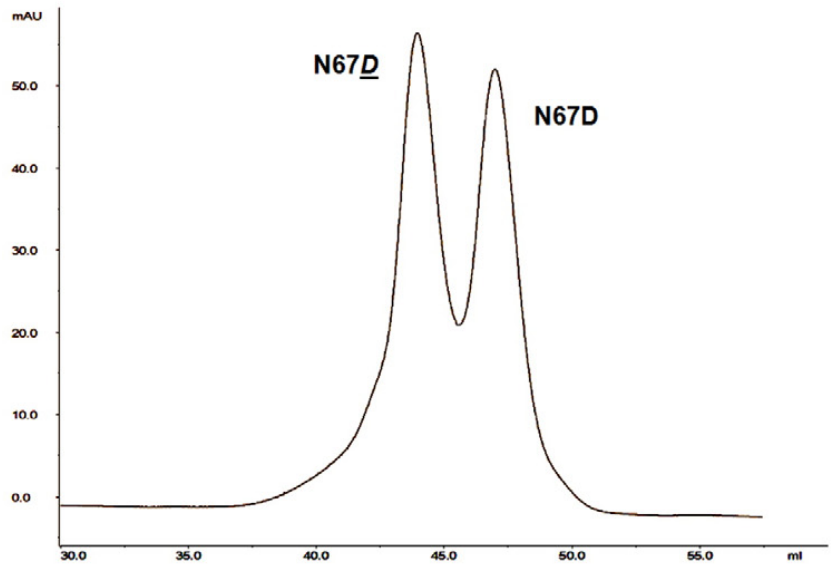

Figure 3.5 – HIC purification of N67D from N67*D*. The purification was performed using a Phenyl Sepharose column, starting from 100% 2 M $(NH_4)_2SO_4$, 0.1 M NaPi, pH 6.0, and applying a linear gradient in 90 min, until reaching 100% 0.5 M $(NH_4)_2SO_4$, 0.1 M NaPi, pH 6.0.

After their purification, N67D and N67*D* were separately lyophilized from ddH_2O, redissolved in 40% acetic acid, resubmittet to lyophilization and finally resuspended in 0.4 M NaPi buffer, pH 6.7, at a concentration of 10 mg/ml. The two samples obtained were then separately analyzed through size exclusion chromatography, in parallel with a 1:1 mix of them (Fig. 3.6). Both N67D and N67*D* are able to oligomerize, producing the same oligomers as native RNase A. However, the oligomeric yields obtained, about 31% for N67D and 21% for N67*D*, are lower than the 38% obtained from monomeric RNase A (Table 3.1). Moreover, the yield of the oligomers obtained from N67*D* are lower than N67D, and the mix of the two isoforms produces a quantity of oligomers (about 24%) that is similar to that of N67*D*, but lower than the expected yield calculated from the average quantity of the oligomers obtained by separate N67D and N67*D*. The difference in oligomers' yield is mainly due to the high difference in the amount of C_D produced.

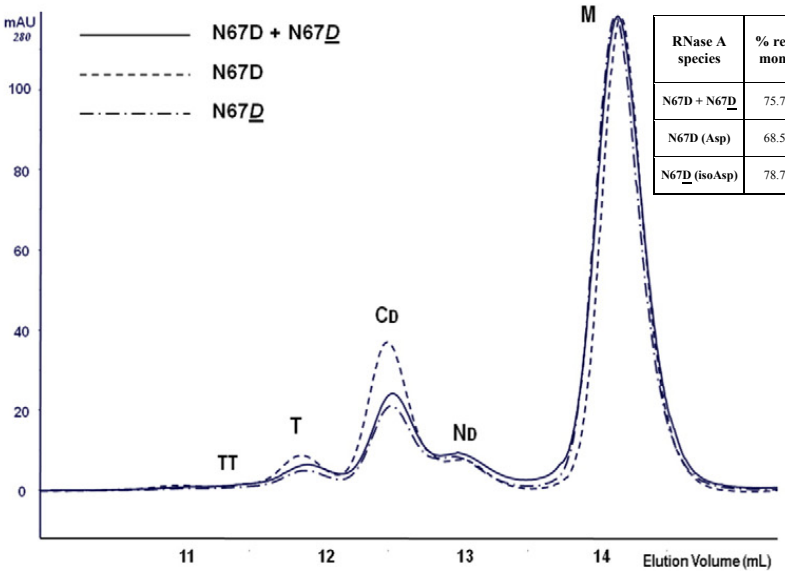

RNase A species	% residual monomer	% N_D	% C_D	% trimers	% large oligomers
N67D + N67D	75.7 ± 2.1	5.5 ± 0.7	14.2 ± 1.1	3.0 ± 0.3	1.6 ± 0.2
N67D (Asp)	68.5 ± 2.0	5.8 ± 0.8	19.2 ± 1.4	4.0 ± 0.4	2.5 ± 0.3
N67D (isoAsp)	78.7 ± 1.2	4.9 ± 0.4	13.1 ± 0.8	2.1 ± 0.2	1.3 ± 0.1

Figure 3.6 – SEC purification through a Superdex 75 HR 10/300 column equilibrated with 0.4 M NaPi buffer, pH 6.7, of the oligomers obtained from 40% acetic acid lyophilization of N67D (dashed line), N67D (dash-dot line) and a 1/1 mix of N67D/N67D (continuous line). M = monomer, N_D = N-terminal domain swapped dimer, C_D = C-terminal domain swapped dimer, T = trimer, TT = tetramers. The table reports the mean percentages of each species calculated from three or four different experiments. Patterns were normalized on the monomer area with the Unicorn 5.01 Software (GE Healthcare).

3.3.6 Extensively polydeamidated RNase A derivatives lose their propensity to oligomerize

A more in-depth analysis was performed also on the *dd* species. As being polydeamidated species, X and *dd* are indeed a mixture of differently charged isoforms. By changing the chromatography conditions equilibrating the cation exchange column with 0.1 M acetic acid/sodium acetate, pH 5.0, NaCl 0.05 M, then performing a linear gradient from 0.05 to 0.35 NaCl in 90 min, it was possible to split the *dd* and X corresponding peaks in further four peaks (Fig. 3.7A). Each peak was collected, lyophilized from ddH_2O, and then from 40% acetic acid. After resuspension in 0.4 M NaPi buffer pH 6.7, each sample was analyzed through SEC (Fig. 3.7B-E). In line with the results obtained from the whole mix of these species,

no oligomers are visible from any peak. This indicates again that polydeamidation of different and/or more sites inhibits the oligomerization propensity of RNase A at all. Traces of aggregates eluting at the void volume are detectable for peak 3 (Fig. 3.7D).

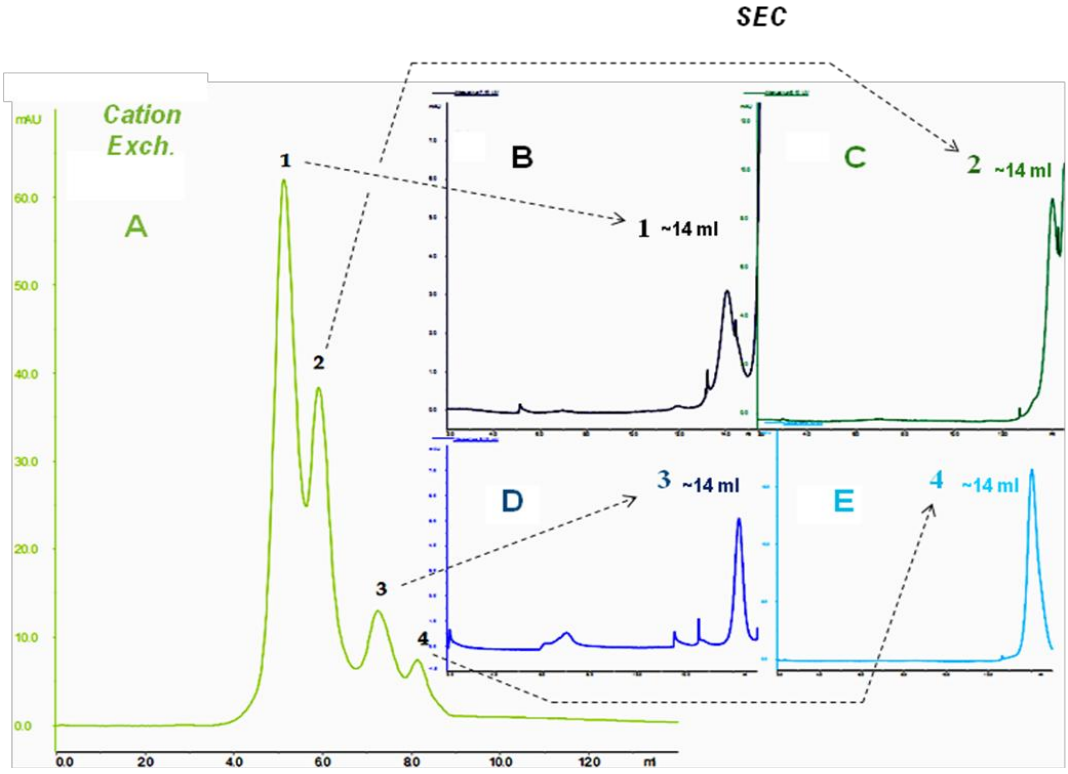

Figure 3.7 – A) *dd* analysis through cation exchange chromatography after the equilibration of a Source 15S 10/10 column with 0.1 M acetic acid/sodium acetate, pH 5.0, NaCl 0.05 M, with the application of a linear gradient from 0.05 to 0.35 NaCl in 90 min. B, C, D, E) SEC analysis of the four peaks eluted from cation exchange chromatography and lyophilized from 40% acetic acid.

3.3.7 Far-UV CD and melting temperatures analysis of the *dd* species

The characterization of peaks 1 (dd_1) and 2 (dd_2) of the *dd* species purified through cation exchange chromatography with the NaCl gradient (Fig. 3.7A) was deepened through far-UV CD analysis. The spectra of native and polydeamidated (*dd*)

monomeric RNase A (Fig. 3.8) are very similar to each other, suggesting that deamidation does not affect the protein's secondary fold.

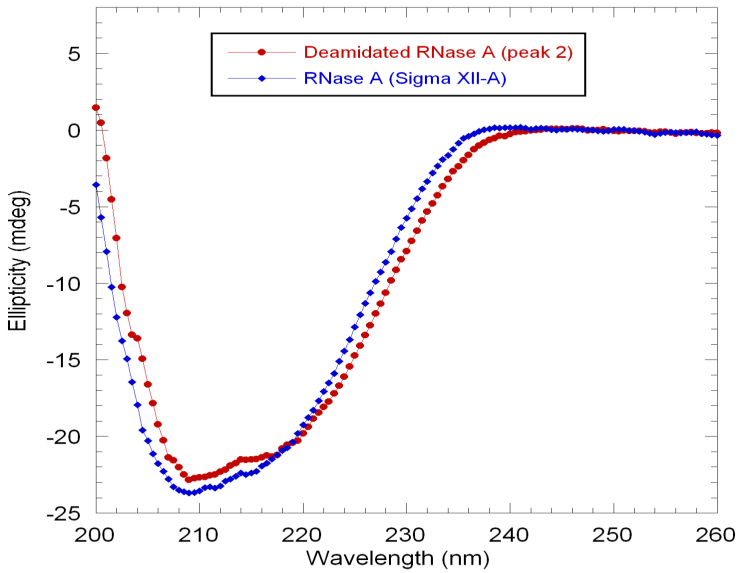

Figure 3.8 – Far-UV CD spectra of native monomeric RNase A (blue) and dd_2 (red) eluting from cation exchange chromatography (Figure 3.7). The concentration of each sample is reported in the Materials and Methods section.

Thermal denaturations were followed with CD at 218 nm, in 10 mM NaPi buffer, pH 6.7 (Fig. 3.9). The calculated T_m of N67D mix (N67D + N67*D*) is slightly lower that of the native RNase A monomer, while the T_m of X and *dd* species are about 5.6 and 4.9 °C lower. These results indicate that the stability of RNase A monomer is minimally affected in case of N67 deamidation, while when the deamidation affects more residues, its stability is more largely compromised, even if deamidation does not induce a dramatic unfolding on the protein.

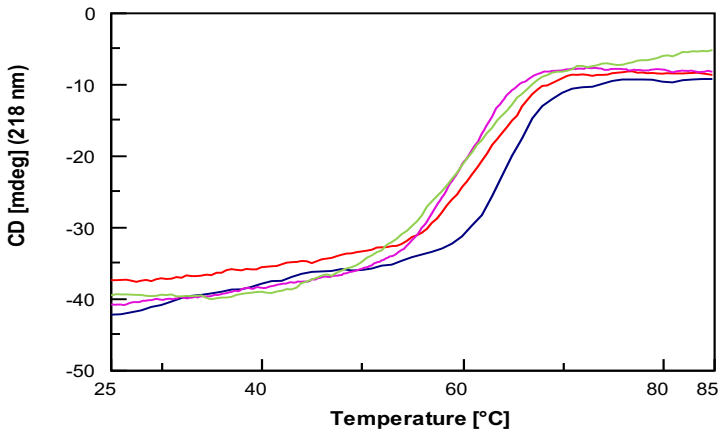

RNase A species	T_m °C
RNase A	64.6 ± 0.5
N67D	62.5 ± 0.7
X	59.0 ± 0.5
dd	59.7 ± 0.6

Figure 3.9 – Denaturation curves of native RNase A monomer (blue curve), N67D (N67D/N67D mix, red curve), X (green curve) and *dd* (violet curve). The thermal denaturation experiments were followed with CD at 218 nm, in 10 mM NaPi buffer, pH 6.7, from 25 to 90 °C. The calculated T_m are reported in the table. The concentration of the samples is reported in the Material and Methods section. The displayed values are the means of three experiments.

3.3.8 NMR analysis of the *dd* species

The 2D ^{1}H NOESY NMR spectra recorded show hundreds of cross-peaks, characteristic of native RNase A, suggesting once again that the folding is not lost upon polydeamidation (Fig. 3.10). Some cross-peaks previously assigned to the side chain amide —CO—NH_2 of some Gln and/or Asn residues in native RNase A, are not detectable, demonstrating that these residues undergo deamidation. One of the cross-peaks whose signal intensity decreases can be tentatively assigned to Asn67. Two additional cross-peaks also lose signal intensity and are very probably due to deamidation of two more Asn/ Gln side chains. Interestingly, the HN signal of Lys66 is split into at least two or, more probably, three parts. Based on similar findings previously reported by D'Ursi et al.[192] and on three distinct NOESY cross-peaks visible between Lys66 HN and HN signals of Asn67, at 10.28 × 7.51, 10.31 × 7.49 and 10.41 × 7.61 ppm, respectively, it could be that Asn67, Asp67, and isoAsp67 species are simultaneously present. However, due to the heterogeneity of the poly-deamidated sample, the overlapping of relevant cross-peaks, and the slight differences in the pH and buffer composition between these samples and those used

to assign RNase A, it was not possible to unambiguously identify which Asn or Gln residues suffer deamidation. Moreover, Asn and Gln peaks could be shifted by the deamidation of a nearby site, because it could alter their conformation. Hence, to further analyze the residues affected by deamidation, a 2D ^{1}H-^{15}N HSQC and a 3D ^{1}H-^{13}C-^{15}N HN(CO)CA and HNCACB NMR spectra were recorded on a ^{13}C,^{15}N-RNase A labeled sample before and after the incubation under deamidation conditions (Section 3.2.2). The comparison of the two sets of spectra shows that ^{13}C,^{15}N-RNase A maintains its folded structure after deamidation, since many signals readily assignable to the native state are observed (Fig. 3.10D)[48,189]. However, deamidation produces a part of unfolded conformers, as notable from the additional broad signals between 7.9 and 8.5 ppM in the ^{1}H dimension. Despite the peak overlap in the 2D ^{1}H-^{15}N HSQC spectra, it was possible to assign and verify the native backbone resonances of Asn and Gln residues, as well as adjacent residues in the 3D spectra in the sample prior to the reaction inducing deamidation. Many of these signals remain strong after deamidation, indicating that Gln11, Asn24, Asn27, Gln28, Gln55, Gln60, Asn103 and Asn113 were not significantly deamidated. On the contrary, signal displacement, broadening or loss of intensity were detected for Asn34, Asn44, Asn67, Gln69, Asn71, Gln74 and Gln101, indicating the reason of possible conformational diversity that would arise from partial or complete deamidation.

All Asn and Gln residues that did not suffer deamidation, except for Asn113 that is resistant because is followed by Pro114[145], are followed by residues whose NH partecipates to the secondary structure and/or is protected against H/D exchange[189]. In these situations, the rigidity afforded is expected to prevent this HN from attacking its neighbor's side chain amide. Conversely, Asn34, Asn67 and Gln69, that suffer deamidation, are not bordered by HN in secondary structure or protected against exchange. Nevertheless, Asn71 and, partly, Gln74 undergo deamidation, even if their neighbors are protected by secondary structure. This strongly suggests that the deamidation of Asn67 and possibly Gln69 may produce a local conformational change, facilitating Asn71 and Gln74 deamidation.

Besides Asn and Gln residues, the ^{1}H-^{15}N signals of Lys66 (adjacent to Asn67), Lys41, His119 (catalytic residue), Phe120, Asp121 and Ala122 were strongly

weakened by deamidation conditions (Fig. 3.10D). On the contrary His12, the other catalytic residue, retains its native-like signal. It has recently been shown that certain RNase A ^{1}H-^{15}N signals are weakened when the protein is not fully bound to phosphate[193]. Considering this, conformational changes in the P0 subsite (Lys66) may cause the spectral changes described. These, like the perturbations at the B2 (Gln69 and Asn71) and the B1 subsites (Phe120)[194], could be involved in the loss of enzymatic activity observed when RNase A undergoes deamidation (Table 3.1).

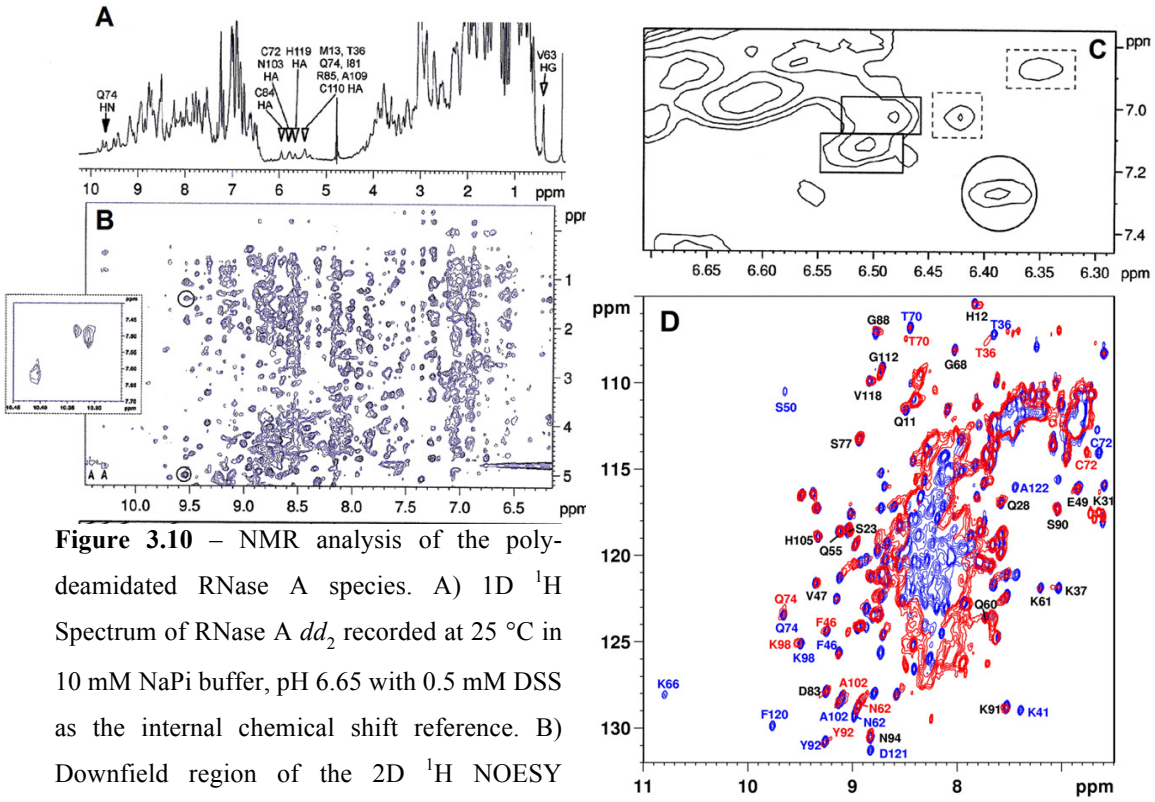

Figure 3.10 – NMR analysis of the poly-deamidated RNase A species. A) 1D ^{1}H Spectrum of RNase A dd_2 recorded at 25 °C in 10 mM NaPi buffer, pH 6.65 with 0.5 mM DSS as the internal chemical shift reference. B) Downfield region of the 2D ^{1}H NOESY spectrum of dd_2, showing hundreds of peaks typical of native RNase A. The crosspeaks circled in red can be putatively assigned to Gln74. The arrowheads in the left of the panel mark distinct HN-Lys66 resonances, which putatively arise from Asn67 deamidation. C) Zoom of the NOESY spectrum showing some Asn and Gln -NH_2 side-chain cross peaks. The signal putatively assigned to Asn67 (circle) appears weaker than two other probable Asn/Gln-NH_2 cross peaks (solid boxes). Additional peaks (dashed boxes) are putatively assigned to additional partially deamidated Asn/Gln -NH_2 groups. D) 2D ^{1}H, ^{15}N HSQC NMR spectra of ^{13}C, ^{15}N- labeled RNase A prior to (blue signals) and after (red peaks) incubation under deamidation conditions, recorded at pH 4.6, 35 °C in 20 mM NaH_2PO_4 buffer. Selected resonances are labeled. Signals that do not substantially change peak width or chemical shift are colored black, while the ones that change are blue or red depending on whether the signal corresponds to the spectrum acquired before or after incubation under deamidation conditions, respectively.

3.3.9 Analysis of RNase A dimers' interface sites containing Asn and/or Gln residues

An *in silico* analysis of both N-dimer (PDB ID:1A2W[81]) and C-dimer (PDB ID: 1F0V[80]) structures was performed in order to obtain more information on the way in which deamidated residues affect RNase A stability and oligomerization tendency. In N_D, three hot-spot regions can be found: 1) Gln11* (*refers to the second subunit in the dimer) and Asn44, 2) Asn24, Asn27 and Asn103*, and 3) Gln101 and Gln101* (Fig. 3.11). In C_D, two hot-spot regions involving 1) Asn67, Gln69, Asn71 belonging to the 65–72 loop, and 2) Asn113 and 113* are visible (Fig 3.11). NMR results demonstrated that only Asn44, Asn67, Gln69, Asn71 and Gln101 underwent extensive deamidation. In N-dimer, the *in silico* analysis shows that Gln11* and Asn44 are involved in two interchain contacts, where also Lys41 side chain takes part (Fig. 3.11B). These contacts are symmetrically present in both N_D subunits, and tether the N-swapping termini. Moreover, Gln101 and Gln101* are asymmetrically positioned[81,105], and form inter-chain H-bonds with Ser21* and Ser22, respectively (Fig. 3.11C). The *in silico* substitution Asn44* $\rightarrow$ Asp/isoAsp, followed by local energy minimization, does not allow the formation of the H-bond connecting Asn44 δ-amide group to the peptide oxygen of Gln11* (Fig. 3.11D,E), while Gln101/Gln101* $\rightarrow$ Glu substitution affects the H-bond with Ser21* and Ser22[105] (Fig. 3.11F).

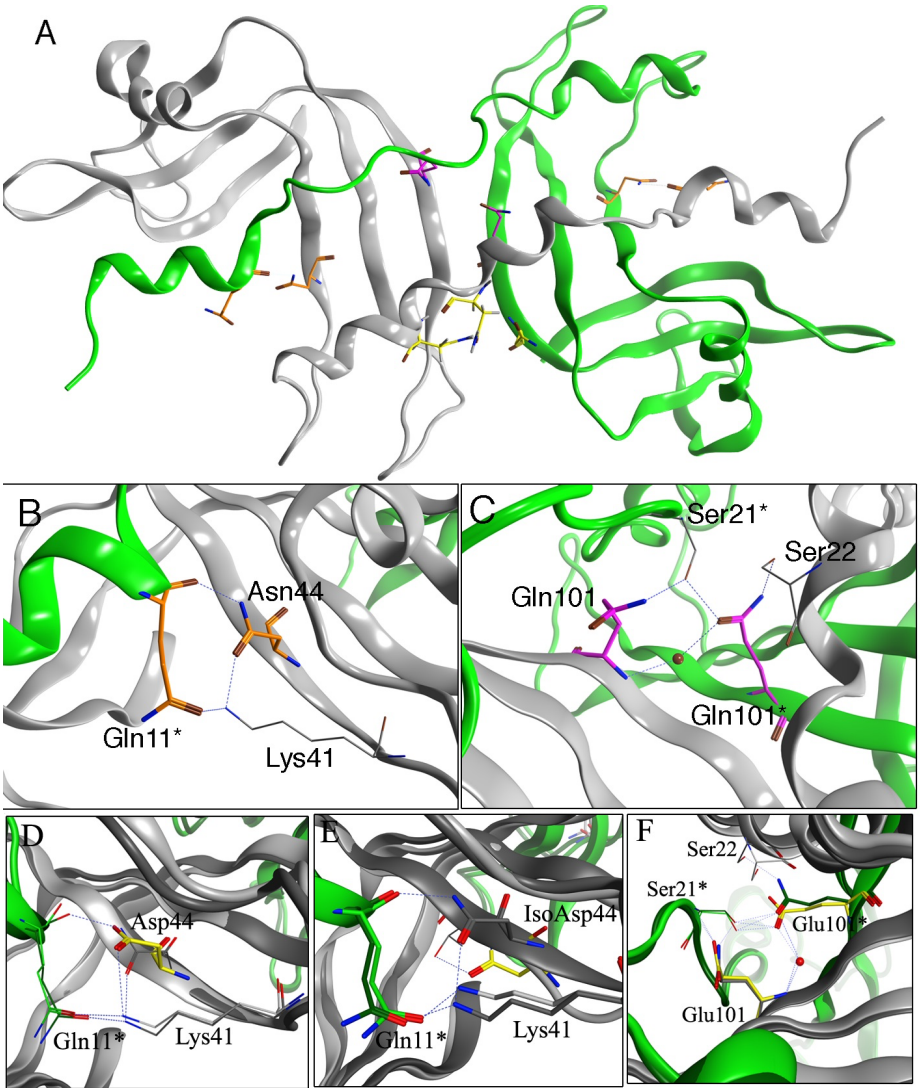

Figure 3.11 – RNase A deamidation sites possibly affecting N-dimer stability. A) Ribbon representation of RNase A whole N_D structure (PDB ID: 1A2W), with the two protomers in green and grey and the relative position of the three deamidation hot-spot residues clusters shown as yellow, orange and magenta sticks, respectively. B, C) Detailed representation of the interaction network of N44 and Q101. D, E and F) Superimposition of the wild-type (dark colors) and the structures of N44D, N44*D* and E101Q mutants (light colors) respectively. Images built using the MOE software (CCG Group).

The loop formed by Cys65 and Cys72 is a crucial nucleation and folding site of RNase A[195]. It generates a symmetrical interaction network present in both C_D subunits, involving Asn67, Gln69, Asn71 and Lys66, which contacts the neighbor Asp121* (Fig. 3.12B). The composition and/or conformation of the 65-72 loop,

tethered to the antiparallel β-strand that connects the two protomers through an H-bond between Asn71 side chain and Cys110, can alter two strong contacts between Lys66 and Asp121*. Moreover, Gln69 side chain interacts with both Asn67 and, through a water molecule, Asn71 (Fig. 3.12B). The Asn71 → Asp deamidation could abolish the contact with Cys110, while the Gln69 → Glu conversion is expected to break the interactions with Asn67 and Asn71. In any case, it is difficult to predict how the conversion Asp → isoAsp could alter the structure of the 65-72 loop, but previous studies showed how this loop affects the stability of RNase A dimers[105,106], and a concomitant deamidation of Asn67, Gln69 and Asn71 could be a deleterious event for the formation of such oligomers.

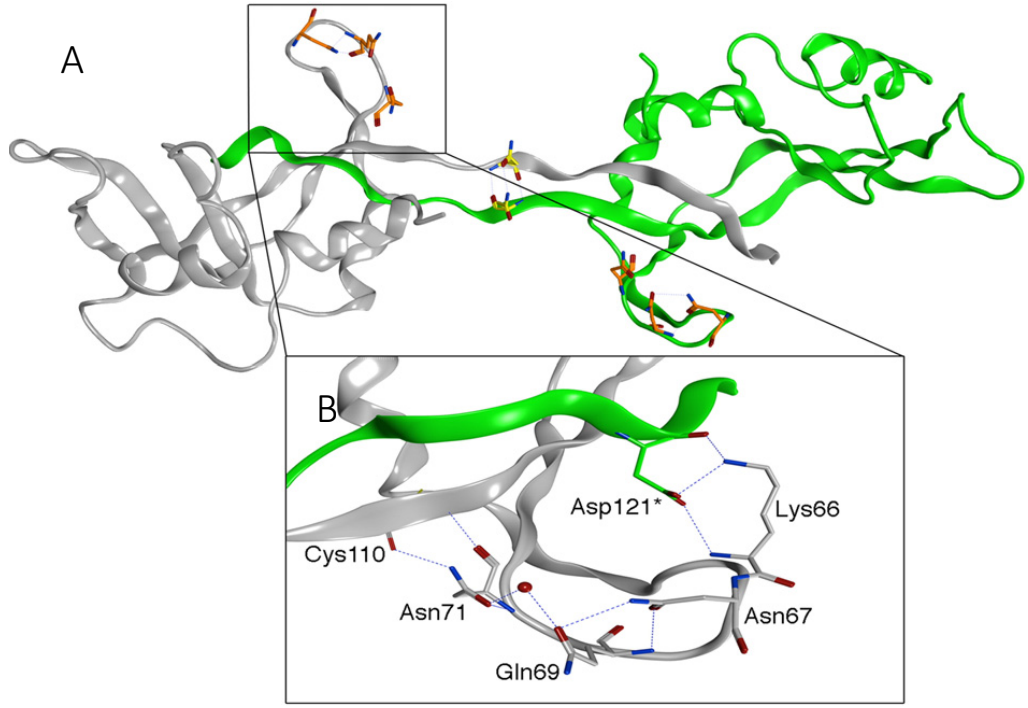

Figure 3.12 – RNase A deamidation sites predicted to affect C-dimer stability. A) RNase A C-dimer structure with the two protomers represented in grey and green (residues marked with *). The two hot-spot clusters are shown as orange and yellow sticks. B) Zoom on the interaction network between N67, Q69, K66 and D121*. The images were produced with MOE software (CCG Group).

3.4 Discussion

In this work we report that extensive deamidation of Asn/Gln residues almost nullifies RNase A oligomerization through 3D-DS. Recent papers indicate that non-natural aminoacids, as well as small interference molecules, can inhibit amyloid fibril formation, thus blocking or slowing the onset of neurodegenerative pathologies[196–198]. Certain point mutation(s) can protect proteins against undesired and pathological aggregation[199], whereas others enhance oligomerization and disease[200]. Since deamidation exerts an effect comparable to that induced by a point mutation, it is not surprising that it can affect protein oligomerization.

RNase A deamidation starts with N67, the residue most prone to undergo deamidation, since it is followed by G68, which does not hinder the formation of the cyclic intermediate imide[145,201]. Our studies demonstrated how RNase A N67D, the mixture of N67D and N67*D*[157], deamidation slightly limits the yield of oligomers obtained through its lyophilization from 40% acetic acid (Fig. 3.4 and 3.6), similarly to the effect of deamidation in RNase B[140]. In particular, while the oligomers' yield produced by N67D is similar to that of the native enzyme, N67*D* derivative hinders the oligomerization propensity to a higher extent. This could be due to the extension of the 65-72 loop in the isoAsp derivative, because of the additional $–CH_2–$ in the backbone, or/and by the increased proximity of the carboxylate group to the backbone. This insertion causes the loss of two H-bonds (N67-O^{δ}–N-Q69 and C65-O–N-G68), with the consequent shift of the 65-72 loop toward the main protein body[190]. In presence of N67*D*, C_D production is more affected than that of N_D, likely because of the altered interactions between 65-72 loop and Asp121*, which favor the C-terminal swapping.

When deamidation is extended to other Asn or Gln residues besides N67, RNase A does not oligomerize at all (Fig. 3.4 and 3.7). In the 2D and 3D heteronuclear NMR spectra (Fig. 3.10) Asn34, Asn44, Gln69, Asn71, Gln74, and Gln101 resulted to be deamidated after a week incubation at pH 8.2, at 37 °C. This is in line with an earlier work in which is described how Q69, N71 and and Q74 are the best candidate to suffer this modification[202]. N67, Q69, N71 and Q74 are all residues located in the 65-72 loop, or in its proximity. This loop, delimited by 65-72 disulfide bond, is one

of the first folding nuclei of the protein, and is a dynamically "breathing" loop both in monomeric and oligomeric RNase A[105,106,203]. The influence of this loop on the stability of the C_D[106] was not contradicted by the *in silico* inspection (Fig. 3.12). Furthermore, N67 deamidation may increase the loop flexibility and facilitate the deamidation of other Asn/Gln residues of this short domain[202], in line with the results emerging from ^{13}C, ^{15}N spectra.

2D ^{1}H NOESY NMR (Fig. 3.10) and far-UV CD spectra (Fig. 3.8) indicate that the poly-deamidated derivatives are correctly folded. Hence, the reduced capacity of RNase A to oligomerize may be ascribed to three reasons: 1) the monomer and the oligomers could be destabilized by a remarkable structural modification of 65-72 loop. The oligomers stably form only if the native closed interface is reconstituded[88]; 2) poly-deamidation increases the negative charge density, especially in the 65-72 loop, with a consequent electrostatic repulsion between the subunits[84]; 3) the Asp (Glu) or isoAsp isomers of each deamidated residue may produce a mixture of differently deamidated protomers, that would eliminate the correct complementarity necessary for 3D-DS. This third point is supported by the fact that 1:1 N67D/N67*D* and especially 1:1 *dd*/native RNase mixtures produce a lower amount of oligomers with respect to the predicted yield calculated as the mean obtained from each separate species (Fig. 3.4). This behavior resembles that of other 3D-DS proteins, such as human prion protein, which struggles to form hetero-oligomers[199].

According to molecular modeling (Fig. 3.11), N44 and Q101 deamidation detected by NMR would reduce N_D stability. On the other hand, C_D stability could be theoretically destabilized by the deamidation of N113. However, this residue is resistant to deamidation, because it is followed by a Pro that prevents the formation of the cyclic imide[145], in line with our 2D and 3D heteronuclear NMR results, which demonstrate that N113 does not suffer deamidation. Consequently, the key residues that may hinder C_D formation upon deamidation should be N67, Q69 and N71 (Fig. 3.12).

Overall, deamidation of RNase A seems to inhibit its ability to oligomerize by: 1) modifications of the protein structure and of the approach dynamics of the subunits, in particular when isoAsp derivative is present, or also when racemization with the

consequent formation of D-derivatives may occur[204]; 2) variation of the charge density and/or exposure of the approaching protomers; 3) key H-bonds and contacts depletion affecting the dimers.

In conclusion, the deamidation event, which is naturally linked to protein aging, could be a protective mechanism against self-association of RNase A. In fact, since several neurodegenerative pathologies are related to protein aging that leads to protein self-association, with the consequent formation of toxic oligomers, we could propose, considering RNase A as a protein model, that deamidation may become an aging strategy of proteins to avoid or limit pathological aggregation. This would be in line with the fact that D76N β_2-microglobulin increases its propensity to aggregate, with respect to wt[150]. However, an opposite behavior was demonstrated for other proteins, such as γD-crystalline, amylin and SOD1[151–153], whose aggregation propensity is enhanced by deamidation. So, it is difficult to generally predict the effect of the deamidation on the aggregation propensity of a protein, and further investigations are needed to withdraw general conclusion.

Chapter 4

Different properties of RNase A dimers depend on the oligomerization process of the protein

4.1 Materials

RNase A type XII-A (highest purity available), polyadenylic acid-polyuridylic acid [poly(A):poly(U)] and Subtilisin "Carlsberg" were purchased from Sigma. Yeast RNA was purchased from Boheringer, and ANS from Molecular Probes. All other chemicals were of the highest purity available.

4.2 Methods

4.2.1 RNase A oligomerization

a) Lyophilization from acetic acid

Oligomerization of monomeric RNase A was induced by lyophilizing a solution of the protein dissolved in 40% acetic acid at a concentration of about 50 mg/ml[78]. The powder was then resuspended at a concentration of 10 mg/ml in 50 mM phosphate buffer (NaPi), pH 6.7.

b) Thermally-induced oligomerization

RNase A oligomers were obtained also by incubating the protein dissolved at about 200-250 mg/ml at 60 °C for 2 hours in 20% or 40% EtOH[79]. Thereafter, 1 ml of 0.2 M NaPi buffer, pH 6.7, (preheated at 60 °C) was added to the sample. Once the resulting mixture spontaneously cooled to 25 °C, it was put in an ice-bath till further analyses.

4.2.2 Monomers and dimers purification

Samples that underwent the treatments described were separately purified through cation exchange chromatography, using a Source 15S 10/10 column connected to an ÄKTA-FPLC system (GE Healthcare). The separation of the different species was carried out starting with NaPi, pH 6.7, at a concentration of 70 mM to elute RNase A monomer, then increasing it to 90 mM to elute the N-dimer, and subsequently performing a 1h linear gradient from 90 mM to 200 mM to elute the C-dimer and to purify it from higher order-oligomers[107]. Hence, RNase A monomer, N-dimer and C-dimer were separately collected and used for further analyses in parallel with the native, untreated, monomer.
The NaPi concentration was lowered to 50 mM in each sample, and then protein concentration was concentrated to 0.7/0.8 mg/ml, with Amicon plus or Amicon mini ultrafilters (3 kDa or 10 kDa c.o.), until use.

4.2.3 Enzymatic activity

a) Single strand (ss-)RNA activity

The activity of RNase A monomers was tested using yeast ss-RNA as substrate, following the protocol of Kunitz[187]. Assays were performed with a substrate concentration of 0.6 mg/ml ($A_{300} \approx 0.6$), in 0.10 M sodium acetate/acetic acid buffer, pH 5.0. Enzyme concentration was 0.75 ng/µl, in each reaction. The catalytic activity was determined at 300 nm in the linearity range, measuring the absorbance decrease over time per µg of enzyme. The blank measure was performed measuring the absorbance of 0.1 M sodium acetate buffer pH 5.0. Negative controls were performed by measuring the absorbance of the yeast-RNA solution without the addition of the enzyme, in order to exclude the presence of contaminant RNases.

b) Double stranded (ds-)RNA activity

Activity was tested on synthetic poly(A):poly(U) diluted to 0.045 mg/ml in 400 µl of 0.150 M NaCl/ 0.015 M sodium citrate, pH 7.0[116]. In each assay, 12 µg of RNase A monomer(s) or 5 µg of dimer(s) were added. The reaction was followed at 260 nm, for 300s, in the linearity range. Blank was determined measuring the absorbance of 0.150 M NaCl/ 0.015 M sodium citrate solution, pH 7.0. To confirm the absence of contaminant RNases, negative controls were performed measuring the absorbance of poly(A):poly(U) solution, without the addition of the enzyme. The catalytic activity was calculated as the absorbance increase per min and per µg of enzyme.

4.2.4 Nondenaturing cathodic PAGE

Nondenaturing cathodic PAGE[188] was performed with 15%-18% acrylamide gel. Protein migration was carried out in cathodic electrode buffer (0.35% β-alanine/acetic acid buffer, pH 4.0) at a constant voltage of 200 V, for 90 min, in ice bath. The gel was subsequently transferred in 12% trichloroacetic acid (TCA) for 90 min, stained with 0.1% Coomassie Brilliant Blue and destained in 10% CH_3COOH, 20% EtOH solution.

4.2.5 Circular dichroism spectroscopy and thermal denaturation analyses

Far- and near-UV CD spectra of RNase A monomers were recorded at 25 °C from 190 to 240 nm and from 240 to 340 nm, respectively, in 10 mM NaPi buffer, pH 6.7, using a Jasco-J-810 spectropolarimeter. Near-UV data were recorded with a protein concentration ranging from 0.28 to 0.60 mg/ml, while far-UV data with a protein concentration comprised between 0.27 and 0.34 mg/ml. All spectra were normalized against concentration. The far-UV CD spectra deconvolution was

performed by means of DichroWeb Server (http://dichroweb.cryst.bbk.ac.uk/html/home.shtml), considering the range 190-240 nm and using the CONTIN algorithm.

The thermal denaturation of the monomers was followed by far-UV CD, at 218 nm, with a Jasco J-810 spectropolarimeter. Each sample, dissolved in 10 mM NaPi buffer, was subjected to a temperature increase of 1.5 °C/min, from 25 °C to 90 °C. The T_m of each monomer was hence derived from the 50% far-UV CD signal.

4.2.6 1-Anilinonaphthalene-8-Sulfonic acid (1,8-ANS) fluorescence

In order to measure the fluorescence of 1-Anilinonaphthalene-8-Sulfonic acid (1,8-ANS)-protein complex, each differently treated monomer was incubated with 90 μM ANS for 1 h, in 10 mM NaPi, at a protein concentration of 0.90 mg/ml, in parallel with the native monomer. The spectrum of each sample was then measured using a JASCO FP-750 spectrofluorimeter. Samples were excited at 365 nm, and emission was recorded from 380 to 550 nm. The bandwidth of both excitation and emission was 2 nm. Fluorescence data were obtained subtracting the ANS emission contribution from that of each ANS-monomer complex.

4.2.7 Limited proteolysis with subtilisin

RNase A monomers were proteolyzed with subtilisin in 0.2 M Tris-HCl pH 8.0, at a protein concentration of 0.8 mg/ml[205]. Subtilisin was added in a subtilisin:RNase A weight ratio of 1:1000. Eight μg of each sample were withdrawn at different times (0, 15, 30, 60, 120, 240, 480, 1500 min). In order to stop the reaction, PMSF (in ethanol solution) was added to each aliquot at a final concentration of 1.5 mM. Loading buffer was immediately added, and each sample analyzed with SDS-PAGE.

4.3 Results

4.3.1 RNase A oligomerization

RNase A N- and C-dimers, obtained through lyophilization from 40% acetic acid and thermal treatments from 20 or 40% EtOH highly concentrated solutions, were purified through cation exchange chromatography, as described in section 4.2.2. Figure 4.1 shows the corresponding chromatograms.

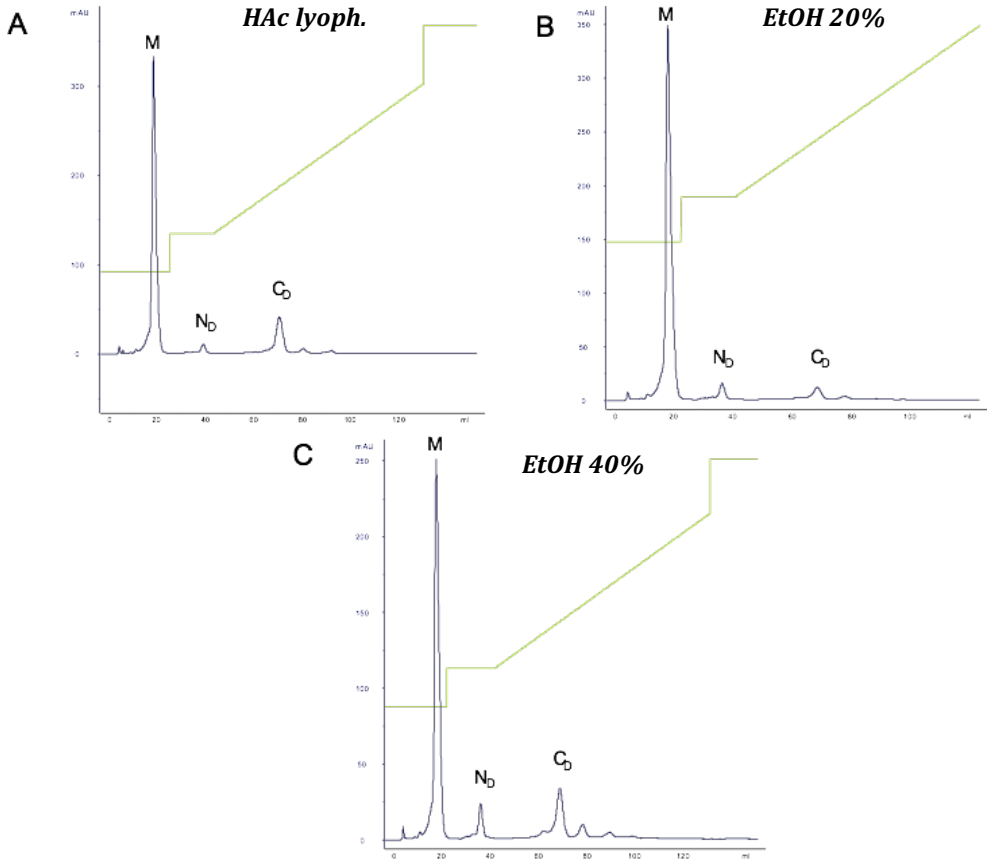

Figure 4.1 – Cation exchange chromatography of RNase A oligomers performed with a Source 15S HR 10/10 column. RNase A oligomers were obtained through A) lyophilization of 1.5 mg protein from acetic acid 40%, B) thermal treatment of 1.5 mg protein at 60 °C in EtOH 20% and C) thermal treatment of 1 mg protein at 60 °C in EtOH 40%. The separation of RNase A monomer, N-dimer and C-dimer was performed increasing NaPi buffer, pH 6.7, concentration from 70 to 90 mM, with a subsequent 1h linear gradient from 90 mM to 200 mM. M= RNase A monomer, N_D = N-dimer, C_D = C-dimer. The green line shows the NaPi buffer concentration.

RNase A monomer, N-dimer and C-dimer elute at 70, 90 and about 120 mM phosphate concentration, respectively[107]. It is evident that the yield of C-dimer is higher when obtained through lyophilization from acetic acid or thermal treatment from 40% EtOH, in line with previous investigations[79,107]. On the other hand, N-dimer is more abundant when obtained by thermal treatment from 40% EtOH solution.

4.3.2 Enzymatic activity

a) Kunitz assays

Kunitz assays performed against yeast ss-RNA using each species produced by the different treatments described show, as expected, that the activity of the monomers was higher than that of both dimers, with C-dimers showing in turn a lower activity than N-dimers (Fig. 4.2). Assays showed no significantly different activities among the same RNase A species (monomers, N-dimers, or C-dimers) obtained under different solvent and treatment conditions. It has to be noticed here that RNase A monomer degradates yeast-RNA more efficiently with respect to N- and C-dimers. These results indicate that the catalytic activity of monomer and N- and C- dimer against yeast ss-RNA is not significantly compromised by solvents and/or temperatures used to induce RNase A oligomerization.

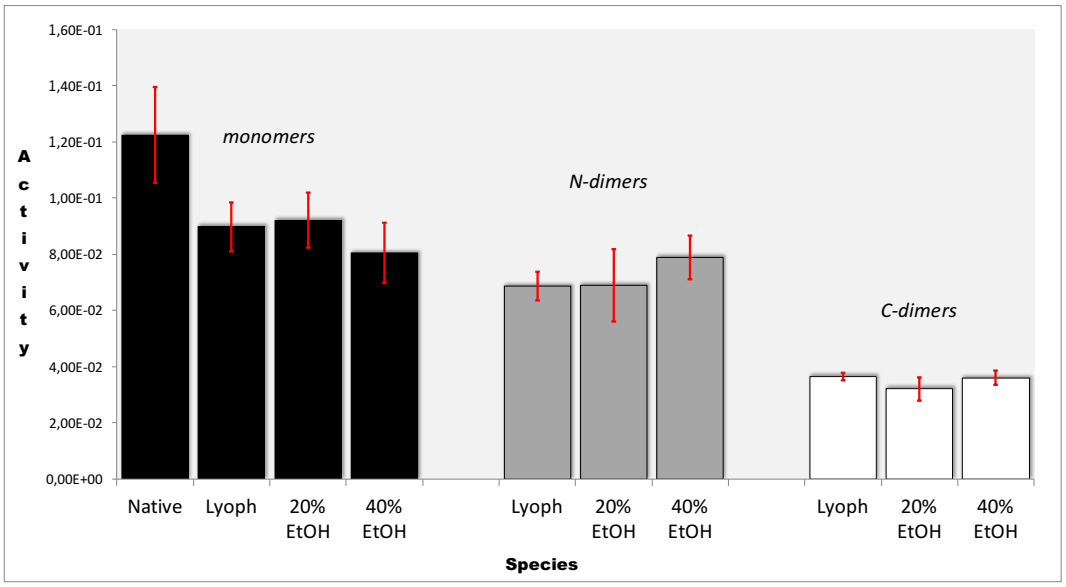

Figure 4.2 – Kunitz activities of monomers (black histograms), N-dimers (gray histograms) and C-dimers (white histograms) obtained with different treatments. Single stranded yeast RNA was used as substrate. The enzymatic activity (*Abs/µg*min*) is plotted against each protein species. Activities are reported as the mean of five independent experiments. Red indicators represent standard deviations. M = RNase A monomer, N_D = N-dimer, C_D = C-dimer.

b) RNase A - Poly(A):poly(U) enzymatic assays

The activity values (*Abs/µg*min*) of monomers and dimers against synthetic ds-RNA poly(A):poly(U) are reported in figure 4.3.

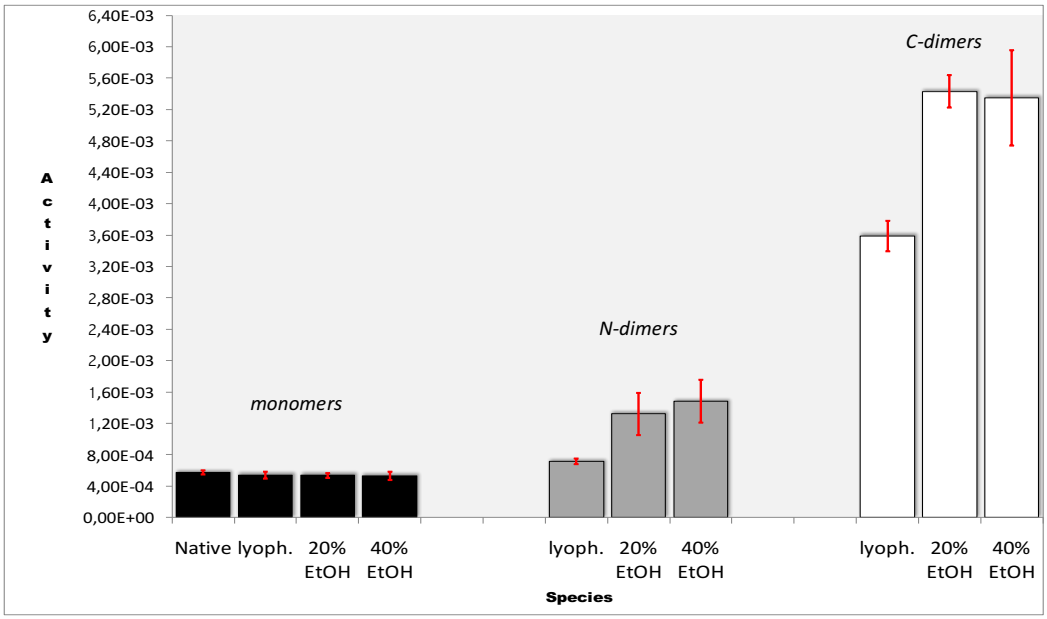

Figure 4.3 – Activities against synthetic Poly(A):poly(U) substrate of monomers (black histograms), N-dimers (gray histograms) and C-dimers (white histograms) obtained with different treatments. The enzymatic activity (*Abs/µg*min*) is plotted against each protein species. Activities are reported as the mean of five independent experiments. Red indicators represent standard deviations. M = RNase A monomer, N_D = N-dimer, C_D = C-dimer.

Monomers obtained with different solvent exposure do not display different activities within one another and with respect to native, untreated monomer. On the other hand, N-dimers and C-dimers obtained from thermal treatments in 20% or 40% ethanol are definitely more active against poly(A):poly(U) than the same species formed through lyophilization from 40% aqueous acetic acid.

4.3.3 Nondenaturing cathodic PAGE

In order to investigate if the different activities against poly(A):poly(U) of N- and C-dimers obtained with different treatments could be related to conformational changes induced by incubation in various solvents and/or temperatures, all the

species produced were analyzed through nondenaturing cathodic PAGE (Figure 4.4).

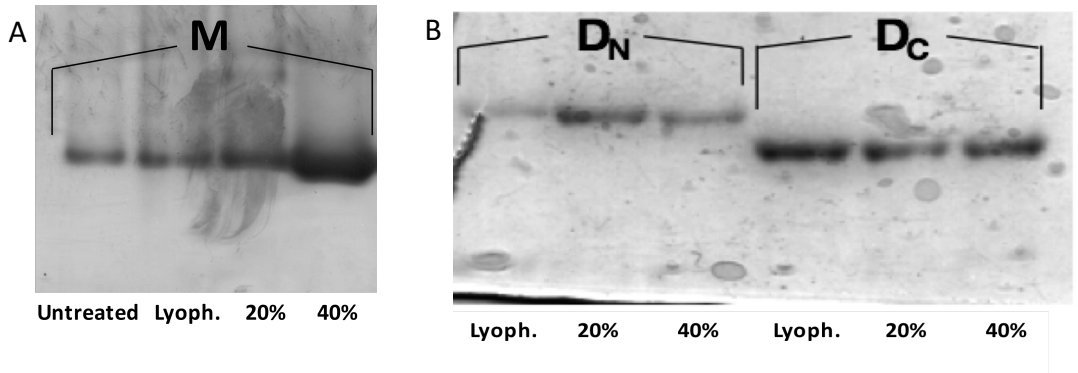

Figure 4.4 – Gel electrophoresis under nondenaturing conditions of A) RNase A monomers (M) and B) N- (N_D) and C–dimers (C_D) obtained through lyophilization from acetic acid and thermal treatments in 20 or 40% EtOH. 5 μg of each sample were loaded in a 15% polyacrilamide gel.

As expected, mobility differences are visible among N-dimers and C-dimers, due to both different mass and basic charge exposure[107]. However, no significant mobility differences are detectable within the same oligomer type obtained after incubation with different solvents.

4.3.4 CD-spectroscopy

The study of the possible structural differences among monomers exposed to different treatments was deepened using far- and near-UV CD spectroscopy. Far-UV spectra of each sample were recorded in 10 mM NaPi buffer, pH 6.7. Data derived from spectra deconvolutions are reported in Table 4.1.

Samples	Helix (%)	β-strand (%)	β-turn (%)	Unordered (%)	NRMSD
Native M	17.8	27.6	21.7	32.9	0.101
Liophylized M	18.4	28.6	22.6	30.4	0.075
20% EtOH M	18.5	26.8	22.4	32.3	0.119
40% EtOH M	16.7	29.9	22.5	30.9	0.051

Table 4.1 – Percentages of helix, β-strand and β-turn and unordered motives resulting from far-UV CD spectra deconvolutions of each type of monomer. The value of the normalized root-mean-square deviation (NRMSD) obtained by each fitting is reported. Each value is the mean of the two best results computed by the algorithm.

Although the monomers recovered from acetic acid lyophilization and 20% EtOH thermal treatment display a slightly higher amount of helix with respect to the other monomeric samples, and considering that the RMSDs calculated for all monomers vary between 0.051 and 0.119, the modest differences detected cannot be considered significant.

Near-UV spectra of the differently treated monomers were recorded from 240 to 340 nm, in 10 mM NaPi buffer, pH 6.7, and are reported in figure 4.5.

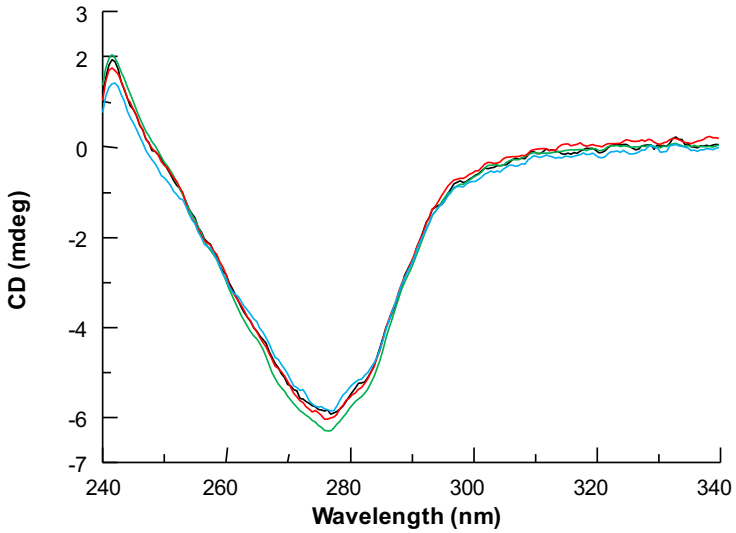

Figure 4.5 – Near-UV spectra of native RNase A (green curve), and of RNase A lyophilized from 40% acetic acid (red curve), or incubated at 60 °C in 20% (black curve) or 40% EtOH (cyan curve). Spectra were recorded from 240 to 340 nm in 10 mM NaPi, pH 6.7. The concentration of each sample is reported in the Material and Methods section.

The CD spectra are minimally affected by the tertiary structure, rather by the secondary structure.

The thermal denaturation of each monomer was analyzed following the variation of its 218 nm far-UV CD signal as a function of temperature. Each sample was exposed to a temperature increase of 1.5 °C/min, starting from 25 to 90 °C. Figure 4.6 reports the denaturation curves and the calculated T_m of each monomer.

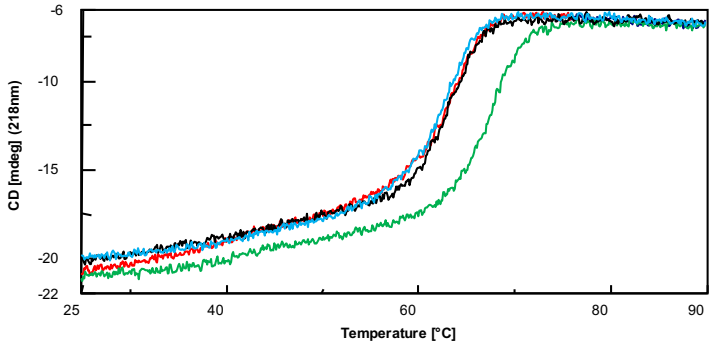

Type of RNase A monomer	T_m (°C)
Untreated	67.6
Lyophilized	63.4
20% EtOH	63.5
40% EtOH	62.7

Figure 4.6 – Denaturation curves and calculated T_m of native RNase A (green curve), and of RNase A lyophilized from 40% acetic acid (red curve), or incubated at 60 °C in 20% (black curve) or 40% EtOH (cyan curve). Data were obtained following the denaturations with far-UV CD, at 218 nm, in 10 mM NaPi, pH 6.7. The concentration of each sample is reported in the Material and Methods section.

All monomers exposed to acetic acid or ethanol display a melting temperature of approximately 63 °C. On the other hand, the melting temperature of RNase A is higher (67.6 °C) when the protein is not treated with solvents. This indicates that both acetic acid and ethanol treatments and/or high temperatures partially destabilize RNase A monomer[206].

4.3.5 1-Anilinonaphthalene-8-Sulfonic Acid (1,8-ANS) fluorescence

In order to study if different treatments could cause some conformational changes and a different exposure of hydrophobic regions, RNase A monomers (0.9 mg/ml)

recovered from different treatments were incubated with 90 µM 1,8-ANS fluorophore in 10 mM NaPi buffer, pH 6.7. Fluorescence spectra recorder after 1 h of incubation are shown in figure 4.7.

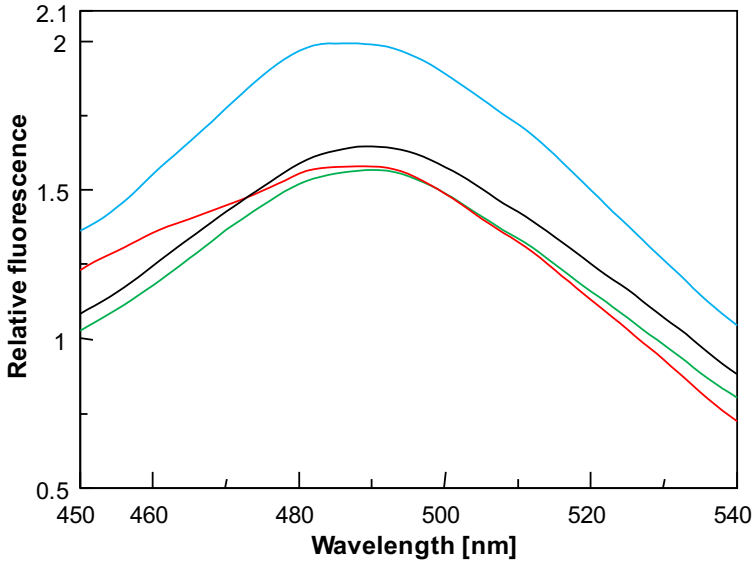

Figure 4.7 – ANS fluorescence emission after 1 h incubation with native RNase A monomer (green curve), or with monomers recovered from 40% acetic acid lyophilization (red curve), or thermally treated in 20% (black curve), or 40% (cyan curve) EtOH. Data were acquired from 450 to 540 nm in 10 mM NaPi, pH 6.7.

When the monomer recovered from 40% EtOH is incubated with ANS, a hyperchromic effect is observed, together with a shifting of the peak from 490 to 485 nm. This is different compared to other monomers and could be due to different local conformational changes, inducing a global major exposure of hydrophobic regions.

4.3.6 Limited proteolysis with subtilisin

Subtilisin is a non-specific serine protease that specifically hydrolizes RNase A peptide bonds between A20-S21 and S21-S22. Subtilisin reaction was performed

to investigate if a specific conformational change occured in the N-terminal region, or in the protein motives interacting with it.
SDS-PAGE of the products deriving from monomeric RNase A samples subjected to proteolysis with subtilisin is shown in figure 4.8.

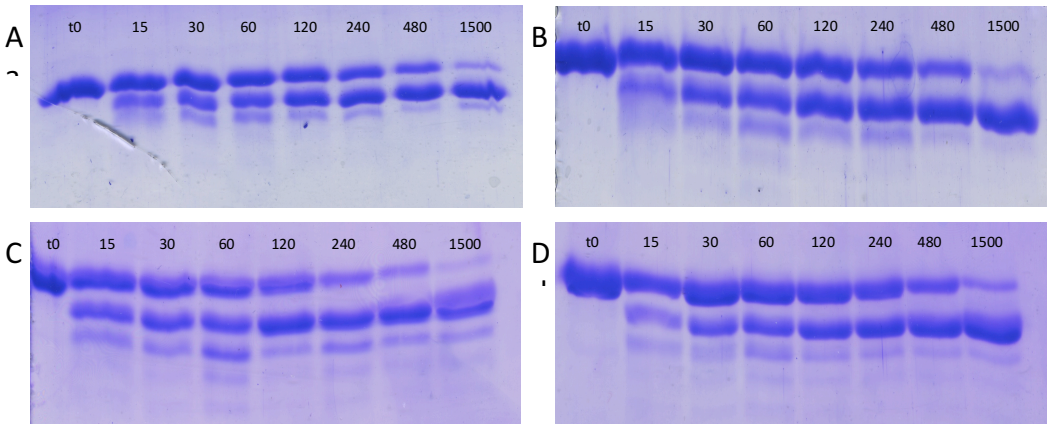

Figure 4.8 – SDS-PAGE showing the products of limited proteolysis performed with subtilisin on A) native RNase A monomer, B) RNase A monomer lyophilized from 40% acetic acid, C) RNase A monomer thermally treated in 20% EtOH, D) RNase A monomer thermally treated 40% EtOH. Reaction was stopped after 0 (t0), 15, 30, 60, 120, 240, 480 and 1500 min, as reported in the labels of the lanes.

No significative differences can be detected in the rate of reaction detected with the different species, even if the monomer incubated in 20% EtOH seems to be slightly more prone to subtilisin cleavage. This suggests that the different treatments do not significantly alter the conformation of the N-terminus of RNase A monomer.

4.4 Discussion

3D-DS, the mechanism through which RNase A is able to oligomerize, has been detected to be one of the mechanisms of amyloid fibers formation. It was demonstrated that in the context of amyloid-related pathologies, the toxicity is due to the oligomers that are the precursor of amyloid fibers, and they can be toxic or not depending on the way they form. Even if there is not evidence that RNase A forms amyloid type fibrils, we studied the structural and functional differences of its oligomers obtained through different ways: 1) lyophilization from 40% acetic acid solution, 2) thermal treatment at 60 °C in 20% ethanol solution and 3) thermal treatment at 60 °C in 40% ethanol solution.

Chromatographic experiments (Fig. 4.1) revealed that the C-dimer is more abundant when obtained through lyophilization from acetic acid or thermal treatment in 40% EtOH than the one deriving from thermal treatment in 20% EtOH. N-dimer, instead, is more aboundant after the treatment in 40% EtOH. Since 40% acetic acid lyophilization and thermal treatment at 60° in 40% EtOH solution generate a stronger denaturing environment than thermal treatment at 60 °C in 20% EtOH, they could favor the almost complete denaturation of RNase A monomer[207], with the possibly consequent higher yield of C-dimer formed after the addition of phosphate buffer. Moreover, the 40% ethanol thermal treatment could somehow favor the swapping of RNase A N-terminal domain more than the other two incubation types, leading to the generation of more N-dimer. However, no significant structural differences are detectable with nondenaturing cathodic PAGE (Fig. 4.4) and with far- and near-UV CD spectroscopy (Fig. 4.5, 4.6 and Table 4.1), although acetic acid lyophilization and 20% EtOH thermal treatment seem to lead to a slightly higher helix content. Then, the overlapping of the near-UV spectra may be considered as a confirmation of the actual absence of differences in the secondary structure of the different monomers. Anyway, since the RNase A number of aromatic residues is low, and their distribution not uniform, an actual modest variation of the secondary structure could not be visible as a dichroic signal variation in the near-UV.

On the contrary, the calculated T_m of each monomer demonstrate that all treatments promote their destabilization. In fact, when not submitted to any type of treatment, RNase A monomer is more stable, with a T_m of 67.6 °C, that is about 4-5 °C higher than the T_m of the monomers that underwent the three different treatments (Fig. 4.6). Despite the undetectable structural differences with CD analyses, ANS fluorescence showed that different treatments may cause a difference in hydrophobic residues exposure (Fig. 4.7). In fact, when incubated at 60°C in 40% EtOH, RNase A monomer exposes more hydrophobic residues than the native form and the same species treated in the other two ways. The combination of harsh conditions, i. e., relative high EtOH concentration and high temperature, could therefore cause some structural changes that may be accompanied with hydrophobic regions exposure. On the other hand, limited proteolysis with subtilisin did not show any significant conformational change at the N-terminus of the differently treated monomers (Fig. 4.8).

Finally, lyophilization from acetic acid or thermal treatments in ethanol do not significantly affect the activity of RNase A monomer and dimers against ss-RNA (Fig. 4.2). On the contrary, both N- and C- dimers activities against ds-RNA are enhanced after thermal treatments in presence of EtOH. This indicates that EtOH could somehow alter the composed catalytic site region or environment that generates after the protein resuspension in NaPi buffer, favoring the increasing of dimeric activity (Fig.4.3).

Thus, we show here how the same protein submitted to different oligomerization pathways may produce slightly structurally and functionally different oligomers. This is not in contraddiction wity amyloidogenic proteins even if it is well known that wt RNase A does not form fibrils.

Chapter 5

Onconase oligomerizes producing a cytotoxic 3D domain-swapped dimer

5.1 Materials

Recombinant ONC was produced and purified from *E. coli*. Aminopeptidase from *Aeromonas proteolytica* (AAP), yeast RNA, poly(A):poly(U) and divinyl sulfone (DVS) were purchased from Sigma-Aldrich. SOC medium was from Invitrogen. Gemcitabine (2′,2′-difluoro-2′-deoxycytidine; GEM) was provided by Accord Healthcare (Milan, Italy) and solubilized in sterile water. All other chemicals were used at the highest purity available.

5.2 Experimental procedures

5.2.1 wt ONC competent cells preparation

The cDNA of ONC, inserted in the plasmidic vector pET-22b(+) between Nde I/Bam HI restriction sites, was kindly provided by prof. D. Picone and dr. E. Notomista (University of Naples, Federico II).

BL21(DE3) cells were incubated with 100 ng of plasmidic DNA, transferred in ice for 30 min, and then immediately at 42 °C for two min. After other two min in ice, 200 µl TB were added, and the mixture was incubated at 37 °C for 1 h. Then, 100 µl of solution were transferred in a "Petri" plate containing 15 ml of LB-agar and 15 mg ampicillin, and colonies were grown overnight. A colony was then collected, transferred in 5 ml LB containing 5 mg ampicillin, and grown at 37 °C, overnight. Subsequently, 500 µl of culture were mixed with 500 µl glycerol, and immediately frozen to -80 °C.

5.2.2 H10A ONC mutant construction and production

Primers 5'-TCCAGAAAAAAGCTATCACTAACACTCGTG-3' and 5'-CACGAGTGTTAGTGATAGCTTTTTTCTGGA-3' were used to produce the H10A mutant. The PCR was carried out using the QuikChangeII (Agilent) mutation kit, and containing 0.5 µl of 117 ng/µl plasmidic DNA, 5 µl of 10X Buffer, 1 µl of 10 mM dNTPs mix, 1.25 µl of each 25 µM primer, 1 µl of PFU polymerase, 40 µl of ddH_2O. PCR was performed with the following cycles: 30 sec at 95 °C, 16 x (30 sec at 95 °C, 1 min at 57 °C, 12 min at 68 °C), 12 sec at 68 °C. The amplification product was detected through electrophoresis (100 V, 20 min) on a 0.8 % agarose gel, enriched with 1/10 SYBR® dye solution (Invitrogen). The amplification product was digested with DpnI at 37 °C, for 1h.

TOP10 cells (Invitrogen) were incubated with 5 µl of PCR product, transferred in ice bath for 30 min, then 30 sec at 42 °C and again 2 min in ice bath. Successively, 250 µl of SOC medium (Sigma-Aldrich) were added and the sample was incubated at 37 °C for 1 h. 80 µl of bacteria were than grown overnight on a "Petri" plate, in 15 ml of LB-agar containing 15 mg ampicillin. Two colonies were separately collected, transferred in 5 ml LB containing 5 mg ampicillin, and grown at 37 °C. The plasmidic DNA was purified (PureLink Quick Plasmid Miniprep Kit, Invitrogen), sequenced, and the one extracted from a selected colony was used to transform BL21(DE3) cells following the same procedure described in section 5.2.1.

5.2.3 wt and H10A onconase expression and purification

Competent cells were grown for 6 h in 5 ml LB and 5 mg AMP, at 37 °C, and then overnight in 150 ml of the same broth, at the same temperature. The inoculum was subsequently mixed with 1 L of TB, 1 g AMP, incubated at 37 °C, and induced with 0.4 mM IPTG when the OD_{600} of 2.4 was reached. Then it was left at 37 °C, overnight, under agitation. Cell lysis was performed resuspending the pellet in 10 ml of 0.1 M Tris-acetate pH 8.4, 5 mM protease inhibitor PMSF, and 2 mg of

lysozyme, for 20 min. Then, 32 mg of deoxycholic acid were added, and the solution was transferred at 37 °C, for 40 min. After that, 320 Kunitz Units of DNase and $MgCl_2$ at the final concentration of 5 mM were added, and the solution was incubated 30 min at room temperature. The pellet was then solubilized in 0.1 M Tris-acetate, pH 8.4, 10 mM EDTA, 2% Triton X and 2M Urea. After 30 min incubation, the "washing" was repeated three times, one with the same buffer and two with only 0.1 M Tris-acetate, pH 8.4, plus 10 mM EDTA. The pellet was subsequently redissolved in 0.1 M Tris-acetate, pH 8.4, 10 mM EDTA, 6 M GdnHCl, and DTT was added at the concentration of 100 mM. A flow of nitrogen was used to avoid oxidizing conditions, and the pellet was incubated at 37 °C for 3 h. The sample was then dialyzed twice against 2 L of 20 mM acetic acid, for 3 h, and finally against 5 L, overnight. After pellet removal, the solution was diluted in 200 ml of 0.1 M Tris-acetate, 0.5 M L-arginine, pH 8.4. A mix of reduced and oxidized gluthatione (3 mM/0.6 mM) was added and the sample saturated of nitrogen for 22 h. At the end of the reaction, the solution containing the protein was transferred in 100 ml of 0.2 M potassium-phosphate pH 8.0, 20 mM $ZnSO_4$, and aminopeptidase extracted from *Aeromonas proteolytica* (AAP) was added in a molar ratio AAP:ONC of 1:1000. The solution was incubated for four days at 37 °C. Subsequently, EDTA was added at a final concentration of 10 mM. ONC was further purified using a Superdex 75 HR 10/300 column, connected to an AKTA-FPLC system (GE-Healthcare), in 0.1 M Tris-acetate pH 8.4, 0.3 M NaCl, at a flow rate of 0.2-0.3 ml/min. After the final purification step, ONC quantity was spectrophotometrically determined at 280 nm, $\varepsilon^{1\%}_{280}$ = 8.84 $M^{-1}cm^{-1}$ (calculated with ProtParam tool), with a Jasco V-650 spectrophotometer, and the protein was lyophilized from ddH_2O. 10 μg of protein sample were resuspended in 100 μl of 0.1% HCOOH and were analyzed by a high-resolution mass spectrometry on a Xevo G2-S Q-TOF instruments (Waters, MA, USA). Experimental conditions: capillary potential, 1.5kV; source temperature, 100°C; desolvation gas temperature, 350°C; collision energy, 20-30V. The mass versus charge signals, visualized as BPI (base peak intensity) by the program MassLynx V4.1, were deconvoluted by the software MaxEnt1 to achieve the peaks average masses.

5.2.4 Onconase oligomerization

To induce its oligomerization, the ONC powder aliquots of 50 to 1000 μg were lyophilized from 40% acetic acid, following the procedure described by Crestfield & coll. for RNase A[78]. Some ONC samples were also lyophilized after incubation in 0.25-1 mM DTT, 40% acetic acid at 25 °C, for 24 h, or after incubation in 0.5 mM DTT, 10 mM NaPi, pH 6.7, at 25 °C, for 24 h, before the acetic acid solution. The resulting powder was then suspended at concentrations ranging from 1 to 10 mg/ml, in 0.4 M NaPi, pH 6.7, and separately analyzed through SEC, with a Superdex 75 HR 10/300 column attached to an ÄKTA-FPLC system (GE-Healthcare). The column was equilibrated with the same NaPi buffer and mixtures were eluted at a flow rate of 0.10-0.15 ml/min. Chromatographic patterns and areas of the resulting peaks were analyzed with the Unicorn 5.01 Software (GE Healthcare).

5.2.5 Enzymatic activity on single strand (ss-) RNA

Kunitz assays were performed on 0.6 mg/ml ($A_{300} \approx 0.6$) yeast ss-RNA solubilized in 0.10 M sodium acetate buffer, pH 5.0, using a Jasco V-650 spectrophotometer. RNase A concentration was 0.75 ng/μl, while ONC monomer and dimer concentration was 12,5-25 ng/μl. The catalytic activity was determined at 300 nm in the linearity range, measuring the absorbance decrease over time per μg of enzyme. The blank measure was performed measuring the absorbance of 0.1 M sodium acetate buffer pH 5.0. Negative controls were performed by measuring the absorbance of the yeast-RNA solution without the addition of the enzyme, in order to exclude the presence of contaminant RNases.

5.2.6 Nondenaturing cathodic PAGE

Nondenaturing cathodic PAGE[188] was performed using a 12.5-15% acrylamide gel,

in β-alanine (0.35%)/acetic acid buffer, pH 4.0. ONC samples were electrophoresed with a constant voltage of 200 V, for 90 min., in ice. Gels were subsequently transferred in 12.5% 2,2,2-trichloroacetic acid for 1.5 h, stained with 0.1% Coomassie Brilliant Blue, and destained in 10% CH_3COOH, 20% EtOH solution.

5.2.7 ONC dimer stability

ONC dimer stability was studied incubating it at 37 °C, for 100 h, at a concentration of 0.8 mg/ml in 10 mM NaPi Buffer, pH 6.7, in parallel with RNase A N- and C-dimers. 5 μg aliquots were withdrawn at different time intervals and run in a 15% cathodic nondenaturing PAGE. The stability of ONC dimer in sodium acetate/acetic acid buffer, pH 5.0, was studied incubating it at 25 °C, for 120 h. 5 μg were withdrawn at different time intervals and analyzed in 15% cathodic nondenaturing PAGE. The stability of ONC dimer in RPMI 1640 containing glutamine, gentamicin sulfate, was studied incubating it at 37 °C, with or without the addition of FBS. At different time intervals, 5 μg were withdrawn and analyzed in a 15% cathodic nondenaturing PAGE.

5.2.8 Cross-linking with divinyl sulfone (DVS)

ONC dimer was cross-linked with DVS at a concentration of 0.25 mg/ml in 0.1 M sodium acetate/acetic acid buffer, pH 5.0, or at 0.6 mg/ml in 0.025, 0.05 and 0.1 M sodium acetate/acetic acid buffer, pH 5.0. 10% DVS in ethanol solution was added in a DVS/protein molar ratio of 1000. Reactions were carried out at 8 or 25 °C. 15 μg aliquots were withdrawn at times comprised between 0 and 165 h, and the reaction was stopped with β-mercaptoethanol (0.2 M final concentration). The reaction time-course was electrophoretically analyzed with SDS-PAGE (15% polyacrylamide, Tris/glycine buffer, pH 8.3). Gels were run at 200 V, for 60 min.

5.2.9 Circular dichroism and fluorescence

Near-UV and far-UV spectra were acquired between 350-240 and 260-190 nm, respectively, using a Jasco J-810 spectropolarimeter, performing five total scans for each experiment. The far-UV CD spectra deconvolution was performed by means of DichroWeb Server (http://dichroweb.cryst.bbk.ac.uk/html/home.shtml), considering the range 190-260 nm and using the CONTIN algorithm.
Fluorescence spectra were acquired using a Jasco FP-750 spectrofluorimeter. The excitation wavelength were 280 and 295 nm, and emission was respectively recorded from 295 to 550 nm or from 315 to 550 nm.
For all CD and fluorescence experiments ONC monomer and dimer concentration were 0.17 and 0.18 mg/ml, respectively.

5.2.10 ONC dimer modeling

Two models of N-swapped ONC dimer were obtained in collaboration with dr. A. Pica (University of Naples, Federico II), starting from two different crystallographic templates: i) the non-covalent N-swapped dimer (N_D) of wild-type RNase A (pdb code 1A2W)[81], and ii) the dimeric deletion mutant of human pancreatic ribonuclease des(16-20)-HP-RNase (pdb code 4KXH)[208]. They were called N_D-like model and desHP-like model respectively. The two models were obtained superimposing the structure of monomeric ONC (pdb code 2I5S)[169] onto each structural unit of the domain-swapped dimer templates RNase A-N_D or des(16-20)-HP-RNase. Then, the eight residues located in the loop connecting His10 (corresponding to His12 in RNase A) to Cys19 (Cys26 in RNase A) were manually modeled using the template structures as a guide.
MD simulations were performed to compare the two protein models and evaluate their stability. The N_D-like model was immersed in a box of 7.985x6.646x6.518 nm^3 volume and filled with 10203 water molecules. In order to neutralize the overall protein charge (+12) and simulate physiological conditions, sodium and chloride ions were added to the box at a concentration of 100 mM, corresponding

to 21 sodium cations and 33 chloride anions. The desHP-like model was immersed in a box of 5.900x7.492x7.687 nm^3 filled with 10114 water molecules with the addition of 20 sodium cations and 32 chloride anions. Equilibration was conducted in two phases. The first phase was to stabilize the temperature of the systems to 300 K, the second to equilibrate pressure to 1 atm. Before starting the MD simulation, energies were minimized by fixing the protein atoms and then without restraints.

5.2.11 Cytotoxic activity of ONC oligomers: cell proliferation and apoptosis assays

ONC cytotoxicity was measured against PaCa44 human pancreatic adenocarcinoma cell line grown in RPMI 1640 supplemented with 2 mM glutamine (Life Technologies, Milan, Italy), 10% FBS, and 50 μg/mL gentamicin sulfate (BioWhittaker, Lonza, Bergamo, Italy), at 37 °C with 5% CO_2.

Cells were then seeded in 96-well plates (2.5 x 10^3 cells/well) and, the day after, incubated with 5, 10 and 25 μg/mL of ONC monomer or dimer, supplemented, or not, with 50 nM gemcitabine (GEM)[178]. After 96 h, cells were stained with a Crystal Violet solution (Sigma, Milan, Italy) and the dye was solubilized in PBS containing 1% SDS to spectrophotometrically analyse the cell growth at 595 nm.

In apoptosis assays, cells were seeded in 96-well plates (2.5 x 10^3 cells/well) and, the day after, treated for 96 h with 10 μg/ml of the mentioned compounds. At the end of the treatment, cells were fixed for 30 min with 2% paraformaldehyde in PBS solution at RT, then washed twice with PBS and stained for 10 min in the dark at RT with annexinV/FITC (Bender MedSystem, Milan, Italy) in the binding buffer 10 mM HEPES/HCl pH 7.4, 140 mM NaCl, and 2.5 mM $CaCl_2$. Finally, cells were washed with a binding buffer solution and fluorescence was measured with a multimode plate reader (λ_{exc} 485 nm and λ_{em} 535 nm) (GENios Pro, Tecan, Milan, Italy). Values were normalized on cell proliferation with a Crystal Violet assay.

5.3 Results

5.3.1 wt ONC expression and purification

Figure 5.1 displays a 18% SDS-PAGE performed after the expression and purification steps of wt ONC.

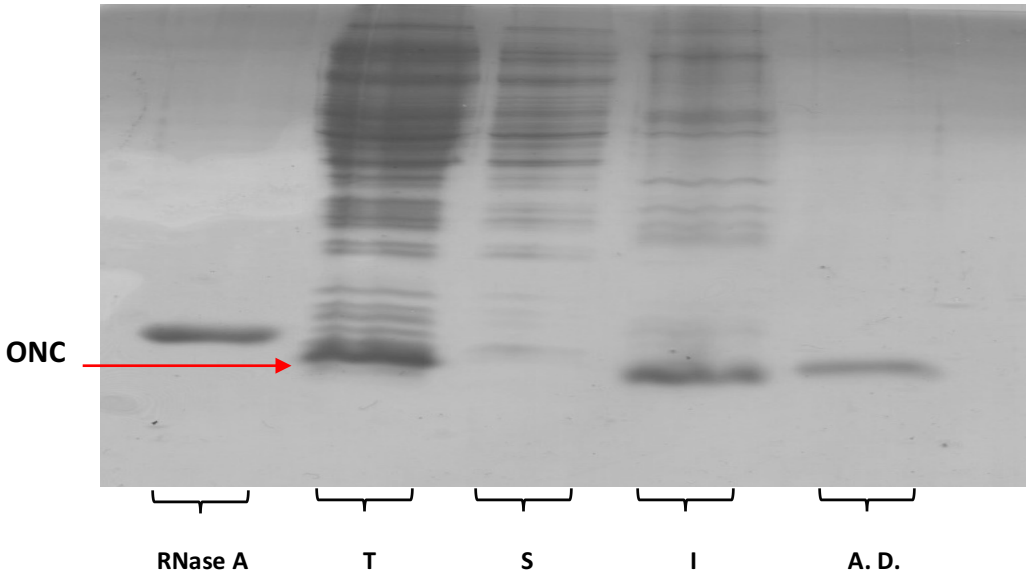

Figure 5.1 – 18% SDS-PAGE analysis of the total (T), soluble (S) and insoluble (I) fractions deriving from the lysis of BL21(DE3) cells. ONC is detectable in the insoluble fraction (red arrow), and moves in the soluble fraction after the dialysis (A. D.). RNase A was used as a MW control.

As expected, ONC is detectable in the insoluble fraction, since it is incorporated in inclusion bodies, like RNase A. After dialysis against 20 mM acetic acid, all the undesidered proteins precipitate, but the ONC monomer moves in the soluble fraction. The additional N-terminal residue N-Met was removed by incubating the protein for 96h in 0.2 M potassium-phosphate buffer, pH 8.0, containing *Aeromonas proteolytica* Aminopeptidase (AAP), with an AAP/protein molar ratio

of 1:1000, at 37 °C. After the reaction, the protein was transferred in 0.1 M acetic acid pH 8.4, 0.3 M NaCl, and further purified through SEC, in order to remove AAP traces. Fig. 5.2 shows that ONC elutes slightly after RNase A, as expected.

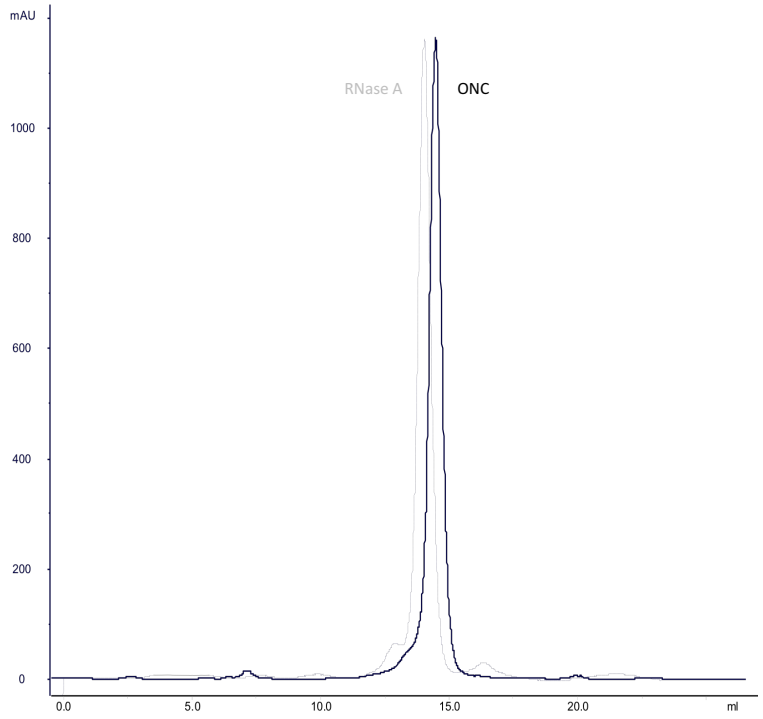

Figure 5.2 – Superimposed SEC patterns of ONC monomer (blue curve) after the N-terminal Met removal performed with AAP and of RNase A monomer (grey curve). Chromatographies were carried out with a Superdex 75 HR 10/300 column equilibrated with 0.1 M acetic acid, pH 8.4, 0.3 M NaCl buffer. Patterns were normalized on the RNase A monomer area with the Unicorn 5.01 Software (GE Healthcare).

The peak was collected and its content spectrophotometrically quantified, transferred in ddH_2O and lyophilized. 10 μg of sample were analyzed by a high-resolution mass spectrometry on a Xevo G2-S Q-TOF instruments (Waters, MA, USA). The N-term-Met cleavage occurred successfully for the 78% of the protein, while the 22% maintained the N-Met (Data not shown). Mass spectrometry confirmed that ONC monomer was correctly expressed. Moreover, ONC catalytic activity was tested against yeast ss-RNA, with Kunitz assays and the results are in line with those reported in literature[209] (Table 5.2).

5.3.2 ONC oligomers production, purification and characterization

In order to obtain ONC oligomers, ONC monomer was lyophilized from 40% acetic acid acqueus solution. The resulting powder was resuspended in 0.4 M NaPi buffer pH 6.7, at a concentration ranging from 1 to 10 mg/ml, and analyzed through SEC. Figure 5.3 shows the chromatographic pattern of ONC oligomers purification. The presence of two peaks before ONC monomer indicates the increasing yield of a peak that could be supposed as to be a dimer (eluting at about 13 ml) and the formation of a trace of a larger oligomer (eluting at about 12.3 ml). The elution volumes of the most abundant species, in fact, is similar the one of RNase A N-dimer (gray dotted pattern in Fig. 5.3). Moreover, the higher the concentration of ONC after the resolubilization in NaPi buffer, the higher the yield of the dimer obtained. In fact, we noticed that dimer yield increases from 9.5 to about 13.5% if the powder was resuspended at a concentration increasing from 1 to 10 mg/ml (Table 5.1).

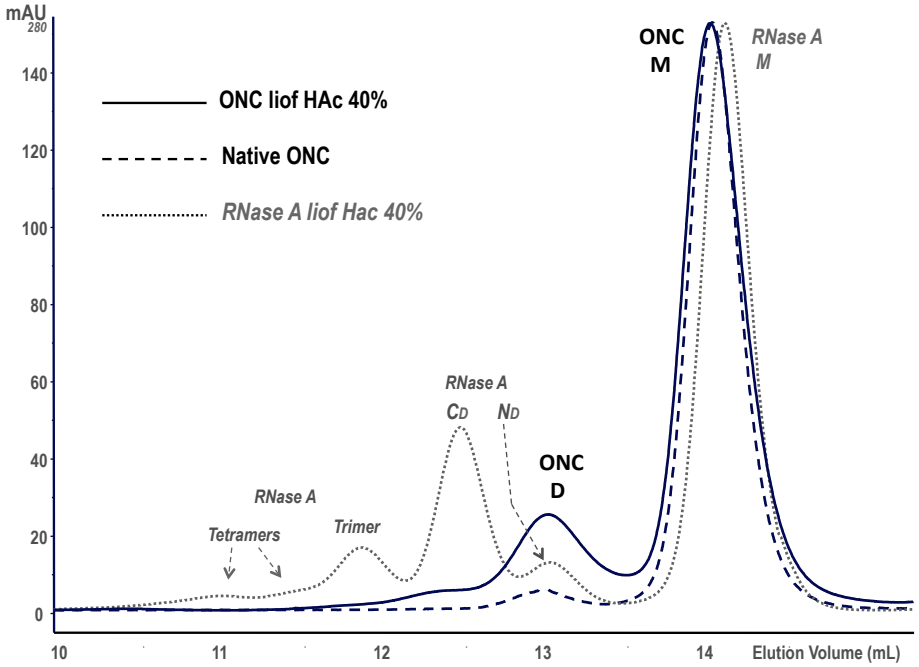

Figure 5.3 – SEC purification of ONC before (dashed line) and after (continuous line) the induced oligomerization through lyophilization from 40% acetic acid solution. Traces of ONC dimer are constitutively present (dashed line), but after the induction of oligomerization, the yield of the dimer increases. Traces of a larger oligomer are also detectable. The RNase A pattern is superimposed in grey (dotted line). Patterns were normalized on the RNase A monomer area with the Unicorn 5.01 Software (GE Healthcare).

ONC species	Monomer %	Dimer %	Larger oligomers %
No HAc lyophilization	96.9 ± 0.4	3.1 ± 0.3	-----
1 mg/mL	89.8 ± 0.2	9.7 ± 0.2	0.6 ± 0.2
2 mg/mL	87.7 ± 0.8	11.4 ± 0.5	0.9 ± 0.3
4 mg/mL	85.6 ± 0.2	12.8 ± 0.3	1.5 ± 0.2
10 mg/mL	85.0 ± 0.4	13.4 ± 0.4	1.7 ± 0.6

Table 5.1 – Yields (%) of dimer and larger oligomers obtained after lyophilizing ONC from 40% acetic acid buffer and resuspending it in 0.4 M NaPi buffer, pH 6.7 at concentration ranging from 1 to 10 mg/ml. The quantity of each species was calculated as the area of each peak eluted with SEC purifications and the percentage calculated as ratio of (each peak area/total peak area)·100%. The values reported are the mean of three or more different experiments.

Since it is known that the C-terminus of ONC is blocked by the disulfide bond that links Cys87 to Cys104, and that RNase A disulfide bonds are not affected by acetic acid[207], some ONC fractions were lyophilized after incubation in 0.25-1 mM DTT, 40% acetic acid at 25 °C, for 24 h, or after incubation in 0.5 mM DTT, 10 mM NaPi, pH 6.7, at 25 °C, for 24 h, before the acetic acid solution, in order to try to make the C-terminal residues available for the swapping. However, no traces of an additional ONC dimer are detected in SEC after these treatments (Fig 5.4).

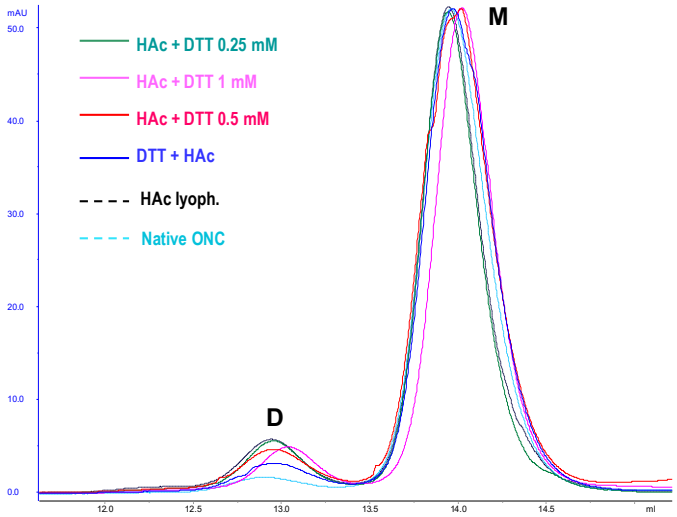

Figure 5.4 – SEC purification of ONC: untreated (light blue curve), lyophilized from 40% acetic acid solution (black curve), lyophilized after incubation in 40% acetic acid with the addition of 0.25 (green curve), 0.5 (red curve) and 1 mM (violet curve) DTT at 25 °C, for 24 h, and lyophilized from 40% acetic acid solution after incubation with 0.5 mM DTT, 10 mM NaPi, pH 6.7, at 25 °C, for 24h. Each sample was resuspended in 0.4 M NaPi buffer, pH 6.7, before the SEC analysis. Patterns were normalized on the monomer area with the Unicorn 5.01 Software (GE Healthcare).

5.3.3 Comparison of the catalytic activities of ONC monomer and dimer against ss-RNA

Kunitz assays were performed in order to measure the enzymatic activity of ONC dimer against ss-RNA and compare it to that of the monomer (Table 5.2).

Species	%Kunitz activity
RNase A	100.0
ONC monomer	3.5
ONC dimer	1.4

Table 5.2 – Kunitz activity of RNase A monomer, ONC monomer and ONC dimer. The activities of all the species are reported as percentages of RNase A monomer activity (100%). Data shown are the average of five different assays.

Recombinant refolded ONC is less active than RNase A, in line with previous results[209], and ONC dimer displays about 3.5% activity compared to ONC monomer. This result recalls the behavior of RNase A oligomers, whose formation leads to the loss of about 40% catalytic activity against ss-RNA[79,83,107,112].

5.3.4 Nondenaturing cathodic PAGE

In order to analyze the electrophoretic behavior of ONC dimer under nondenaturing conditions, the samples collected from SEC were desalted to lower NaPi concentration to 50 mM, and 4 μg of ONC monomer and dimer were separately subjected to a 12.5 % acrylamide gel electrophoresis under nondenaturing conditions[188].

Monomeric ONC maintains the same electrophoretic mobility before and after the lyophilization treatment, indicating that harsh conditions do not affect the overall protein structure (Fig. 5.5, lane 3 and 4). The dimeric sample obtained after ONC lyophilization from 40% acetic acid (Fig. 5.5, lane 2) displays a lower mobility with respect to that of ONC monomer. Moreover, it maintains the same mobility of the corresponding species present before treatment (Fig. 5.5, lane 1), demonstrating that dimer traces are actually constitutively present after ONC purification. Finally, the presence of a single band demonstrates that the peak corresponding to ONC dimer is not a mixture of different dimeric conformers, but it contains only one isoform.

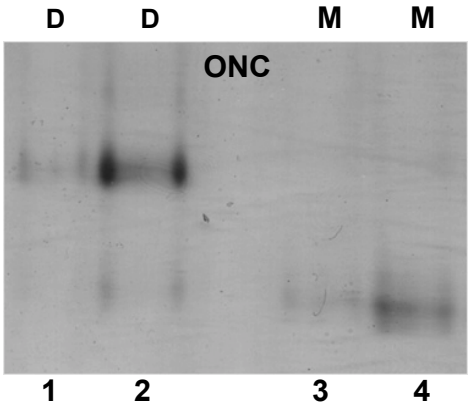

Figure 5.5 – 12.5% acrylamide cathodic nondenaturing PAGE of: ONC dimer isolated before (lane 1) and after 40% acetic acid lyophilization (lane 2), ONC monomer before (lane 3) and after (lane 4) 40% acetic acid lyophilization.

5.3.5 ONC dimer stability

The stability of ONC dimer in 10 mM NaPi buffer, pH 6.7, was studied incubating ONC dimer or N- or C-dimers of RNase A at 37 °C, at a concentration of 0.8 mg/ml. 5 μg aliquots were withdrawn at different times (0, 1, 2, 4, 10, 24, 48, 72, 100 h), and run in a cathodic nondenaturing PAGE (Fig. 5.6). Under these conditions, traces of ONC dimer are detectable until 72 h, whereas C-dimer and N-dimer persist until 24 and 48h, respectively. This indicates that ONC dimer is a more stable species than N- and C-dimers of RNase A.

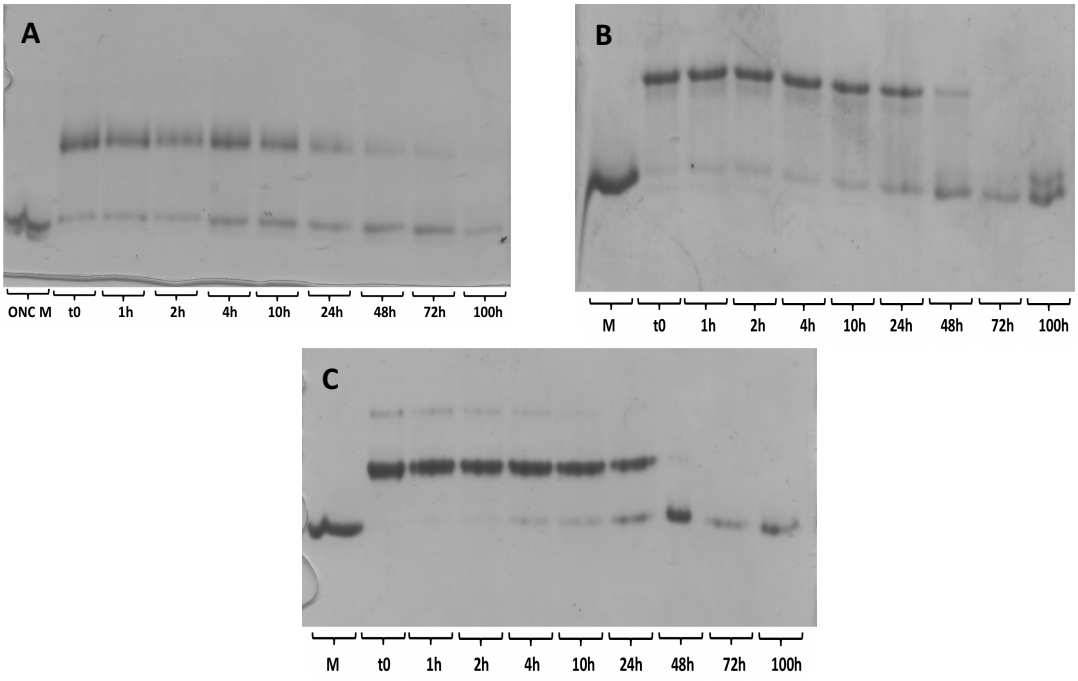

Figure 5.6 – A) ONC dimer, B) RNase A N-dimer and C) C-dimer stability until 100 h at 37 °C, assayed with cathodic nondenaturing PAGE. 5 μg of each species were withdrawn at 0, 1, 2, 4, 10, 24, 48, 72 and 100 h and run on the gel. ONC M = ONC monomer, M = RNase A monomer.

5.3.6 Far- and near-UV circular dichroism and fluorescence analyses

The differences of secondary and tertiary structure detectable among ONC monomer and dimer were studied also through circular dichroism. Far-UV CD spectra were measured from 190 to 260 nm (Fig. 5.7A). The results of far-UV spectra deconvolution are reported in Table 5.3. No significant differences among the secondary structures of ONC monomer and dimer were detected through far-UV CD analysis, as they display about the same amounts of α-helices, β-sheets and random coils.

Near-UV CD data were measured from 240 to 350 nm (Fig. 5.7B), while fluorescence was measured exciting at 280 and 295 nm, and recording the emission spectra from 300 to 450 nm and from 315 to 450 nm, respectively (Fig. 5.7C/D).

Near-UV CD spectra of ONC monomer and dimer do not show significant differences, indicating that dimerization does not compromise the global tertiary fold of ONC, and therefore that the swapped N-terminal domains would re-establish the same contacts present in the monomer (closed interface) with the other subunit, as the 3D-DS mechanism foresees[88]. Fluorescence experiments (λ_{em} of 280 and 295 nm) reveal a 2-3 nm maximum intensity shift of ONC dimer with respect to the monomer, in dicating a slightly lower exposition to the solvent of the dimer's aromatic side chains. On the other hand, the similar fluorescence intensities shown by ONC monomer and dimer confirm that no significant conformational changes occur as a consequence of dimerization.

Samples	Helix (%)	β-Strand (%)	β-Turn (%)	Unordered (%)	NRMSD
ONC monomer	18.1	32.8	19.6	29.5	0.243
ONC dimer	19.4	27.6	21.8	31.2	0.223

Table 5.3 – Percentages of helix, β-strand and β-turn and unordered motives resulting from far-UV CD spectra deconvolutions of ONC monomer and dimer. The value of the normalized root-mean-square deviation (NRMSD) obtained by each fitting is reported. Each value is the mean of the two best results computed by the algorithm.

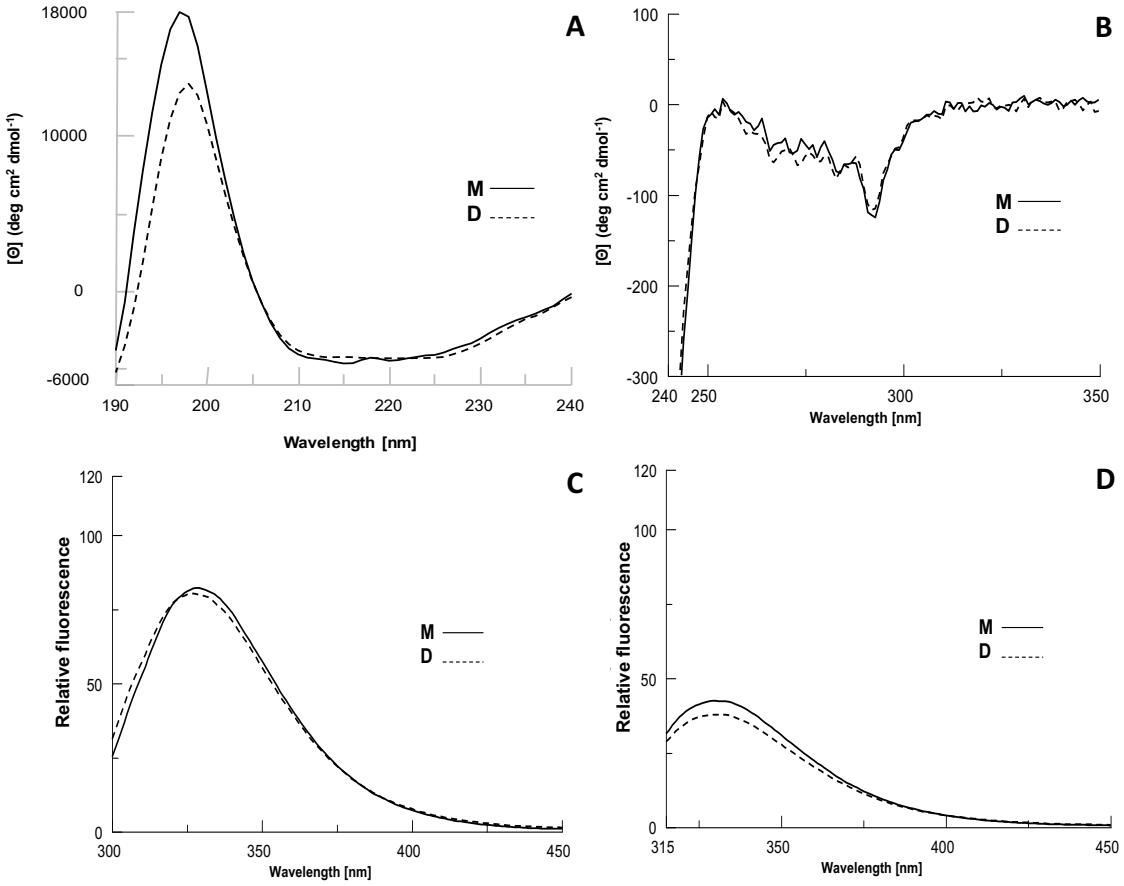

Figure 5.7 – A) Far-UV and B) near-UV CD spectra of ONC monomer (M, continuous line) and dimer (D, dashed line). Far- and near-UV CD spectra were measured from 190 to 240 nm and from 240 to 350 nm, respectively. C) Fluorescence at λ_{ex} = 280 nm, λ_{em} = 300-450 nm and D) fluorescence at λ_{ex} = 295 nm, λ_{em} = 315-450 nm of ONC monomer (M, continuous line) and dimer (D, dashed line). All spectra were measured in 50 mM NaPi buffer, pH 6.7. The concentrations of the samples are reported in the Materials and Methods section.

5.3.7 DVS cross-linking: investigating the presence of 3D-DS

The reaction of pancreatic-type RNases with DVS allows to covalently link the two His residues of the active site that belong to the two N- and C-termini. This reaction allows to assess if the oligomers form through 3D-DS because if 3D-DS took place, an SDS-PAGE performed after DVS reaction would reveal a covalently stabilized dimer formed by the swapping of one terminus, or both.

Thus, the ONC dimer was incubated with DVS at different protein and buffer concentrations. Reaction aliquots were collected up to 165 h, adding β-mercaptoethanol, and four μg of each sample were analyzed in SDS-PAGE. As shown in fig. 5.8A-E, the presence of two bands demonstrates that the 3D-DS mechanism occurs in the ONC dimer formation. In ONC, the two His residues composing the active site are His97, which belongs to the C-terminus, blocked by the disulfide involving Cys104, and His10, which is located in the N-terminus. It is therefore reasonable that ONC dimer forms through the swapping of ONC N-terminus.

In order to ensure that the dimer did not dissociate during the DVS reaction, ONC dimer stability was tested incubating it in the same buffer of the DVS experiment, at 25 °C (Fig. 5.8F). ONC dimer results to be stable at least for 120 h.

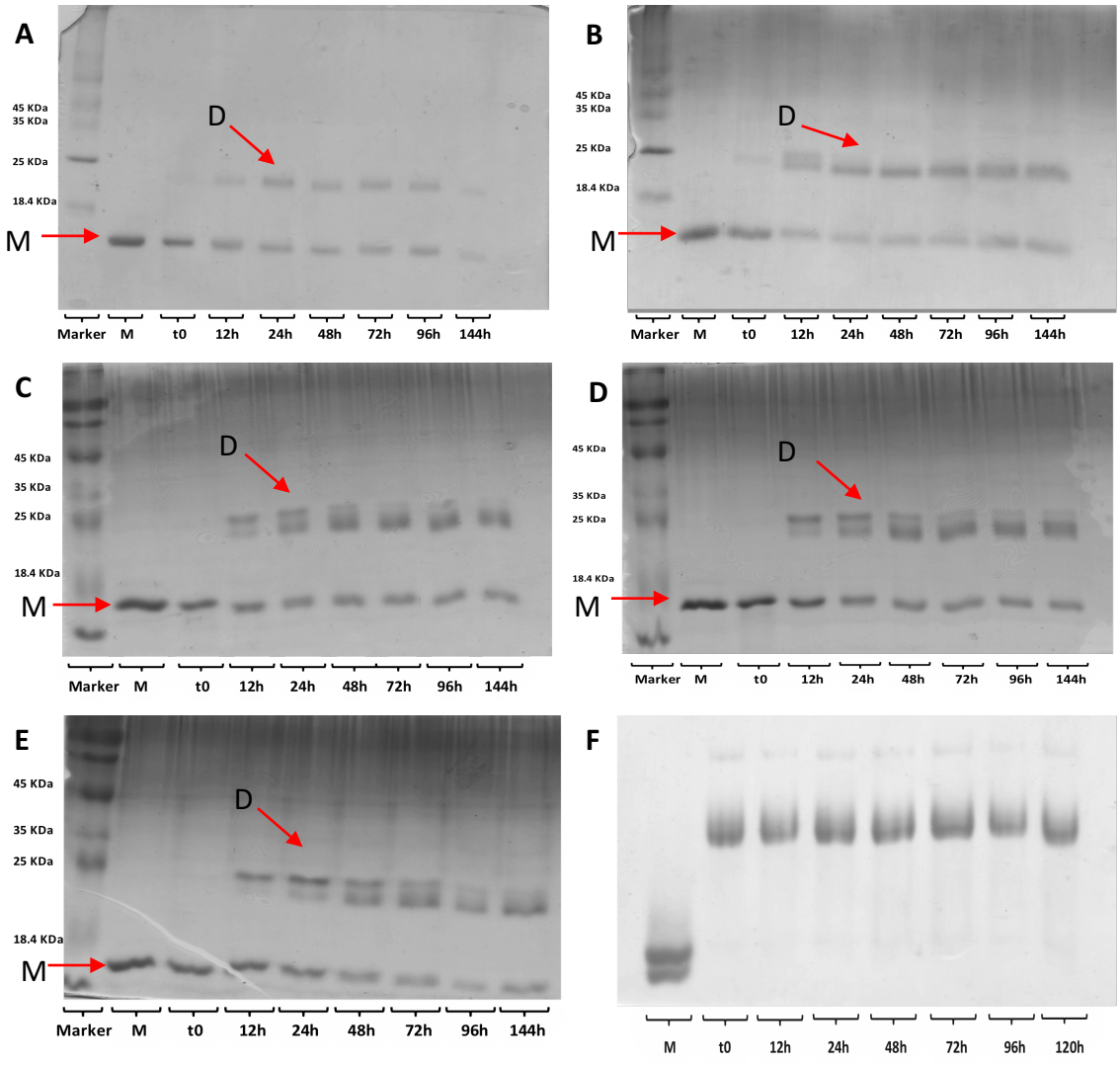

Figure 5.8 – 15% SDS-PAGE analysis of the cross-linking reactions obtained with divinyl sulfone on ONC dimer (0.6 mg/ml) in 0.10 M sodium acetate/acetic acid buffer, pH 5.0 at A) 8 °C and B) 25 °C, C) in 0.05 M sodium acetate/acetic acid buffer, pH 5.0, at 25 °C, D) in 0.025 M sodium acetate/acetic acid buffer, pH 5.0, at 25 °C, and E) on ONC dimer (0.25 mg/ml) in 0.10 M sodium acetate/acetic acid buffer, pH 5.0. At different times (0, 12, 24, 48, 74, 118, 165 h), 15 µg aliquots were withdrawn and 4 µg were analyzed in SDS-PAGE. M = monomer, D = dimer. F) Stability of ONC dimer in sodium acetate/acetic acid buffer, pH 5.0, at 25 °C. 5 µg were withdrawn at different times (0, 12, 24, 48, 72, 96, 120 h) and analyzed in 15% cathodic nondenaturing PAGE.

While the ONC dimer maintains catalytic activity on ss-RNA (Table 5.2), Kunitz assays showed no ss-RNA cleavage by the cross-linked dimer collected after the

reaction with DVS (165 h), in line with the covalent modifications of the active site His induced by the cross-linking reaction. In fact, the two His of the active site, linked by DVS, are not available for the catalytic reaction anymore.

However, beyond the two His of the active site, a third histidine, His29, is present in ONC. In order to exclude the possibility of the cross-linking between His29 and His97 during the DVS reaction, that would lead to the formation of a dimer in absence of 3D-DS, the H10A mutant was hence constructed and produced (Section 5.2.2). If the formation of ONC dimer occurred through 3D-DS, then the cross-linking with DVS performed on H10A ONC would not produce a covalent dimer, due to the absence of one of the two His involved in the reaction. The H10A ONC was purified with Superdex 75 HR 10/300, and its CD and fluorescence analyses showed that it was correctly folded. Moreover, as expected, no catalytic activity against ss-RNA was detected, in line with the substitution of His10. However, we did not obtain analyzable quantity of dimer after the lyophilization of H10A ONC monomer from 40% acetic acid. A possible explanation could be the lack of a stabilizing interaction formed by a phosphate ion that links the two histidines of the composed active site of ONC dimer, in the first phases of its folding. In fact, the product yield of RNase A oligomerization through 3D-DS depends also by the presence of phosphate ions in the buffer, which would allow the interaction between His12 and His119 of two different subunits, favoring the swapping. This is supported by the fact that when ONC powder derived from lyophilization from 40% acetic acid is resuspended in ddH_2O, the yield of the dimer is significantly lower compared to that obtained with resuspension in phosphate buffer (Fig. 5.9).

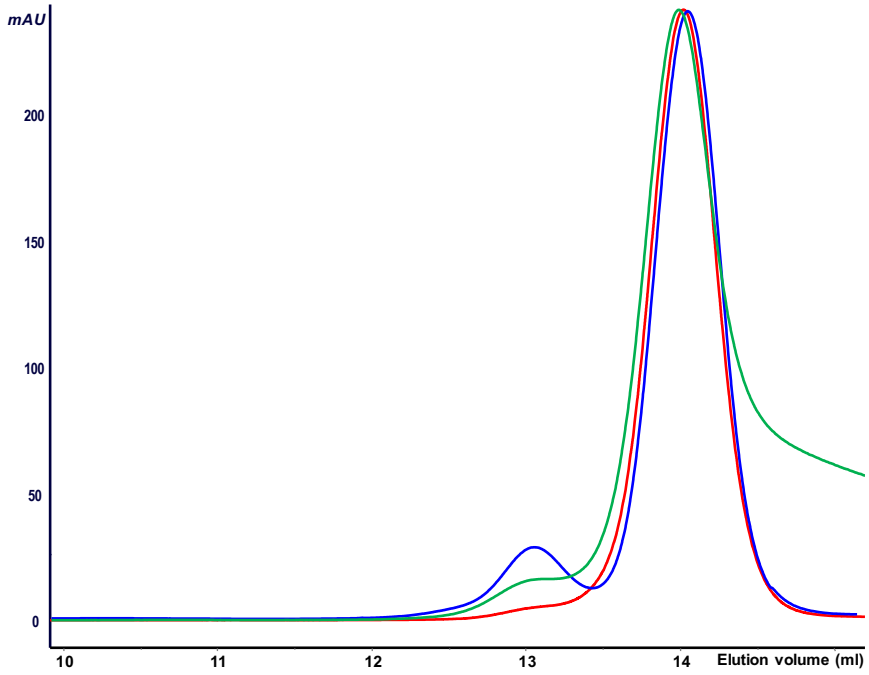

Figure 5.9 – SEC patterns superimposition of wt ONC after lyophilization from 40% acetic acid buffer and resuspension in 0.4 M NaPi buffer, pH 6.7 (blue curve) or ddH_2O (green curve) and of H10A ONC after lyophilization from 40% acetic acid buffer and resuspension in 0.4 M NaPi buffer, pH 6.7 (red curve). Patterns were normalized on the monomer area with the Unicorn 5.01 Software (GE Healthcare).

Due to the lack of His10, H10A ONC dimerization could be hindered even after its resuspension in phosphate buffer. This demonstrates that His10 is essential for the dimer formation, and that dimerization occurs through the formation of new interactions involving ONC N-terminal domain. DVS demonstrated that these interactions produce a 3D N-terminal domain-swapped ONC dimer.

5.3.8 Modeling of the domain-swapped ONC dimer

The 3D structure of ONC dimer was modeled firstly assuming that the protein is free to swap only its amino-terminus. Indeed, the C-terminal swapping is precluded by the disulfide involving ONC C-terminal cysteine. Models were obtained starting from the structure of monomeric ONC (pdb code 2I5S)[169] using two different

dimeric templates that display different relative orientations between the two subunits: a) the N-swapped dimer of RNase A-N_D, (pdb code: 1A2W)[81] and b) the dimer of des(16-20)-HP-RNase (desHP, pdb code: 4KXH)[208], as detailed in the Materials and Methods section. Like ONC, both the crystallographic structures of RNase A dimers retain the standard folding of pancreatic-type RNases. The two dimeric ONC models are reported in Fig. 5.10A and B, paralleled in Fig. 5.10C and D by the structures of their parent templates, i.e., RNase A-N_D and des(16-20)-HP-RNase, respectively.

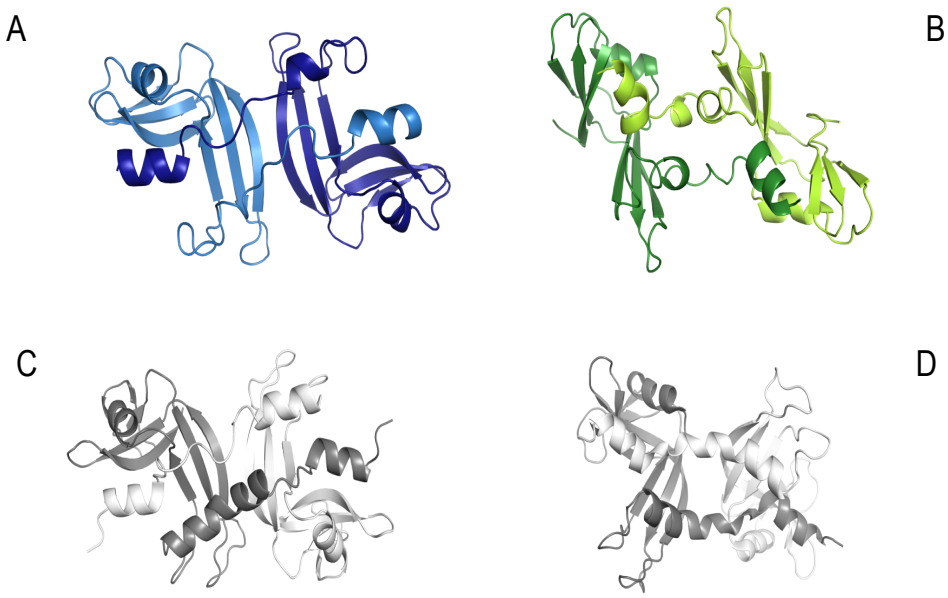

Figure 5.10 – Molecular modeling of the N-swapped ONC dimer. A) RNase A N_D-like ONC dimeric model; B) desHP-like ONC dimeric model; C) RNase A N-dimer, N_D[81]; D) des(16-20)-HP RNase dimer[208]. MD simulations were performed to compare the models and test their validity.

In the N_D-like model, several interactions contribute to form the open interface[88] between the two ONC subunits and stabilize the quaternary structure. In particular, as reported in Fig. 5.11, four strong H-bonds form between the backbones of NH and CO of Leu79 of subunit A and Lys81 of subunit B, and vice-versa. It has to be underlined, then, that only two H-bonds are present in the same region of the parent RNase A-N_D[81]. In addition, three extra H-bonds (between Asp18A and Thr14B,

Asp18B and Tyr64A, Lys81A and Arg15B) and two symmetric salt bridges between Arg73A and Glu62B, and vice-versa, are present in the N_D-like dimeric ONC model with respect to the parent template of RNase A. Accordingly, the interface area between the two subunits in the N_D-like model is 2121 Å^2, about 10% higher than that of the RNase A-N_D (1963 Å^2)[81].

As far as the other desHP-like model is concerned (panel 5.10B), its quaternary structure is less compact. Indeed, the open interface is stabilized by only two H-bonds occurring between the two subunits. Consequently, the interface area is 1573 Å^2, thus, definitely smaller than the one of the N_D-like model.

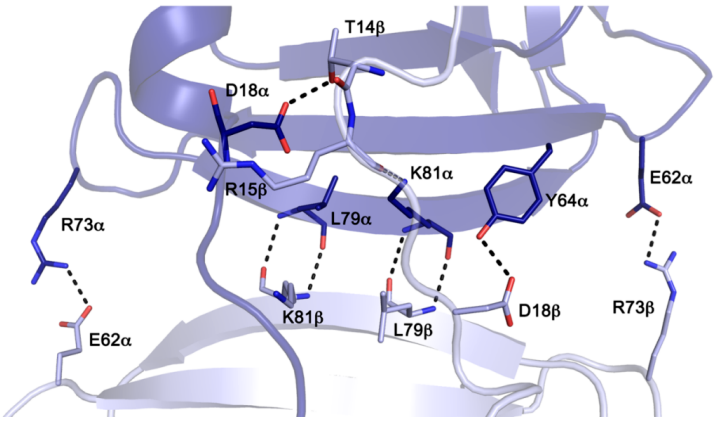

Figure 5.11 – In the N_D-like model, four strong H-bonds form between the backbones of NH and CO of Leu79 of subunit A and Lys81 of subunit B, and vice-versa, in addition to the hydrogen bonds between Asp18A and Thr14B, Asp18B and Tyr64A, Lys81A and Arg15B, and two symmetric salt bridges between Arg73A and Glu62B.

5.3.9 Cell proliferation and apoptosis assays

In order to test if ONC dimer was active against PaCa44 cell line, cells were treated with 5,10 and 25 μg/ml of each ONC species, both in presence and in absence of gemcitabine. The experiment was made in collaboration with prof. M. Donadelli. Fig. 5.12 shows the results obtained with Crystal Violet assay.

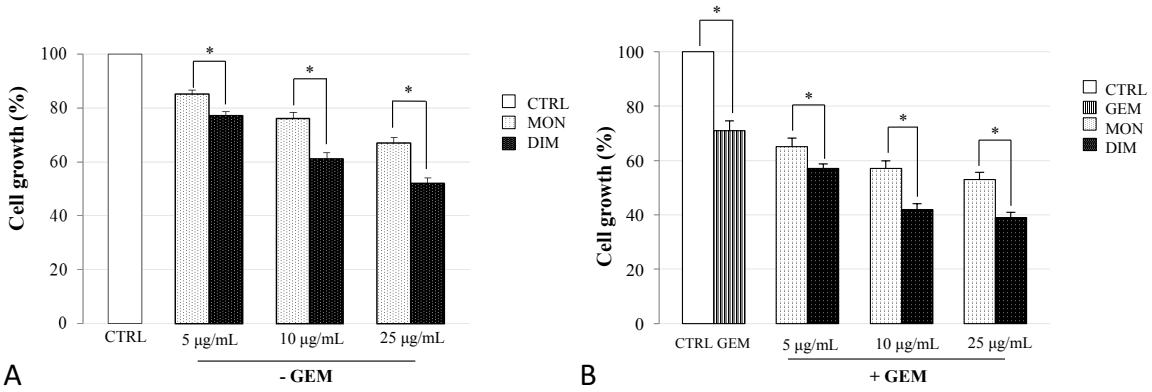

Figure 5.12 – Effects of ONC monomer and dimer on cell growth of PaCa44 pancreatic adenocarcinoma cells determined with Crystal Violet colorimetric assay. Cells were seeded in 96-well plates, incubated overnight, and treated with native ONC monomer and dimer, at the indicated concentrations, in the absence A) or presence B) of 50 nM GEM for 96 h. Values are means (±SD) of three independent biological replicates, each performing three technical replicates. Statistical analysis: * $p < 0.05$.

Both ONC monomer and dimer resulted to induce cell death of PaCa44 cell line, and the effect of the dimer is higher with respect to that of the monomer. The difference in cytotoxicity detected between monomer and dimer is strengthened when the two species are combined with the addition of gemcitabine (GEM). The higher cytotoxicity of ONC dimer could be ascribed to the higher amount of its positive net charge with respect to the monomer[108], that causes a stronger interaction with cancer cell membranes, promoting cell death after its endocytosis[108,210].

Apoptosis induction by ONC monomer and dimer was measured against the same cell line and the results are shown in Fig. 5.13.

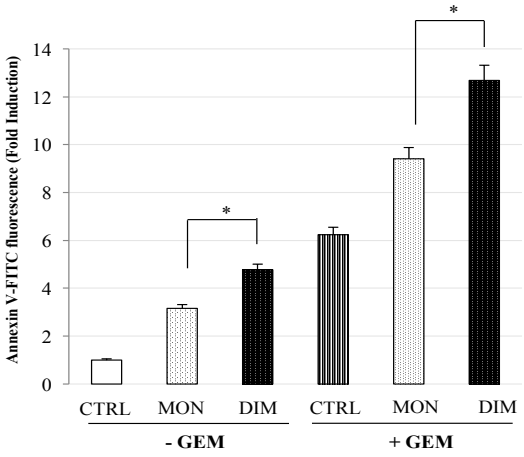

Figure 5.13 – In vivo effects of ONC monomer and dimer associated to chemotherapy. Apoptosis of PaCa44 pancreatic adenocarcinoma cells was determined with annexinV/FITC binding assay. Cells were seeded in 96-well plates, incubated overnight, and treated with 10 μg/ml native ONC monomer and dimer, in the absence or presence of 50 nM GEM for 96 h. Values are means (±SD) of three independent biological replicates, each performed using three technical replicates. Statistical analysis: * $p < 0.05$.

ONC monomer and dimer demonstrated to be able to induce apoptotis on PaCa44 cell line. The dimer is more pro-apoptotic with respect to the monomer. The apoptotic effect is further increased in presence of gemcitabine (GEM).

In order to ensure that ONC dimer did not dissociate during the 96 h of incubation with Paca44 cells, it was incubated at 37 °C with or without the addition of FBS in RPMI 1640 containing glutamine, gentamicin sulfate. At different time intervals (0, 12, 24, 48, 72, 96 h), 5 μg of each sample were withdrawn and analyzed in cathodic nondenaturing PAGE (Fig. 5.14). The presence of the band corresponding to ONC dimer in both cathodic nondeanturing PAGEs demonstrates that a certain amount of ONC dimer survived after 96 hours of incubation.

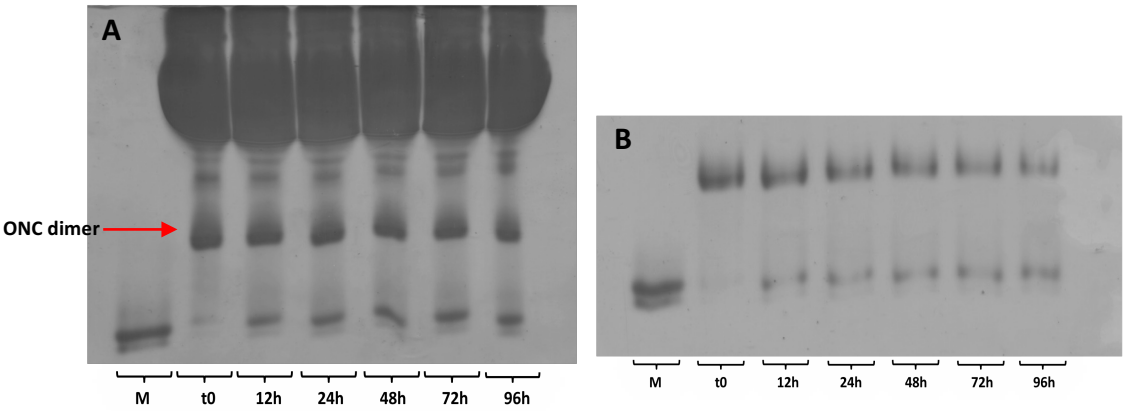

Figure 5.14 – Stability of ONC dimer in RPMI 1640 containing glutamine, gentamicin sulfate, with A) or without B) the addition of FBS. At different time intervals (0, 12, 24, 48, 72, 96 h), 5 μg of each sample were withdrawn and analyzed in 15% cathodic nondenaturing PAGE. M = ONC monomer.

4.4 Discussion

In this study we demonstrated that ONC is able to oligomerize, even if at lower extent compared to RNase A and BS-RNase. As expected, in fact, ONC forms only a type of dimer (Fig. 5.3 - 5.6), due to the fact that a disulfide bond blocks its C-terminal, preventing its swapping[211], and few traces of larger oligomers, with a residual monomer never decreasing below 83-84%. Moreover, 3% of dimer, more than the 1-2% of RNase A N-dimer[141], is natively formed by ONC (Table 5.1). The yield of ONC dimer is substantially increased after lyophilizing ONC from 40% acetic acid and resuspending it in NaPi buffer, and the increased concentration of the solubilized powder allows an augment, although not dramatic, of the dimeric species up to 13% (Table 5.1).

The ONC dimer formed after lyophilization from acetic acid is identical to the one spontaneously formed by the protein (Fig. 5.5), and DVS cross-linking reaction demonstrated that it forms through the swapping of the N-terminus of ONC monomer (Fig. 5.8). This result is not in contrast with what was previously envisaged to explain ONC partial unfolding occurring at the N-terminus[212]. These conclusions are also supported by the almost identical volume of ONC dimer and N-dimer of RNase A, that is in turn different from that of RNase A C-dimer[80] (Fig. 5.3).

The overall structure of the proposed ONC dimer model is more compact than the parent RNase A N_D, because of the wider contact area of the former (2121 $Å^2$ versus 1963 $Å^2$) and the higher number of H-bonds and other stabilizing interactions (Fig. 5.10, 5.11). In particular, two strong and symmetrical salt bridges (Arg73A-Glu62B and Arg73B-Glu62A) located at the edges of the open interface lock the dimer and stabilize the compact quaternary structure. This is supported by the stability analysis in 10 mM NaPi buffer, pH 6.7, at 37 °C, in which ONC dimer resulted to be more stable with respect to RNase A N-dimer (and also to C-dimer) (Fig 5.6). ONC dimer is also stable for 96 h in RPMI 1640 containing glutamine, gentamicin sulfate, with or without the addition of FBS (Fig. 5.14) and is even more stable when incubated in 0.1 M sodium acetate/acetic acid buffer, pH 5.0, until 120 h (Fig. 5.8F). Anyway, since 3D-DS oligomer stability depends on several factors such as

temperature, ionic strength, buffer nature, protein concentration[92,93,95], further analyses could be performed to deepen the knowledge of the factors affecting ONC dimer stability. All these results, also considering that only a single ONC species is detectable in nondenaturing cathodic PAGE, suggest that the proposed RNase A N_D-like model could represent the real ONC dimer structure.

As a consequence of dimerization, ONC increases its cytotoxic activity at low concentrations (from 5 to 25 μg/ml) against PaCa44 pancreatic cancer cell line (Fig. 5.12). The ability to induce an antiproliferative effect in presence of gemcitabine, that is higher with respect to the monomeric form, suggests a possible future therapeutic implication of ONC dimer, that could decrease both ONC and GEM concentration and side effects. The increased cytotoxicity induced by ONC dimerization is not only ascribable to the cytosolic RNase inhibitor (RI) evasion, as it is for many pancreatic-type RNases[186], since also ONC monomer is able to avoid it[57]. It could rather derive by its higher basic charge density, that would cause a higher affinity for cancer cell membrane and/or target substrates, with respect to the monomer[210,213–215]. It was demonstrated that ONC monomer is able to cause Panc1 pancreatic cancer cell line apoptosis through an autophagy-mediated pathway induced by LC3 and Beclin1 expression and by UCP2 and MnSOD inhibition[178]. A similar mechanism may be proposed for the treatment of PaCa44 cells with ONC monomer and dimer, but further studies are certainly needed to further explain the cause of their different cytotoxicity.

Besides the production and the structural and functional characterization of a dimeric form of ONC, this study can set the basis for future developments with the aim of enhance the oligomerization capacity of ONC, that could produce new species with possible therapeutic applications.

Bibliography

1. Gesteland RF, Atkins JF. The RNA world : the nature of modern RNA suggests a prebiotic RNA world. *Cold Spring Harb Monogr Ser*. 1993.
2. Ilinskaya ON, Makarov AA. Why ribonucleases induce tumor cell death. *Mol Biol*. 2005;39(1):1–10.
3. Benito A, Ribó M, Vilanova M. On the track of antitumour ribonucleases. *Mol Biosyst*. 2005;1(4):294–302.
4. Rybak SM, Newton DL. Natural and Engineered Cytotoxic Ribonucleases: Therapeutic Potential. *Exp Cell Res*. 1999;253(2):325–335.
5. Ilinskaya O, Decker K, Koschinski A, Dreyer F, Repp H. Bacillus intermedius ribonuclease as inhibitor of cell proliferation and membrane current. *Toxicology*. 2001;156(2):101–107.
6. Sevcik J, Urbanikova L, Leland PA, Raines RT. X-ray structure of two crystalline forms of a streptomycete ribonuclease with cytotoxic activity. *J Biol Chem*. 2002;277(49):47325–47330.
7. Olmo N, Turnay J, de Buitrago GG, de Silanes IL, Gavilanes JG, Lizarbe MA. Cytotoxic mechanism of the ribotoxin α-sarcin. *Eur J Biochem*. 2001;268(7):2113–2123.
8. Juan G, Ardelt B, Li X, et al. G(1) arrest of U937 cells by onconase as associated with suppression of cyclin D3 expression, induction of p16(INK4A), P21(WAF1/CIP1) and p27(KIP) and decreased pRb phosphorylation. *Leukemia*. 1998;12(8):1241–1248.
9. Arnold U, Ulbrich-Hofmann R. *Natural and engineered ribonucleases as potential cancer therapeutics*. Vol 28.; 2006:1615–1622.
10. Arnold U. Aspects of the cytotoxic action of ribonucleases. *Curr Pharm Biotechnol*. 2008;9(3):161–168.
11. Di Donato A, Cafaro V, D'Alessio G. Ribonuclease-A can be transformed into a dimeric ribonuclease with antitumor-activity. *J Biol Chem*. 1994;269(26):17394–17396.
12. Leland PA, Schultz LW, Kim BM, Raines RT. Ribonuclease A variants with potent cytotoxic activity. *Proc Natl Acad Sci U S A*. 1998;95(18):10407–10412.
13. Gaur D, Swaminathan S, Batra JK. Interaction of human pancreatic ribonuclease with human ribonuclease inhibitor: Generation of inhibitor-resistant cytotoxic variants. *J Biol Chem*. 2001;276(27):24978–24984.
14. Leland PA, Staniszewski KE, Kim BM, Raines RT. Endowing Human Pancreatic Ribonuclease with Toxicity for Cancer Cells. *J Biol Chem*. 2001;276(46):43095–43102.
15. Bosch M, Benito A, Ribó M, Puig T, Beaumelle B, Vilanova M. A Nuclear Localization Sequence Endows Human Pancreatic Ribonuclease with Cytotoxic Activity. *Biochemistry*. 2004;43(8):2167–2177.
16. Futami J, Maeda T, Kitazoe M, et al. Preparation of potent cytotoxic ribonucleases by cationization: enhanced cellular uptake and decreased

interaction with ribonuclease inhibitor by chemical modification of carboxyl groups. *Biochemistry*. 2001;40(25):7518–7524.
17. Futami J, Kitazoe M, Maeda T, et al. Intracellular delivery of proteins into mammalian living cells by polyethylenimine-cationization. *J Biosci Bioeng*. 2005;99(2):95–103.
18. De Lorenzo C, Arciello A, Cozzolino R, et al. A fully human antitumor immunoRNase selective for ErbB-2-positive carcinomas. *Cancer Res*. 2004;64(14):4870–4874.
19. Boix E, Wu Y, Vasandani VM, et al. Role of the N terminus in RNase A homologues: differences in catalytic activity, ribonuclease inhibitor interaction and cytotoxicity. *J Mol Biol*. 1996;257(5):992–1007.
20. Sierakowska H, Shugar D. Mammalian nucleolytic enzymes. *Prog Nucleic Acid Res Mol Biol*. 1977;20:59–130.
21. Weickmann JL, Elson M, Glitz DG. Purification and characterization of human pancreatic ribonuclease. *Biochemistry*. 1981;20(5):1272–1278.
22. Weickmann JL, Glitz DG. Human ribonucleases. Quantitation of pancreatic-like enzymes in serum, urine, and organ preparations. *J Biol Chem*. 1982;257(15):8705–8710.
23. Morita T, Niwata Y, Ohgi K, Ogawa M, Irie M. Distribution of two urinary ribonuclease-like enzymes in human organs and body fluids. *J Biochem*. 1986;99(1):17–25.
24. De Prisco R, Sorrentino S, Leone E, Libonati M. A ribonuclease from human seminal plasma active on double-stranded RNA. *Biochim Biophys Acta*. 1984;788(3):356–363.
25. Chu TM, Wang MC, Kuciel R, Valenzuela L, Murphy GP. Enzyme markers in human prostatic carcinoma. *Cancer Treat Rep*. 61(2):193–200.
26. Kurihara M, Ogawa M, Ohta T, et al. Purification and immunological characterization of human pancreatic ribonuclease. *Cancer Res*. 1982;42(11):4836–4841.
27. Sorrentino S, De Prisco R, Libonati M. Human seminal ribonuclease. Immunological quantitation of cross-reactive enzymes in serum, urine and seminal plasma. *Biochim Biophys Acta*. 1989;998(1):97–101.
28. Dalaly BK, Eitenmiller RR, Friend BA, Shahani KM. Human milk ribonuclease. *Biochim Biophys Acta*. 1980;615(2):381–391.
29. Sorrentino S, Libonati M. Human pancreatic-type and nonpancreatic-type ribonucleases a direct side-by-side comparison of their catalytic properties. *Arch Biochem Biophys*. 1994:340–348.
30. Sorrentino S, Libonati M. Structure-function relationships in human ribonucleases: Main distinctive features of the major RNase types. *FEBS Lett*. 1997;404(1):1–5.
31. Sorrentino S, Tucker GK, Glitz DG. Purification and characterization of a ribonuclease from human liver. *J Biol Chem*. 1988;263(31):16125–16131.
32. Ohta T, Ogawa M, Kurihara M, Kitahara T, Kosaki G. Purification, characterization and development of radioimmunoassay of human liver ribonuclease. *Clin Chim Acta*. 1982;124(1):51–62.
33. Yasuda T, Mizuta K, Sato W, Kishi K. Purification and characterization of a ribonuclease from human spleen. Immunological and enzymological comparison with nonsecretory ribonuclease from human urine. *Eur J*

Biochem. 1990;191(2):523–529.
34. Mizuta K, Awazu S, Yasuda T, Kishi K. Purification and characterization of three ribonucleases from human kidney: comparison with urine ribonucleases. *Arch Biochem Biophys*. 1990;281(1):144–151.
35. Iwama M, Kunihiro M, Ohgi K, Irie M. Purification and properties of human urine ribonucleases. *J Biochem*. 1981;89(4):1005–1016.
36. Jones W. THE ACTION OF BOILED PANCREAS EXTRACT ON YEAST NUCLEIC ACID. *Am J Physiol -- Leg Content*. 1920;52(1):203–207.
37. BARNARD EA. Biological Function of Pancreatic Ribonuclease. *Nature*. 1969;221(5178):340–344.
38. Liang CJ, Yamashita K, Kobata a. Structural study of the carbohydrate moiety of bovine pancreatic ribonuclease B. *J Biochem*. 1980;88(1):51–58.
39. Rudd PM, Scragg IG, Coghill E, Dwek RA. Separation and analysis of the glycoform populations of ribonuclease B using capillary electrophoresis. *Glycoconj J*. 1992;9(2):86–91.
40. Fu D, Chen L, O'Neill RA. A detailed structural characterization of ribonuclease B oligosaccharides by 1H NMR spectroscopy and mass spectrometry. *Carbohydr Res*. 1994;261(2):173–186.
41. Plummer TH. Glycoproteins of bovine pancreatic juice. Isolation of ribonucleases C and D. *J Biol Chem*. 1968;243(22):5961–5966.
42. Baynes JW, Wold F. Effect of glycosylation on the in vivo circulating half-life of ribonuclease. *J Biol Chem*. 1976;251(19):6016–6024.
43. Hirs CHW, Moore S, Stein WH. The sequence of amino acid residues in performic acid-oxidized ribonuclease. *J Biol Chem Biol Chem*. 1960;235:633–647.
44. Smyth DG, Stein WH, Moore S. The Sequence of Amino Acid Residues in Bovine Pancreatic Ribonuclease: Revisions and Confirmations. *J Biol Chem*. 1963;238(1):227–234.
45. KARTHA G, BELLO J, HARKER D. Tertiary Structure of Ribonuclease. *Nature*. 1967;213(5079):862–865.
46. Klink TA, Woycechowsky KJ, Taylor KM, Raines RT. Contribution of disulfide bonds to the conformational stability and catalytic activity of ribonuclease A. *Eur J Biochem*. 2000;267(2):566–572.
47. Laity JH, Shimotakahara S, Scheraga HA. Expression of wild-type and mutant bovine pancreatic ribonuclease A in Escherichia coli. *Proc Natl Acad Sci U S A*. 1993;90(2):615–619.
48. Shimotakahara S, Rios CB, Laity JH, Zimmerman DE, Scheraga HA, Montelione GT. NMR structural analysis of an analog of an intermediate formed in the rate-determining step of one pathway in the oxidative folding of bovine pancreatic ribonuclease A: automated analysis of 1H, 13C and 15N resonance assignments for wild-type and [C65S, C72S] mutant forms. *Biochemistry*. 1997;36:6915–6929.
49. Ul N. Isoelectric points and conformation of proteins: I. Effect of urea on the behavior of some proteins in isoelectric focusing. *Biochim Biophys Acta - Protein Struct*. 1971;229(3):567–581.
50. Libonati M, Gotte G. Oligomerization of bovine ribonuclease A: structural and functional features of its multimers. *Biochem J*. 2004;380(Pt 2):311–327.

51. Wlodawer A, Miller M, Sjölin L. Active site of RNase: neutron diffraction study of a complex with uridine vanadate, a transition-state analog. *Proc Natl Acad Sci U S A*. 1983;80(12):3628–3631.
52. Lee FS, Vallee BL. Structure and action of mammalian ribonuclease (angiogenin) inhibitor. *Prog Nucleic Acid Res Mol Biol*. 1993;44:1–30.
53. Shapiro R. Cytoplasmic ribonuclease inhibitor. *Methods Enzymol*. 2001;341:611–628.
54. Klink TA, Raines RT. Conformational stability is a determinant of ribonuclease A cytotoxicity. *J Biol Chem*. 2000;275(23):17463–17467.
55. Lee FS, Shapiro R, Vallee BL. Tight-binding inhibition of angiogenin and ribonuclease A by placental ribonuclease inhibitor. *Biochemistry*. 1989;28(1):225–230.
56. Vicentini AM, Kieffer B, Matthies R, et al. Protein chemical and kinetic characterization of recombinant porcine ribonuclease inhibitor expressed in Saccharomyces cerevisiae. *Biochemistry*. 1990;29(37):8827–8834.
57. Rutkoski TJ, Raines RT. Evasion of ribonuclease inhibitor as a determinant of ribonuclease cytotoxicity. *Curr Pharm Biotechnol*. 2008;9(3):185–189.
58. Wu Y, Mikulski SM, Ardelt W, Rybak SM, Youle RJ. A cytotoxic ribonuclease. Study of the mechanism of onconase cytotoxicity. *J Biol Chem*. 1993;268(14):10686–10693.
59. Kim JS, Soucek J, Matousek J, Raines RT. Structural basis for the biological activities of bovine seminal ribonuclease. *J Biol Chem*. 1995;270(18):10525–10530.
60. Kobe B, Deisenhofer J. Mechanism of ribonuclease inhibition by ribonuclease inhibitor protein based on the crystal structure of its complex with ribonuclease A. *J Mol Biol*. 1996;264(5):1028–1043.
61. Felsenfeld G, Sandeen G, Vonhippel PH. The destabilizing effect of ribonuclease on the helical DNA structure. *Proc Natl Acad Sci U S A*. 1963;50(4):644–651.
62. Jensen DE, Von Hippel PH. DNA «melting» proteins. Effects of bovine pancreatic ribonuclease binding on the conformation and stability of DNA. *J Biol Chem*. 1976;251(22):7198–7214.
63. Record MT, Lohman ML, De Haseth P. Ion effects on ligand-nucleic acid interactions. *J Mol Biol*. 1976;107(2):145–158.
64. McPherson A, Brayer G, Cascio D, Williams R. The mechanism of binding of a polynucleotide chain to pancreatic ribonuclease. *Science*. 1986;232(4751):765–768.
65. Aguilar CF, Thomas PJ, Mills A, Moss DS, Palmer RA. Newly observed binding mode in pancreatic ribonuclease. *J Mol Biol*. 1992;224(1):265–267.
66. Katoh H, Yoshinaga M, Yanagita T, et al. Kinetic studies on turtle pancreatic ribonuclease: a comparative study of the base specificities of the B2 and P0 sites of bovine pancreatic ribonuclease A and turtle pancreatic ribonuclease. *Biochim Biophys Acta (BBA)/Protein Struct Mol*. 1986;873(3):367–371.
67. RUSHIZKY GW, KNIGHT CA, SOBER HA. Studies on the preferential specificity of pancreatic ribonuclease as deduced from partial digests. *J Biol Chem*. 1961;236:2732–2737.
68. Irie M, Watanabe H, Ohgi K, et al. Some Evidence Suggesting the Existence of P2 and B3 Sites in the Active Site of Bovine Pancreatic Ribonuclease A.

J Biochem. 1984;95(3):751–759.
69. Raines RT. Ribonuclease A. *Chem Rev*. 1998;98(3):1045–1066.
70. Delcardayré SB, Ribó M, Yokel EM, Quirk DJ, Rutter WJ, Raines RT. Engineering ribonuclease a: Production, purification and characterization of wild-type enzyme and mutants at Gln11. *Protein Eng Des Sel*. 1995;8(3):261–273.
71. Panov KI, Kolbanovskaya EY, Okorokov AL, et al. Ribonuclease A mutant His119Asn: the role of histidine in catalysis. *FEBS Lett*. 1996;398(1):57–60.
72. Trautwein K, Holliger P, Stackhouse J, Benner SA. Site-directed mutagenesis of bovine pancreatic ribonuclease: Lysine-41 and aspartate-121. *FEBS Lett*. 1991;281(1–2):275–277.
73. Thompson JE, Raines RT. Value of General Acid-Base Catalysis to Ribonuclease A. *J Am Chem Soc*. 1994;116(12):5467–5468.
74. Thompson JE, Kutateladze TG, Schuster MC, Venegas FD, Messmore JM, Raines RT. Limits to Catalysis by Ribonuclease A. *Bioorg Chem*. 1995;23(4):471–481.
75. Messmore JM, Fuchs DN, Raines RT. Ribonuclease a: revealing structure-function relationships with semisynthesis. *J Am Chem Soc*. 1995;117(31):8057–8060.
76. FINDLAY D, HERRIES DG, MATHIAS AP, RABIN BR, ROSS CA. The active site and mechanism of action of bovine pancreatic ribonuclease. *Nature*. 1961;190:781–784.
77. DelCardayre SB, Raines RT. Structural determinants of enzymatic processivity. *Biochemistry*. 1994;33(20):6031–6037.
78. CRESTFIELD AM, STEIN WH, MOORE S. On the aggregation of bovine pancreatic ribonuclease. *Arch Biochem Biophys*. 1962;Suppl 1:217–222.
79. Gotte G, Vottariello F, Libonati M. Thermal aggregation of ribonuclease A. A contribution to the understanding of the role of 3D domain swapping in protein aggregation. *J Biol Chem*. 2003;278(12):10763–10769.
80. Liu Y, Gotte G, Libonati M, Eisenberg D. A domain-swapped RNase A dimer with implications for amyloid formation. *Nat Struct Biol*. 2001;8(3):211–214.
81. Liu YS, Hart PJ, Schlunegger MP, Eisenberg D. The crystal structure of a 3D domain-swapped dimer of RNase A at a 2.1-angstrom resolution. *Proc Natl Acad Sci U S A*. 1998;95(7):3437–3442.
82. Liu Y, Gotte G, Libonati M, Eisenberg D. Structures of the two 3D domain-swapped RNase A trimers. *Protein Sci*. 2002;11(2):371–380.
83. Libonati M, Bertoldi M, Sorrentino S. The activity on double-stranded RNA of aggregates of ribonuclease A higher than dimers increases as a function of the size of the aggregates. *Biochem J*. 1996;318 (Pt 1):287–290.
84. López-Alonso JP, Gotte G, Laurents D V. Kinetic analysis provides insight into the mechanism of Ribonuclease A oligomer formation. *Arch Biochem Biophys*. 2009;489(1–2):41–47.
85. Liu Y, Eisenberg D. 3D domain swapping: as domains continue to swap. *Protein Sci*. 2002;11(6):1285–1299.
86. Bennett MJ, Choe S, Eisenbergt D. Domain swapping: Entangling alliances between proteins (diphtheria toxin/evolution of oligomers). *Biochemistry*. 1994;91:3127–3131.

87. Gronenborn AM. Protein acrobatics in pairs--dimerization via domain swapping. *Curr Opin Struct Biol*. 2009;19(1):39–49.
88. Bennett MJ, Schlunegger MP, Eisenberg D. 3D domain swapping: A mechanism for oligomer assembly. *Protein Sci*. 1995;4(12):2455–2468.
89. Kuhlman B, O'Neill JW, Kim DE, Zhang KY, Baker D. Conversion of monomeric protein L to an obligate dimer by computational protein design. *Proc Natl Acad Sci U S A*. 2001;98(19):10687–10691.
90. Rousseau F, Schymkowitz JW, Wilkinson HR, Itzhaki LS. Three-dimensional domain swapping in p13suc1 occurs in the unfolded state and is controlled by conserved proline residues. *Proc Natl Acad Sci U S A*. 2001;98(10):5596–5601.
91. Schymkowitz JW, Rousseau F, Wilkinson HR, Friedler a, Itzhaki LS. Observation of signal transduction in three-dimensional domain swapping. *Nat Struct Biol*. 2001;8(10):888–892.
92. Ercole C, Colamarino RA, Pizzo E, Fogolari F, Spadaccini R, Picone D. Comparison of the structural and functional properties of RNase A and BS-RNase: A stepwise mutagenesis approach. *Biopolymers*. 2009;91(12):1009–1017.
93. Giovanni Gotte, Massimo Donadelli, Douglas V. Laurents, Francesca Vottariello, Manuela Morbio and, Massimo Libonati. Increase of RNase A N-terminus Polarity or C-terminus Apolarity Changes the Two Domains' Propensity To Swap and Form the Two Dimeric Conformers of the Protein. 2006.
94. Nenci A, Gotte G, Bertoldi M, Libonati M. Structural properties of trimers and tetramers of ribonuclease A. *Protein Sci*. 2001;10(10):2017–2027.
95. Vottariello F, Giacomelli E, Frasson R, Pozzi N, De Filippis V, Gotte G. RNase A oligomerization through 3D domain swapping is favoured by a residue located far from the swapping domains. *Biochimie*. 2011;93(10):1846–1857.
96. Ercole C, López-Alonso JP, Font J, et al. Crowding agents and osmolytes provide insight into the formation and dissociation of RNase A oligomers. *Arch Biochem Biophys*. 2011;506(2):123–129.
97. Bucci E, Vitagliano L, Barone R, Sorrentino S, D'Alessio G, Graziano G. On the thermal stability of the two dimeric forms of ribonuclease A. *Biophys Chem*. 2005;116(2):89–95.
98. Murray AJ, Lewis SJ, Barclay AN, Brady RL. One sequence, two folds: a metastable structure of CD2. *Proc Natl Acad Sci U S A*. 1995;92(16):7337–7341.
99. Green SM, Gittis a G, Meeker a K, Lattman EE. One-step evolution of a dimer from a monomeric protein. *Nat Struct Biol*. 1995;2:746–751.
100. Kortt AA, Malby RL, Caldwell JB, et al. Recombinant anti-sialidase single-chain variable fragment antibody. Characterization, formation of dimer and higher-molecular-mass multimers and the solution of the crystal structure of the single-chain variable fragment/sialidase complex. *Eur J Biochem*. 1994;221(1):151–157.
101. Perisic O, Webb PA, Holliger P, Winter G, Williams RL. Crystal structure of a diabody, a bivalent antibody fragment. *Structure*. 1994;2(12):1217–1226.

102. Trinkl S, Glockshuber R, Jaenicke R. Dimerization of PB2-crystallin: The role of the linker peptide and the N-and C-terminal extensions. *Protein Sci*. 1994;3:1392–1400.
103. Fruchter RG, Crestfield AM. Preparation and properties of two active forms of ribonuclease dimer. *J Biol Chem*. 1965;240(10):3868–3874.
104. Park C, Raines RT. Dimer formation by a «monomeric» protein. *Protein Sci*. 2000;9(10):2026–2033.
105. Merlino A, Vitagliano L, Ceruso MA, Mazzarella L. Dynamic Properties of the N-Terminal Swapped Dimer of Ribonuclease A. *Biophys J*. 2004;86(4):2383–2391.
106. Merlino A, Ceruso MA, Vitagliano L, Mazzarella L. Open Interface and Large Quaternary Structure Movements in 3D Domain Swapped Proteins: Insights from Molecular Dynamics Simulations of the C-Terminal Swapped Dimer of Ribonuclease A. *Biophys J*. 2005;88(3):2003–2012.
107. Gotte G, Bertoldi M, Libonati M. Structural versatility of bovine ribonuclease A. Distinct conformers of trimeric and tetrameric aggregates of the enzyme. *Eur J Biochem*. 1999;265(2):680–687.
108. Matousek J, Gotte G, Pouckova P, et al. Antitumor activity and other biological actions of oligomers of ribonuclease A. *J Biol Chem*. 2003;278(26):23817–23822.
109. Gotte G, Laurents D V, Libonati M. Three-dimensional domain-swapped oligomers of ribonuclease A: identification of a fifth tetramer, pentamers and hexamers, and detection of trace heptameric, octameric and nonameric species. *Biochim Biophys Acta*. 2006;1764(1):44–54.
110. Cozza G, Moro S, Gotte G. Elucidation of the ribonuclease a aggregation process mediated by 3D domain swapping: A computational approach reveals possible new multimeric structures. *Biopolymers*. 2008;89(1):26–39.
111. Fruchter RG, Crestfield AM. On the structure of ribonuclease dimer. Isolation and identification of monomers derived from inactive carboxymethyl dimers. *J Biol Chem*. 1965;240(10):3875–3882.
112. Libonati M. Molecular aggregates of ribonucleases. Some enzymatic properties. *Ital J Biochem*. 1969;18(6):407–417.
113. Parés X, Nogués M V, de Llorens R, Cuchillo CM. Structure and function of ribonuclease A binding subsites. *Essays Biochem*. 1991;26:89–103.
114. Nogués MV, Vilanova M, Cuchillo CM. Bovine pancreatic ribonuclease A as a model of an enzyme with multiple substrate binding sites. *Biochim Biophys Acta (BBA)/Protein Struct Mol*. 1995;1253(1):16–24.
115. Usher DA, Erenrich ES, Eckstein F. Geometry of the first step in the action of ribonuclease-A (in-line geometry-uridine2',3'-cyclic thiophosphate- 31 P NMR). *Proc Natl Acad Sci U S A*. 1972;69(1):115–118.
116. Libonati M. Degradation of poly A and double-stranded RNA by aggregates of pancreatic ribonuclease. *Biochim Biophys Acta*. 1971;228(2):440–445.
117. Wu Y, Saxena SK, Ardelt W, et al. A study of the intracellular routing of cytotoxic ribonucleases. *J Biol Chem*. 1995;270(29):17476–17481.
118. De Lamirande G. Action of Deoxyribonuclease and Ribonuclease on the Growth of Ehrlich Ascites Carcinoma in Mice. *Nature*. 1961;192:52–54.
119. ROTH JS. Ribonuclease activity and cancer: a review. *Cancer Res*. 1963;23:657–666.

120. Ilinskaya ON, Dreyer F, Mitkevich VA, Shaw KL, Pace CN, Makarov AA. Changing the net charge from negative to positive makes ribonuclease Sa cytotoxic. *Protein Sci*. 2009;11(10):2522–2525.
121. Garcia-Ortega L, Masip M, Mancheño JM, et al. Deletion of the NH2-terminal beta-hairpin of the ribotoxin alpha-sarcin produces a nontoxic but active ribonuclease. *J Biol Chem*. 2002;277(21):18632–18639.
122. Klink TA, Raines RT. Conformational stability is a determinant of ribonuclease A cytotoxicity. *J Biol Chem*. 2000;275(23):17463–17467.
123. Haigis MC, Kurten EL, Raines RT. Ribonuclease inhibitor as an intracellular sentry. *Nucleic Acids Res*. 2003;31(3):1024–1032.
124. Johnson RJ, McCoy JG, Bingman CA, Phillips GN, Raines RT. Inhibition of Human Pancreatic Ribonuclease by the Human Ribonuclease Inhibitor Protein. *J Mol Biol*. 2007;368(2):434–449.
125. Libonati M, Sorrentino S, Galli R, Montagna R La, Donato A Di. Degradation of DNA:RNA hybrids by aggregates of pancreatic ribonuclease. *BBA Sect Nucleic Acids Protein Synth*. 1975;407(3):292–298.
126. Bretscher LE, Abel RL, Raines RT. A ribonuclease A variant with low catalytic activity but high cytotoxicity. *J Biol Chem*. 2000;275(14):9893–9896.
127. Patutina OA, Mironova NL, Ryabchikova EI, et al. Tumoricidal Activity of RNase A and DNase I. *Acta Naturae*. 2010;2(1):88–94.
128. Glenner GG, Eanes ED, Page DL. The relation of the properties of Congo red-stained amyloid fibrils to the -conformation. *J Histochem Cytochem*. 1972;20(10):821–826.
129. Cohen AS, Shirahamata T, Skinner M. Electron microscopy of amyloid. *Electron Microsc Proteins*. 1982;3:165–205.
130. COHEN AS, CALKINS E. Electron microscopic observations on a fibrous component in amyloid of diverse origins. *Nature*. 1959;183(4669):1202–1203.
131. Glenner GG. Amyloid Deposits and Amyloidosis. *N Engl J Med*. 1980;302(24):1333–1343.
132. Jaskólski M. 3D domain swapping, protein oligomerization, and amyloid formation. *Acta Biochim Pol*. 2001;48(4):807–827.
133. Eakin CM, Attenello FJ, Morgan CJ, Miranker AD. Oligomeric Assembly of Native-like Precursors Precedes Amyloid Formation by β-2 Microglobulin †. *Biochemistry*. 2004;43(24):7808–7815.
134. Nilsson M, Wang X, Rodziewicz-Motowidlo S, et al. Prevention of Domain Swapping Inhibits Dimerization and Amyloid Fibril Formation of Cystatin C: use of engineered disulfide bridges, antibodies, and carboxymethylpapain to stabilize the monomeric form of Cystatin C. *J Biol Chem*. 2004;279(23):24236–24245.
135. Sanders A, Jeremy Craven C, Higgins LD, et al. Cystatin forms a Tetramer through Structural Rearrangement of Domain-swapped Dimers prior to Amyloidogenesis. *J Mol Biol*. 2004;336(1):165–178.
136. Torrent M, Odorizzi F, Nogués MV, Boix E. Eosinophil Cationic Protein Aggregation: Identification of an N-Terminus Amyloid Prone Region. *Biomacromolecules*. 2010;11(8):1983–1990.
137. Sambashivan S, Liu Y, Sawaya MR, Gingery M, Eisenberg D. Amyloid-like

fibrils of ribonuclease A with three-dimensional domain-swapped and native-like structure. *Nature*. 2005;437(7056):266–269.
138. Teng PK, Anderson NJ, Goldschmidt L, Sawaya MR, Sambashivan S, Eisenberg D. Ribonuclease A suggests how proteins self-chaperone against amyloid fiber formation. *Protein Sci*. 2012;21(1):26–37.
139. Campioni S, Mannini B, Zampagni M, et al. A causative link between the structure of aberrant protein oligomers and their toxicity. *Nat Chem Biol*. 2010;6(2):140–147.
140. Gotte G, Libonati M, Laurents D V. Glycosylation and specific deamidation of ribonuclease B affect the formation of three-dimensional domain-swapped oligomers. *J Biol Chem*. 2003;278(47):46241–46251.
141. Gotte G, Vottariello F, Libonati M. Thermal Aggregation of Ribonuclease A. *J Biol Chem*. 2003;278(12):10763–10769.
142. Capasso S, Mazzarella L, Sica F, et al. Kinetics and mechanism of succinimide ring formation in the deamidation process of asparagine residues. *J Chem Soc Perkin Trans 2*. 1993;262(4):679.
143. Capasso S, Kirby AJ, Salvadori S, et al. Kinetics and mechanism of the reversible isomerization of aspartic acid residues in tetrapeptides. *J Chem Soc Perkin Trans 2*. 1995;8(3):437.
144. Robinson AB, Rudd CJ. Deamidation of glutaminyl and asparaginyl residues in peptides and proteins. *Curr Top Cell Regul*. 1974;8(0):247–295.
145. Robinson NE, Robinson AB. Prediction of protein deamidation rates from primary and three-dimensional structure. *Proc Natl Acad Sci U S A*. 2001;98(8):4367–4372.
146. Di Donato A, D'Alessio G. Heterogeneity of bovine seminal ribonuclease. *Biochemistry*. 1981;20(25):7232–7237.
147. Voorter CEM, Roersma ES, Bloemendal H, de Jong WW. Age-dependent deamidation of chicken αA-crystallin. *FEBS Lett*. 1987;221(2):249–252.
148. Reissner KJ, Aswad DW. Deamidation and isoaspartate formation in proteins: unwanted alterations or surreptitious signals? *Cell Mol Life Sci*. 2003;60(7):1281–1295.
149. Nilsson MR, Driscoll M, Raleigh DP. Low levels of asparagine deamidation can have a dramatic effect on aggregation of amyloidogenic peptides: implications for the study of amyloid formation. *Protein Sci*. 2002;11(2):342–349.
150. Mangione PP, Esposito G, Relini A, et al. Structure, folding dynamics, and amyloidogenesis of D76N β2-microglobulin: roles of shear flow, hydrophobic surfaces, and α-crystallin. *J Biol Chem*. 2013;288(43):30917–30930.
151. Flaugh SL, Mills IA, King J. Glutamine deamidation destabilizes human gammaD-crystallin and lowers the kinetic barrier to unfolding. *J Biol Chem*. 2006;281(41):30782–30793.
152. Dunkelberger EB, Buchanan LE, Marek P, Cao P, Raleigh DP, Zanni MT. Deamidation Accelerates Amyloid Formation and Alters Amylin Fiber Structure. *J Am Chem Soc*. 2012;134(30):12658–12667.
153. Shi Y, Rhodes NR, Abdolvahabi A, et al. Deamidation of Asparagine to Aspartate Destabilizes Cu, Zn Superoxide Dismutase, Accelerates Fibrillization, and Mirrors ALS-Linked Mutations. *J Am Chem Soc*.

2013;135(42):15897–15908.
154. Curnis F, Longhi R, Crippa L, et al. Spontaneous formation of L-isoaspartate and gain of function in fibronectin. *J Biol Chem*. 2006;281(47):36466–36476.
155. Di Donato a, Galletti P, D'Alessio G. Selective deamidation and enzymatic methylation of seminal ribonuclease. *Biochemistry*. 1986;25(26):8361–8368.
156. Wearne SJ, Creighton TE. Effect of protein conformation on rate of deamidation: Ribonuclease A. *Proteins Struct Funct Genet*. 1989;5(1):8–12.
157. Di Donato A, Ciardiello MA, De Nigris M, Piccoli R, Mazzarella L, D'Alessio G. Selective deamidation of ribonuclease A. Isolation and characterization of the resulting isoaspartyl and aspartyl derivatives. *J Biol Chem*. 1993;268(7):4745–4751.
158. Darzynkiewicz Z, Carter SP, Mikulski SM, Ardelt WJ, Shogen K. Cytostatic and Cytotoxic Effects of Pannon (P30 Protein), A Novel Anticancer Agent. *Cell Prolif*. 1988;21(3):169–182.
159. Dyer KD, Rosenberg HF. The RNase a superfamily: Generation of diversity and innate host defense. *Mol Divers*. 2006;10(4):585–597.
160. Ardelt W, Shogen K, Darzynkiewicz Z. Onconase and amphinase, the antitumor ribonucleases from Rana pipiens oocytes. *Curr Pharm Biotechnol*. 2008;9(3):215–225.
161. Ardelt W, Mikulski SM, Shogen K. Amino acid sequence of an anti-tumor protein from Rana pipiens oocytes and early embryos. Homology to pancreatic ribonucleases. *J Biol Chem*. 1991;266(1):245–251.
162. Liao Y Di, Wang SC, Leu YJ, et al. The structural integrity exerted by N-terminal pyroglutamate is crucial for the cytotoxicity of frog ribonuclease from Rana pipiens. *Nucleic Acids Res*. 2003;31(18):5247–5255.
163. Chen S lin, Le SY, Newton DL, Jr JVM, Rybak SM. A gender-specific mRNA encoding a cytotoxic ribonuclease contains a 3' UTR of unusual length and structure. *Nucleic Acids Res*. 2000;28(12):2375–2382.
164. Mosimann SC, Ardelt W, James MN. Refined 1.7 A X-ray crystallographic structure of P-30 protein, an amphibian ribonuclease with anti-tumor activity. *J Mol Biol*. 1994;236(4):1141–1153.
165. Leland PA, Staniszewski KE, Kim BM, Raines RT. A synapomorphic disulfide bond is critical for the conformational stability and cytotoxicity of an amphibian ribonuclease. *FEBS Lett*. 2000;477(3):203–207.
166. Notomista E, Catanzano F, Graziano G, Di Gaetano S, Barone G, Di Donato A. Contribution of chain termini to the conformational stability and biological activity of onconase. *Biochemistry*. 2001;40(31):9097–9103.
167. Lee JE, Raines RT. Contribution of active-site residues to the function of onconase, a ribonuclease with antitumoral activity. *Biochemistry*. 2003;42(39):11443–11450.
168. Leland PA, Raines RT. Cancer chemotherapy--ribonucleases to the rescue. *Chem Biol*. 2001;8(5):405–413.
169. Lee JE, Bae E, Bingman CA, Phillips GN, Raines RT. Structural Basis for Catalysis by Onconase. *J Mol Biol*. 2008;375(1):165–177.
170. Kelemen BR, Schultz LW, Sweeney RY, Raines RT. Excavating an active site: The nucleobase specificity of ribonuclease A. *Biochemistry*.

2000;39(47):14487–14494.
171. Saxena SK, Sirdeshmukh R, Ardelt W, Mikulski SM, Shogen K, Youle RJ. Entry into cells and selective degradation of tRNAs by a cytotoxic member of the RNase A family. *J Biol Chem*. 2002;277(17):15142–15146.
172. Suhasini AN, Sirdeshmukh R. Transfer RNA cleavages by onconase reveal unusual cleavage sites. *J Biol Chem*. 2006;281(18):12201–12209.
173. Singh UP, Ardelt W, Saxena SK, et al. Enzymatic and Structural Characterisation of Amphinase, a Novel Cytotoxic Ribonuclease from Rana pipiens Oocytes. *J Mol Biol*. 2007;371(1):93–111.
174. Suhasini AN, Sirdeshmukh R. Onconase action on tRNA(Lys3), the primer for HIV-1 reverse transcription. *Biochem Biophys Res Commun*. 2007;363(2):304–309.
175. Ardelt W, Ardelt B, Darzynkiewicz Z. Ribonucleases as potential modalities in anticancer therapy. *Eur J Pharmacol*. 2009;625(1–3):181–189.
176. Wang X. M., Guo Z-Y. Recombinant expression, different downstream processing of the disulfide‐rich anti‐tumor peptide Ranpirnase and its effect on the growth of human glioma cell line SHG‐44. *Biomed Reports*. 2013;1(5):747–750.
177. Smolewski P, Witkowska M, Zwolinska M, et al. Cytotoxic activity of the amphibian ribonucleases onconase and r-amphinase on tumor cells from B cell lymphoproliferative disorders. *Int J Oncol*. 2014;45(1):419–425.
178. Fiorini C, Cordani M, Gotte G, Picone D, Donadelli M. Onconase induces autophagy sensitizing pancreatic cancer cells to gemcitabine and activates Akt/mTOR pathway in a ROS-dependent manner. *Biochim Biophys Acta - Mol Cell Res*. 2015;1853(3):549–560.
179. Mikulski SM, Ardelt A, Shogen K, Bernstein EH, Menduke H. Striking increase of survival of mice bearing M109 madison carcino- ma treated with a novel protein from amphibian embryos. *J Natl Cancer Inst*. 1990;82:151–152.
180. Saxena SK, Gravell M, Wu YN, et al. Inhibition of HIV-1 production and selective degradation of viral RNA by an amphibian ribonuclease. *J Biol Chem*. 1996;271(34):20783–20788.
181. *Youle RJ, D'Alessio G (1997) Antitumor RNases. In: D'Alessio G, Riordan JF (eds), Ribonucleases: structures and functions. Academic Press, New York pp. 491–514*.
182. Iordanov MS, Ryabinina OP, Wong J, et al. Molecular determinants of apoptosis induced by the cytotoxic ribonuclease onconase: evidence for cytotoxic mechanisms different from inhibition of protein synthesis. *Cancer Res*. 2000;60(7):1983–1994.
183. Zhao H, Ardelt B, Ardelt W, Shogen K, Darzynkiewicz Z. The cytotoxic ribonuclease onconase targets RNA interference (siRNA). *Cell Cycle*. 2008;7(20):3258–3261.
184. Gotte G, Libonati M. Oligomerization of ribonuclease A under reducing conditions. *Biochim Biophys Acta*. 2008;1784(4):638–650.
185. Bennett MJ, Sawaya MR, Eisenberg D. Deposition Diseases and 3D Domain Swapping. *Structure*. 2006;14(5):811–824.
186. Gotte G, Laurents D V., Merlino A, Picone D, Spadaccini R. Structural and functional relationships of natural and artificial dimeric bovine

ribonucleases: New scaffolds for potential antitumor drugs. *FEBS Lett*. 2013;587(22):3601–3608.
187. KUNITZ M. A spectrophotometric method for the measurement of ribonuclease activity. *J Biol Chem*. 1946;164(2):563–568.
188. Goldenberg DP. Analysis of protein conformation by gel electrophoresis. *Inf Press Ltd (IRL), Oxford, Oxford, UK*. 1989.
189. RICO M, BRUIX M, SANTORO J, et al. Sequential 1H-NMR assignment and solution structure of bovine pancreatic ribonuclease A. *Eur J Biochem*. 1989;183(3):623–638.
190. Esposito L, Vitagliano L, Sica F, Sorrentino G, Zagari A, Mazzarella L. The ultrahigh resolution crystal structure of ribonuclease A containing an isoaspartyl residue: hydration and sterochemical analysis. *J Mol Biol*. 2000;297(3):713–732.
191. Tarragona-Fiol A, Eggelte HJ, Harbron S, et al. Identification by site-directed mutagenesis of amino acids in the B2 subsite of bovine pancreatic ribonuclease A. *Protein Eng*. 1993;6(8):901–906.
192. D'Ursi A, Oschkinat H, Cieslar C, et al. Assignment and Secondary-Structure Determination of Monomeric Bovine Seminal Ribonuclease Employing Computer-Assisted Evaluation of Homonuclear Three-Dimensional 1H-NMR Spectra. *Eur J Biochem*. 1995;229(2):494–502.
193. Tonelli M, Eller CH, Singarapu KK, et al. Assignments of RNase A by ADAPT-NMR and enhancer. *Biomol NMR Assign*. 2015;9(1):81–88.
194. Moussaoui M, Guasch A, Boix E, Cuchillo CM, Nogués MV. The role of non-catalytic binding subsites in the endonuclease activity of bovine pancreatic ribonuclease A. *J Biol Chem*. 1996;271(9):4687–4692.
195. Milburn PJ, Scheraga HA. Local interactions favor the native 8-residue disulfide loop in the oxidation of a fragment corresponding to the sequence Ser-50-Met-79 derived from bovine pancreatic ribonuclease A. *J Protein Chem*. 1988;7(4):377–398.
196. Sievers SA, Karanicolas J, Chang HW, et al. Structure-based design of non-natural amino-acid inhibitors of amyloid fibril formation. *Nature*. 2011;475(7354):96–100.
197. Landau M, Sawaya MR, Faull KF, et al. Towards a Pharmacophore for Amyloid. Weissman JS, a c. di. *PLoS Biol*. 2011;9(6):e1001080.
198. Cheng P-N, Liu C, Zhao M, Eisenberg D, Nowick JS. Amyloid β-sheet mimics that antagonize protein aggregation and reduce amyloid toxicity. *Nat Chem*. 2012;4(11):927–933.
199. Apostol MI, Sawaya MR, Cascio D, Eisenberg D. Crystallographic studies of prion protein (PrP) segments suggest how structural changes encoded by polymorphism at residue 129 modulate susceptibility to human prion disease. *J Biol Chem*. 2010;285(39):29671–29675.
200. Benilova I, Gallardo R, Ungureanu A-A, et al. The Alzheimer disease protective mutation A2T modulates kinetic and thermodynamic properties of amyloid-β (Aβ) aggregation. *J Biol Chem*. 2014;289(45):30977–30989.
201. Ondetti MA, Deer A, Sheehan JT, Pluscec J, Kocy O. Side reactions in the synthesis of peptides containing the aspartylglycyl sequence. *Biochemistry*. 1968;7(11):4069–4075.
202. Venkatesh YP, Vithayathil PJ. Isolation and characterization of

monodeamidated derivatives of bovine pancreatic ribonuclease A. *Int J Pept Protein Res*. 1984;23(5):494–505.
203. Merlino A, Vitagliano L, Antoine Ceruso M, Di Nola A, Mazzarella L. Global and local motions in ribonuclease A: A molecular dynamics study. *Biopolymers*. 2002;65(4):274–283.
204. Shimizu T, Watanabe A, Ogawara M, Mori H, Shirasawa T. Isoaspartate Formation and Neurodegeneration in Alzheimer's Disease. *Arch Biochem Biophys*. 2000;381(2):225–234.
205. Nenci A, Gotte G, Maras B, Libonati M. Different susceptibility of the two dimers of ribonuclease A to subtilisin. Implications for their structure. *Biochim Biophys Acta*. 2001;1545(1–2):255–262.
206. Navon A, Ittah V, Laity JH, Scheraga HA, Haas E, Gussakovsky EE. Local and long-range interactions in the thermal unfolding transition of bovine pancreatic ribonuclease A. *Biochemistry*. 2001;40(1):93–104.
207. López-Alonso JP, Bruix M, Font J, et al. NMR spectroscopy reveals that RNase A is chiefly denatured in 40% acetic acid: Implications for oligomer formation by 3D domain swapping. *J Am Chem Soc*. 2010;132(5):1621–1630.
208. Pica A, Merlino A, Buell AK, et al. Three-dimensional domain swapping and supramolecular protein assembly: Insights from the X-ray structure of a dimeric swapped variant of human pancreatic RNase. *Acta Crystallogr Sect D Biol Crystallogr*. 2013;69(10):2116–2123.
209. Notomista E, Cafaro V, Fusiello R, Bracale A, D'Alessio G, Di Donato A. Effective expression and purification of recombinant onconase, an antitumor protein. *FEBS Lett*. 1999;463(3):211–215.
210. D'Errico G, Ercole C, Lista M, et al. Enforcing the positive charge of N-termini enhances membrane interaction and antitumor activity of bovine seminal ribonuclease. *Biochim Biophys Acta - Biomembr*. 2011;1808(12):3007–3015.
211. Schulenburg C, Weininger U, Neumann P, et al. Impact of the C-terminal Disulfide Bond on the Folding and Stability of Onconase. *ChemBioChem*. 2010;11(7):978–986.
212. Casares-Atienza S, Weininger U, Cámara-Artigas A, Balbach J, Garcia-Mira MM. Three-state thermal unfolding of onconase. *Biophys Chem*. 2011;159(2–3):267–274.
213. Sundlass NK, Eller CH, Cui Q, Raines RT. Contribution of Electrostatics to the Binding of Pancreatic-Type Ribonucleases to Membranes. *Biochemistry*. 2013;52(37):6304–6312.
214. Notomista E, Mancheno JM, Crescenzi O, Di Donato A, Gavilanes J, D'Alessio G. The role of electrostatic interactions in the antitumor activity of dimeric RNases. *FEBS J*. 2006;273(16):3687–3697.
215. Turcotte RF, Lavis LD, Raines RT. Onconase cytotoxicity relies on the distribution of its positive charge. *FEBS J*. 2009;276(14):3846–3857.